Adaptive Mechanosensory Mechanism of α-Catenin Revealed by Single-molecule Biomechanics

Koichiro MAKI

Doctor Thesis

Adaptive Mechanosensory Mechanism of α-Catenin Revealed by Single-molecule Biomechanics

Koichiro MAKI

Acknowledgements

This dissertation would not have been possible without the guidance and the help of individuals who contributed and extended their valuable assistance in preparation and completion of this study. I owe them my greatest gratitude.

My deepest gratitude goes out to my supervisor, Professor Taiji Adachi at the Institute for Frontier Life and Medical Sciences, Kyoto University. He gave me the opportunity to undertake my doctorial study under his cordial supervision, and provided me with educative and considerate advices to shape me as an independent researcher. I have learned the spirits of challenging, continuing, and enjoying. It is a great honor and unfathomable pleasure to be his student.

I would also like to express my gratitude to my examiners, Professor Hidetoshi Kotera and Professor Osamu Tabata at the Department of Micro Engineering, Kyoto University, who provided encouraging and constructive feedback to this thesis. I am grateful for their thoughtful and detailed comments.

I would like to express my gratitude to the collaborators. Professor Shigenobu Yonemura at the Graduate School of Medical Science, Tokushima University, and Professors Toshio Hakoshima and Yoshinori Hirano at the Graduate School of Biological Sciences, Nara Institute of Science and Technology, provided me with considerable supports and valuable suggestions from the viewpoint of cell biology and structural biology.

Special thanks to Professor Yasuhiro Inoue at the Institute for Frontier Life and Medical Sciences, Kyoto University, for providing insightful comments and discussions on this research from the view point of statistical mechanics.

My gratitude to Dr. Sung-Woong Han at the National Institute for Nanomaterials Technology, Pohang University of Science and Technology, who helped me step in single-molecule biomechanical experiments using atomic force microscopy.

I would also like to express my gratitude to Professor Damien Lacroix at the INSIGNEO Institute, University of Sheffield, and Professor Christopher R. Jacobs, Department of Biomedical Engineering, Columbia University, who hosted me in their laboratories and giving me a lot of experiences what I will never forget. My gratitude to Dr. Edward Hannezo, Mr. Raj Cool, Mr. Arjan Loenen, Ms. Stefania Marcotti, Mr. Áron Horváth, Mr. Milos Spasic, Ms. Emily Moore, Mr. Michael P. Duffy, who supported my scientific activities and life in UK, Scotland, Netherlands, and USA.

My hearty gratitude to all my colleagues at the Laboratory of Biomechanics, Institute for Frontier Life and Medical Sciences, Kyoto University, where the present study was performed. I would like to thank them for always making me feel at home, and furthermore, for their constant support and cooperation throughout my study period. Special thanks to Professor Yoshitaka Kameo, Professor Tsuyoshi Hirashima, Dr. Shinji Matsushita, Dr. Satoru Okuda, Dr. Naoki Takeishi, Dr. Young Kwan Kim, Mrs. Junko Sunaga, Ms. Hiromi Kanai, Mr. Kyohei Morita, Mr. Takato Tamaki, Mr. Yuki Hirohashi and Mr. Nobuhiko Nakao. Their individual attitudes to their researches taught me the excitement to engage in research.

I would also like to thank to the JSPS Research Fellowships for Young Scientists (DC1) for supporting my doctoral research. My gratitude to the Nakatani foundation for supporting the oversea training in Columbia University.

Special recognition goes to my family who have raised me up. My admiration to Dr. Torizo Takahashi, Dr. Fumihiko Maki and Mr. Haruhiko Maki has led me to the academic field. I’m happy to study in between their academic fields of pharmacy, medicine and engineering. Finally, my profound gratitude goes to my mother Hiromi, sister Misako, grandmothers Hide and Fukuko, and aunt Kyoko for their steady warm supports and encouragements.

Contents

Chapter 1

Molecular Biomechanics

in Intercellular Mechanotransduction

1.1 Introduction

Cell-cell adhesion is a basic principle for multicellular organisms. A variety of biological functions in the multicellular organisms are supported or mediated by the contact adhesion between cells. From a mechanical point of view, the cell-cell adhesion stably supports the functional structures in multicellular organs, such as a heart, a brain, and a gut, by connecting cell cytoskeletons between cells. In the meantime, the cell-cell adhesion is known to dynamically change during morphogenesis in an embryonic body to drive cell rearrangement and local tissue deformation. The dynamical changes in the cell-cell adhesion arise from the series of cellular responses to mechanical environment, such as compressive stress, tensile stress and flow shear stress. The cellular process in which mechanical stimulus is transduced to biochemical signal is called as mechanotransduction. Here, adherens junctions, which connect actomyosin

cytoskeletons between cells, dynamically change the adhesion strength and intensity as a result of mechanotransduction in response to intercellular tension. To understand the process of intercellular mechanotransduction is not only one of the important challenges in the current context of biomechanics and biophysics but also a valuable seed for applications in engineering and medical applications.

The mechano-responsive ability of adherens junctions emerges from the functions of their constitutive proteins. Adherens junctions are molecular complex based on a transmembrane protein called as cadherin. α-Catenin, one of the constitutive proteins at adherens junctions, is known to play a pivotal role as a tension-sensor under intercellular tension. Under intercellular tension, α-catenin changes its three-dimensional conformation to associate with vinculin. As vinculin associates with vinculin and nucleates the actin polymerization, the mechanical activation of α-catenin under tension is supposed to initiate the local remodeling of actin cytoskeleton.

Although the roles of α-catenin in intercellular mechanotransduction have been investigated by previous studies of molecular biology and structural biology, the mechanical behaviors that generate the tension-sensitivity remain unclear. For example, there is one paradox to be solved for this type of tension-sensor proteins, since tension itself is known to cause successive unfolding of biomolecules; the tension-sensor proteins definitely require mechanical forces for their activation, however, they have to be stable under such conditions because the mechanical forces function as basic protein denaturants. If α-catenin further unfolds after the conformational change, vinculin cannot associate with α-catenin because there is no functional structure. On the other hand, the architectural flexibility of adherens junctions should also be assured by the constitutive molecules as long as they sustain their innate functions, since the dynamical actin remodeling would cause a strain in the molecular complex. Since cadherin and actin filament are known to play as highly rigid materials under tension, one remaining component, β-catenin, would support the flexibility of adherens junctions. Thereby, α-catenin and β-catenin, as the constitutive proteins of adherens junction, would have

cryptic mechanical behaviors that allow robust mechanotransduction at adherens junctions. The tension-sensitivity of α-catenin seemingly emerges from the structural-functional dynamics under tension.

The present thesis explores mechanical behaviors of α-catenin and β-catenin, which serve as a tension-sensor and a tension-transmitter with the aim of understanding molecular mechanism of mechanotransduction from a viewpoint of single-molecule biomechanics. In this chapter, we undertake a general and broad background review in intercellular mechanotransduction. First, we highlight the current understanding of the roles of intercellular tension in a mature and immature multicellular tissue from a view point of mechanics. Second, we summarize the current single-molecule biomechanical approaches to understand the mechanical behaviors, structures, and biochemical properties of biomolecules by employing atomic force microscopy (AFM) and total internal reflection fluorescence microscopy (TIRFM). Finally, we present the objective of this thesis and outline of chapters.

1.2 Intercellular mechanotransduction

1.2.1 Intercellular tension in a multicellular tissue

Forces orchestrate the morphogenesis process in an embryo (Eiraku *et al*. 2011; Lecuit *et al*. 2011; Hannezo *et al*. 2015) as well as maintain the integrity of a mature biological tissue (Brugués *et al*. 2014). The embryonic development involves dynamical changes in number, size, shape and position of cells (Heisenberg and Bellaïche 2013). This is not surprising because such changes are caused by innate activities of cells. The change in the cell number is induced by the cell division and death, and the change in the cell size is caused by the cell growth. The cellular shape is determined by the intracellular cytoskeleton and the position in a tissue can be determined by migration. However, in a

developmental tissue, these cellular activities need to be orchestrated for proper morphological changes in every stage of development (Fristrom 1988). Especially, the morphological change of a biological tissue requires the large amount of mechanical forces generated by individual cells to drive the local tissue deformation (Hutson *et al*. 2008; Martin *et al*. 2010; Okuda *et al*. 2013). Therefore, how the cells in a tissue cooperatively behave to induce the local force is a fundamental issue in the field of biomechanics. In the past decade, a variety of researches have shown the cellular activities in response to mechanical environment (Sokabe *et al*. 1991; Engler *et al*. 2006; Malone *et al*. 2007; Adachi *et al*. 2009; Miyoshi and Adachi 2014; Spasic *et al*. in press), which is called as mechanotransduction. In a multicellular tissue, the mechanical forces produced by individual cells trigger mechanotransduction in each cell. This intercellular mechanotransduction would allow mechanical communication between cells to accomplish the cooperative cell activities in a tissue. Adherens junctions, one of the major interfaces that directly connect actin cytoskeleton between cells, sense and amplify the intercellular tension as well as stably transmit the intercellular tension into the intracellular structures.

1.2.2 Cadherin-based adherens junctions

Adherens junctions are molecular complex based on a transmembrane protein called as cadherin, as shown in Fig. 1-1 (Harris and Tepass 2010; Yap *et al*. 2015). The extracellular domain of cadherin associates with another cadherin on another cell, which forms the direct link between cells (Takeichi 1988). Thereby, the intracellular domain of cadherin associates with β-catenin and α-catenin to form a cadherin-catenin complex (CCC) (Kobielak and Fuchs 2004). The CCC further associates with actin filament, through which actomyosin cytoskeletons are physically connected between neighboring cells. Although the direct connection between the CCC and actin filament has been controversial as the α-catenin in the CCC cannot associate with actin filament

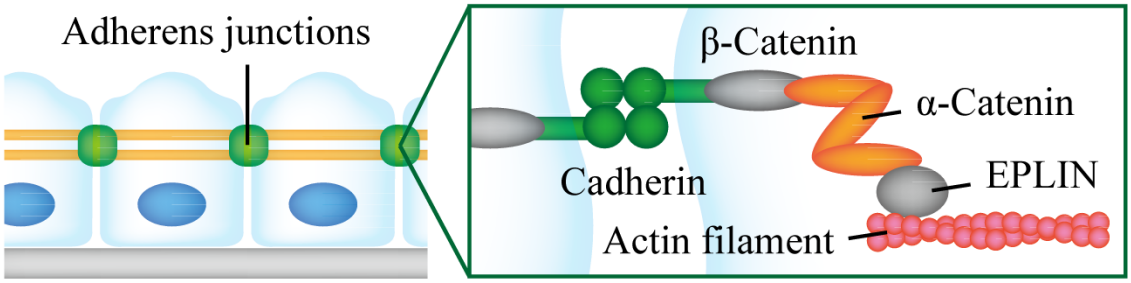

Figure 1-1: Cadherin-based adherens junctions. Several proteins such as β-catenin, α-catenin, and EPLIN mediate the interaction between cadherin and actin filament.

(Yamada *et al*. 2005), some proteins such as vinculin and EPLIN could work as adaptor molecules between α-catenin and actin filament (Pappas and Rimm 2006; Abe and Takeichi 2008). Recently, the adherens junctions can interact with microtubules as well as actin filaments (Waterman-Storer *et al*. 2000; Meng *et al*. 2008), suggesting that the cytoskeletons in cells could be integrally regulated by the adherens junctions.

As illustrated in Fig.1-2, The adherens junctions show dynamical behaviors to cause the apical constriction in the multicellular tissue during development (Takeichi 2014). The apical constriction is induced by the contraction of adherens junctions or by their downwards sliding movement (Wang *et al*. 2012). The direction of epithelial folding can be determined by the alignment of adherens junction along the mediolateral axis of a bending tissue (Nishimura *et al*. 2012). Also, the aligned adherens junctions induce the cell intercalation that drives the directed extension of a tissue along anterior-posterior axis(Rauzi *et al*. 2010; Levayer and Lecuit 2013). Furthermore, the

rotation of epithelial tubule can be driven by asymmetrical constriction of adherens junctions (Taniguchi *et al*. 2011). Such dynamical behaviors of adherens junctions are induced by polarized assembly and disassembly of constitutive molecules as a result of the interaction with other cells. Importantly, adherens junctions have a characteristic ability to sense the intercellular tension by positively remodeling the actin cytoskeleton. Since the strength of adherens junctions correlates with the intercellular tension (Harris *et al*. 2014), such positive tension feedback of adherens junctions could be one of the most important mechanisms in integration of mechanical forces in individual cells for dynamical architectural changes in a biological tissue.

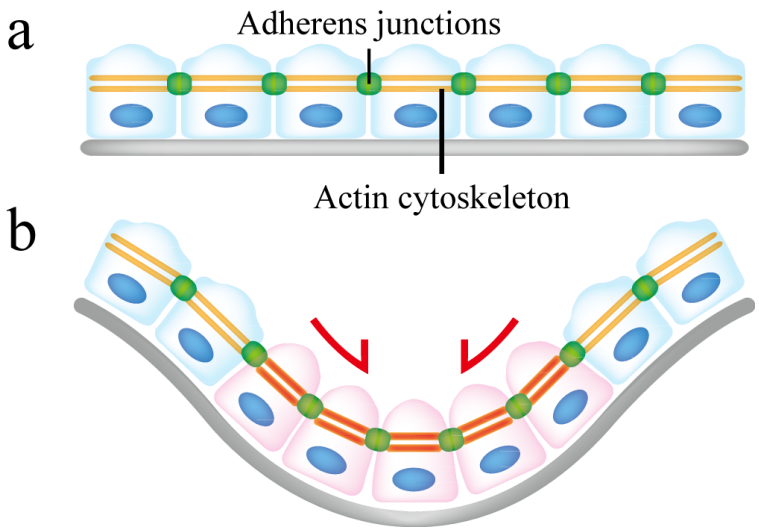

Figure 1-2: Deformation of a multicellular tissue caused by apical constriction. **a.** A planar tissue. Yellow lines and green spots indicate actin cytoskeletons and adherens junctions, respectively. **b.** Tissue deformation caused by apical constriction (orange line).

1.2.3 Mechanotransduction at adherens junctions

The cadherin-based adherens junctions sense the intercellular tension on the basis of functions of their constitutive proteins. As depicted in Fig. 1-3, α-catenin, which links β-catenin and actin filament, is known to play a pivotal role as a tension-sensor under intercellular tension (Yonemura 2011; Maiden and Hardin 2011). Under intercellular tension, α-catenin changes its conformation to associate with vinculin, as shown in Fig. 1-4a (Yonemura *et al*. 2010). As vinculin associates with vinculin and nucleates the actin polymerization, as shown in Fig. 1-4b (Wen *et al*. 2009), the mechanical activation of α-catenin under tension is supposed to initiate the local remodeling of actin cytoskeleton. Furthermore, the contractile force caused by actomyosin activities would be accelerated as a result of actin remodeling. This unique function of α-catenin as a tension-sensor is inevitable in the mechanotransduction via adherens junctions, as the disruption of α-catenin accordingly causes many kinds of diseases such as heart dysfunction (Sheikh *et al*. 2006), hyperproliferation (Vasioukhin *et al*. 2001), tumorigenesis and metastasis (Benjamin and Nelson 2008).

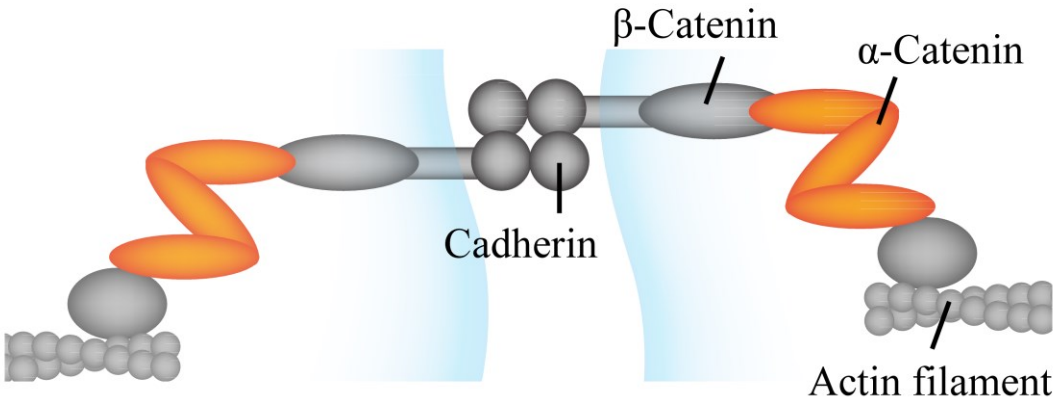

Figure 1-3: The molecular composition of adherens junctions. Cells are directly connected via cadherin, a transmembrane protein. α-Catenin, connecting β-catenin and actin filament, forms an autoinhibited structure against vinculin in free condition.

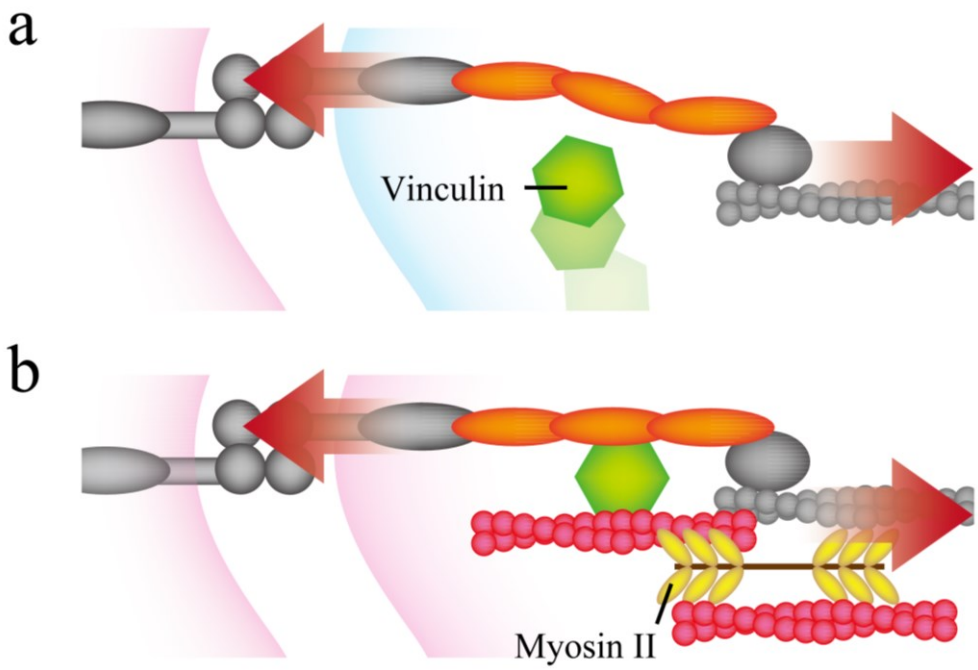

Figure 1-4: Molecular process of mechanotransduction at adherens junctions. **a.** The autoinhibition of α-catenin is disrupted under intercellular tension resulting in vinculin association. **b.** Vinculin nucleates the actin remodeling, in which myosin II is involved in tension generation.

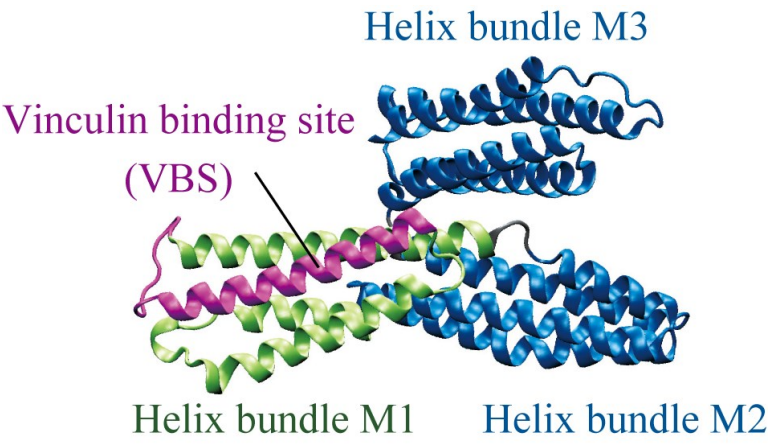

Figure 1-5: The crystal structure of tension-sensory domain α-catenin (residues 277-631) [PDB code: 4K1N] (Ishiyama *et al*. 2013).

The tension-sensory ability of α-catenin is caused by the autoinhibited structure caused by intramolecular domains. The crystal structure of the tension-sensory domain (residues 277-631) of α-catenin, as shown in Fig. 1-5 [PDB code: 4K1N] (Ishiyama *et al*. 2013), shows three four-helix bundles; helix bundle M1 comprising the vinculin binding site (VBS; residues 325-360), helix bundle M2 (residues 391-506), and helix bundle M3 (507-631 residues) (Harris 2012). These helix bundles M2 and M3 are called as modulatory (M) domain that regulates the association of α-catenin with vinculin. Yonemura *et al*. (2010) revealed that the M domain-segmented α-catenin exhibits high vinculin affinity while the autoinhibited α-catenin with M domain exhibited suppressed vinculin affinity, in *in vitro* and *in vivo* experiments. The report also suggested that the autoinhibited structure of α-catenin is open under intercellular tension, by using the specific antibody α18 that binds to a cryptic site in the helix bundle M1. In addition, based on the crystal structural biology study (Rangarajan and Izard 2012), the VBS of α-catenin should be extended to interact with the head domain of vinculin, suggesting the conformational change of the VBS is required for the association with vinculin. Recently, based on the molecular dynamics simulation (Li *et al*. 2015), the helix bundle M1 is proved to be structurally unstable compared to other two helix bundles M2 and M3, and the disruption of the interaction between helix bundles M1 and M2-M3 induces the destabilization of the helix bundle M1. Taken together, the conformational change of α-catenin can be induced by the mechanical disruption of the inter-domain interaction between helix bundles M1 and M2-M3 that causes the destabilization of helix bundle M1 to expose the VBS.

However, there are several questions for the intercellular mechanotransduction process from a view point of molecular biomechanics. First, there is a simple question for the architectural flexibility of adherens junction. Since there are the dynamical assembly and disassembly of protein networks in each cell, the adherens junction at the boundary between the cells is exerted by fluctuated displacement. At the same time, the actin filament and the cadherin as the constitutive proteins are known to play as highly rigid materials (Pittet *et al*. 2008; Matsushita *et al*. 2010). Even though the high rigidity

of actin filament and cadherin is important for stable tension transmission, the flexibility of adherens junctions needs to be supported by the remaining constitutive proteins such as α-catenin and β-catenin.

In addition, one important paradox remains to be solved for α-catenin since tension plays as a denaturant of biomolecules by causing successive unfolding. Previous report (Liu *et al*. 2009) has suggested that some protein completely unfold under physiologically possible small tension. In addition, α-helical secondary structure in α-catenin is known to exhibit lower mechanical stabilities than another type of secondary structure, β-sheet (Hoffmann and Dougan 2012). It is true that the tension-sensor proteins such as α-catenin at adherens junctions and talin at focal adhesions should change the conformation under tension to expose the binding sites for signaling molecules, but they also have to sustain the activated state to await the binding of signaling molecules.

Furthermore, how the mechanically-activated α-catenin associates with vinculin is mysterious, since vinculin forms an autoinhibited structure against α-catenin as α-catenin in free condition does against vinculin (Johnson and Craig 1994; Bakolitsa *et al*. 2004). Although the VBS of α-catenin associates with the head domain of vinculin, the segmented α-catenin (residues 273-510), with exposed VBS, does not associate with full-length vinculin (residues 1-1066) (Choi *et al*. 2012). The difference in the results implies the autoinhibited structure of full-length vinculin against α-catenin. Previous study (Bakolitsa *et al*. 2004) has reported the strong autoinhibiting interaction between the head and tail domains of vinculin. Thereby, there can be an unraveled association mechanism of α-catenin with vinculin mediated by intercellular tension.

Thus, there are three open questions for mechanotransduction at adherens junctions; (1) how the architectural flexibility of adherens junction is maintained under fluctuating intercellular tension, (2) how α-catenin retains its activated state to recruit vinculin by avoiding the successive unfolding under tension, and (3) how α-catenin associates with vinculin under intercellular tension by unlocking its autoinhibition.

1.3 Single-molecule biomechanical approaches based on AFM and TIRFM

1.3.1 AFM nano-tensile testing

In the history of biomechanics, atomic force microscopy (AFM) has been powerfully utilized to explore mechanical behaviors and three dimensional surface profiles of multiscale biological samples from a biological tissue to a single biomolecule such as nucleic acids and proteins (Neuman and Nagy 2008; Lekka and Laidler 2009; Chang *et al*. 2012; Haase *et al*. 2015). The AFM was initially developed by Binning *et al*. (1986) to overcome limitations of the scanning tunneling microscope in imaging nonconductive samples, which enabled AFM to obtain the surface profiles of biomolecules. However, AFM has become an ideal tool for biomechanical researches because of the possibility of modifying the surface and manipulating individual molecules (Engel 1991; Lindsay 1994; Bustamante *et al*. 1995). The advantages of this technique are the possibility of simple and rapid sample preparation and the ability to perform measurements under nearly physiological conditions (Drake *et al*. 1989; Bustamante *et al*. 1997). The special abilities to directly “touch” and “look” the biological samples have provided the new insights in the complex biological systems, in which the mechanical behaviors and the structures of materials are mutually coupled.

AFM is a microscopy that measures forces acting between atoms. Fig. 1-6a describes the basic principle of AFM, which is called as an “optical lever”. The AFM cantilever, the tip of which has a small probe, is exposed by a laser and the reflected laser passes through the long optical path and finally detected by two- or four-segmented photodiode. The base of the cantilever can be displaced along x-, y-, and z-axes by small extensions in piezoelectric elements with the voltages from the controller of AFM. When the cantilever is deflected by the force applied to the probe, the voltages in the photodiode sensitively change. To calibrate the force applied to the

probe from the voltage change in the photo diode, we first need to achieve the two relationships, i.e., the relationship between the voltage change and the cantilever deflection, and the relationship between the cantilever deflection and the force. The relationship can be achieved in a simple measurement to push the surface of a stiff substrate, such as glass or mica. As the displacement of the stiff substrate under small force can be ignored, the displacement of the cantilever is now equal to the displacement of z-axial piezo. Thus, we can obtain the relationship by calculating the slope in the plot on the basis of voltage change in the photodiode and the displacement of z-axial piezo during the pushing experiment. Second, the relationship between the displacement of cantilever and the force is estimated based on the resonance frequency. Thereby, based on the principle of the optical lever in AFM, the small deflection of a cantilever is magnified to the large voltage change in the photodiode as a result of the long optical path length of the deflected laser, and finally calibrated to the force.

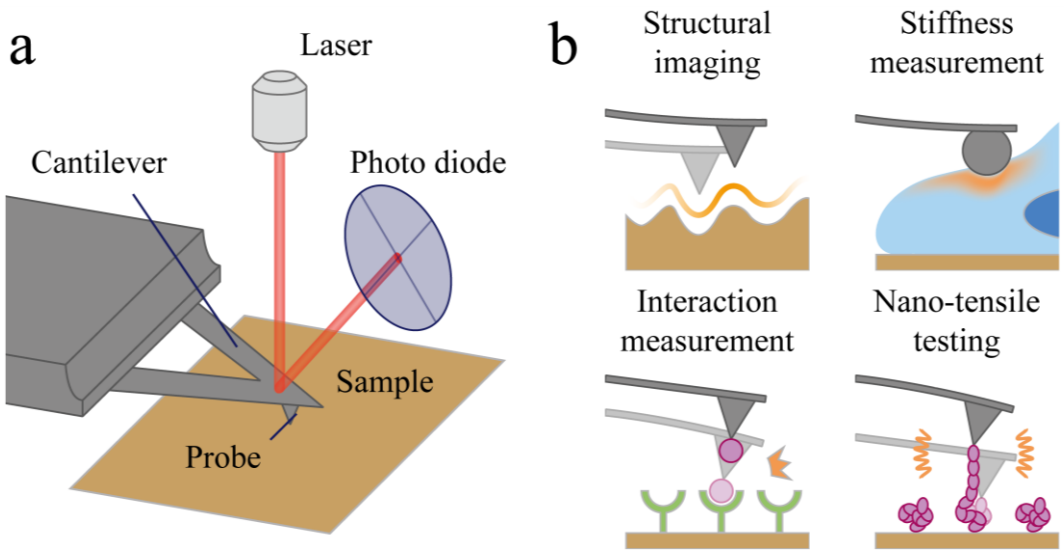

Figure 1-6: Principle of AFM and applications. **a.** An optical lever in AFM system. **b.** Structural imaging, stiffness measurement, interaction measurement, and nano-tensile testing.

The unique ability of AFM to sensitively detect the small force has been utilized to explore the mechanical behaviors of biological materials, as illustrated in Fig. 1-6b (Haase *et al*. 2015). The nano-tensile testing, or single-molecule force spectroscopy, is a strong tool to investigate the forces and motions associated with biological molecules and enzymatic activities (Zhuang and Rief 2003; Lim *et al*. 2006). In the nano-tensile testing, the biomolecules are modified to the AFM tip or substrate, and the AFM probe is contacted to the cover slip to allow the interaction between the molecules on the AFM probe and the cover slip, or the interaction between the AFM probe and the molecules on the cover slip. Finally, the molecules are directly loaded according to the extension of z-axial piezo. After the calibration of the voltage change in the photodiode to the force, we obtain the plot of the force on the basis of the piezo displacement. As the piezo displacement is equal to the summation of the cantilever deflection and the extension of the sample, the force plot is often converted to the force versus extension curve, or shortly force curve. This force curve includes a lot of valuable information in the mechanical behaviors of biomolecules under tension, such as their mechanical properties as a polymer chain, unfolding pathways with multiple intermediate states, and their transient mechanical stabilities. Thereby, this technique can be expressed as “mechanical fingerprinting” (Hoffmann and Dougan 2012).

The first example of single-molecule protein unfolding by AFM nano-tensile testing was reported by Mitsui *et al*. (1996). They modified α2-Macroglobulin on the gold-coated mica surface and applied tension by using gold-coated silicon nitride AFM tip. As a result, saw tooth patterns were observed in force curves, suggesting the multiple intermediate state of the protein during mechanical unfolding. Rief *et al*. (1997) showed the reversible unfolding of titin immunoglobulin domains that proved that the folding pathway could also be explored by AFM nano-tensile testing with cyclic piezo displacement. The reversible mechanical unfolding of RNA structures were reported by Liphardt *et al*. (2001). The AFM nano-tensile testing is now a powerful tool to explore the internal structures of biomolecules. Popa *et al*. (2013) reported the detection of single S-S bond in a protein and Janovjak *et al*. (2003) reported the precise

unfolding pathways of bacteriorhodopsin. Valle-Orero *et al*. (2015) developed the clever method to construct the free energy landscape of a protein based on the result of AFM nano-tensile testing. As the mechanical behaviors of a polymer chain are suggested to change based on the secondary or tertiary structures (Stirnemann *et al*. 2013), the dynamical conformational changes of a protein under mechanical force, including continual breaking of subcomponents, will be more understood by AFM nano-tensile testing.

1.3.2 AFM structural imaging

The other powerful usage of AFM is structural imaging to obtain the three-dimensional profile of biological samples. The sharp AFM probe, of which curvature radius should be small as a few nano-meters, gently traces the sample surface at the constant piezo displacement or the constant force. As a result, the surface profile can be obtained based on the cantilever deflection or the z-axial piezo displacement. The advantage of AFM structural imaging is definitely that we can observe the structures of “living” samples in near-physiological environment.

As shown in Fig. 1-7, There are three types of imaging mode in AFM structural imaging (Jalili and Laxminarayana 2004; Ando *et al*. 2007); (i) constant-height imaging, (ii) constant-force imaging, and (iii) tapping imaging. Constant-height imaging is the simplest type of structural imaging using AFM (Marti *et al*. 1988). In the constant-height imaging, the piezo displacement is clamped during imaging and only the x- and y-axial piezo is displaced in the scanning region. Based on the deflection of cantilever, the sample height is estimated at each scanning point and integrated to one image including the information of the sample height. Although the contact-height imaging is accurate when the sample is much stiffer than the cantilever, it was not applicable for soft samples such as a biological tissue and a protein because the sample

is deformed under force that made the measurement inaccurate. The constant-force imaging overcame the disadvantage by gently scanning the surface at the constant small force, in which the voltage change in the photo diode is fed back to the piezo displacement during the measurement. The constant-force imaging (Häberle *et al*. 1992) enabled the measurement for soft biomaterials while it still cause the drag force on the surface that resulting in the detachment of samples if their adhesion strength to the substrate is weak. Thereby, the samples are occasionally dried up for the strong interaction with the substrate. The tapping imaging, which was invented in 1994 (Zhong *et al*. 1993), broke through in minimizing the drag force. In this type of imaging, the cantilever resonates along z-axis and the difference in the amplitude of vibration caused by the repulsive force from a sample is fed back to the z-axial piezo displacement. As the samples should not be strongly modified to the substrate in tapping imaging, this improvement made the AFM imaging more convenient and useful to visualize the sample surfaces as they were in physiological conditions.

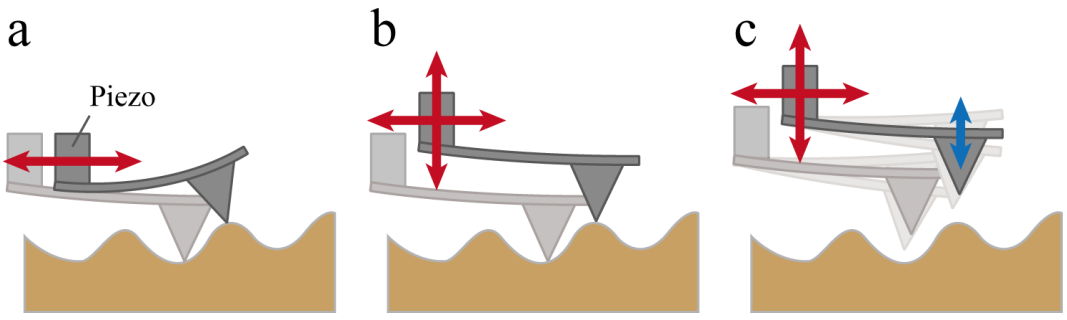

Figure 1-7: Schematics of three types of structural imaging. **a.** Constant-height imaging. **b.** Constant-force imaging. **c.** Tapping imaging.

Recently, new type of very small cantilever with high resonance frequency and the low spring constant have enabled the high speed structural imaging to vividly observe the dynamical motion of proteins in physiological conditions. Previous researches have succeeded to observe the walking motion of myosin proteins on actin filaments (Kodera *et al*. 2010), conformational change of bacteriorhodopsin under optical stimuli (Shibata *et al*. 2010), and the rotational motion of the motor F1-ATPase (Uchihashi *et al*. 2011). This exciting development in AFM imaging is now bridging our understanding on molecular structures and their functions.

1.3.3 TIRFM imaging

Single-molecule fluorescence observation is an implicit technique to understand the biochemical properties of biomolecules. The total internal reflection fluorescence microscopy (TIRFM) enables extremely high signal-to-noise ratio, which is achieved by the illumination of fluorescent molecules only near the coverslip surface without background noise that is caused by fluorescent molecules far away from the coverslip. Thereby, TIRFM has been utilized to explore the dynamics of biomolecules in solution, cells, or even biological tissues (Reck-Peterson *et al*. 2010; Mattheyses *et al*. 2010).

The principle of TIRFM is a total reflection of a beam of light (Axelrod 1981). When the beam goes out of one material and into another material with a smaller refractive index with a small incident angle, the bent is bent with the transmitted angle which is times larger than the incident angle. The relationship between the incident and transmitted angles are determined by the ratio of refraction index of two materials. When the incident angle is equal to the critical angle, the transmitted angle reaches at 90°, i.e., the beam is bent parallel to the interface between two materials. Then, the beam is totally reflected when the incident angle is larger than the critical angle. In the TIRFM observation, the laser perpendicular to the coverslip is serially bent in the

specially made objective lens to obtain the high incident angle, as depicted in Fig. 1-8 (Reck-Peterson *et al*. 2010). The incident angle is regulated by the shift of the laser path from the optical axis. In the condition of total reflection, the electric field of the laser generates an evanescent wave that extends into the second material. Importantly, the evanescent wave exponentially decays with the distance from the substrate and thus the fluorescent molecules only near the substrate can be illuminated.

The first TIRFM experiment was performed by Funatsu *et al*. in 1995, in which they directly observed the motion of myosin on actin filament. After this considerable work, a lot of researches examined the stepping mechanisms of cytoskeletal motor proteins such as myosins, kinesins and dyneins, which contributed to the early stage of nano-biomechanics and molecular biophysics. The TIRFM imaging has also been utilized to understand the kinetics of the interaction between single molecules (Hellen and Axelrod 1991). Even though the small depth of the evanescent wave limits the application to *in vivo* researches using cells, the molecular assembly/disassembly mechanism of focal adhesion, which appears in the thin basement of cells, has been realized based on the TIRFM imaging.

1.4 Thesis objective

The research objective in this thesis is to understand the mechanical behaviors of α-catenin and β-catenin, which serve as a tension-sensor and a tension-transmitter from a viewpoint of molecular biomechanics. The tension-sensitivity of α-catenin would emerge from a dynamical coupling of the structure and the biochemical properties under tension. Therefore, we employed AFM-based nano-tensile testing and structural imaging, and TIRFM-based fluorescent imaging in order to comprehensively understand the tension-sensory mechanism of α-catenin molecule under tension.

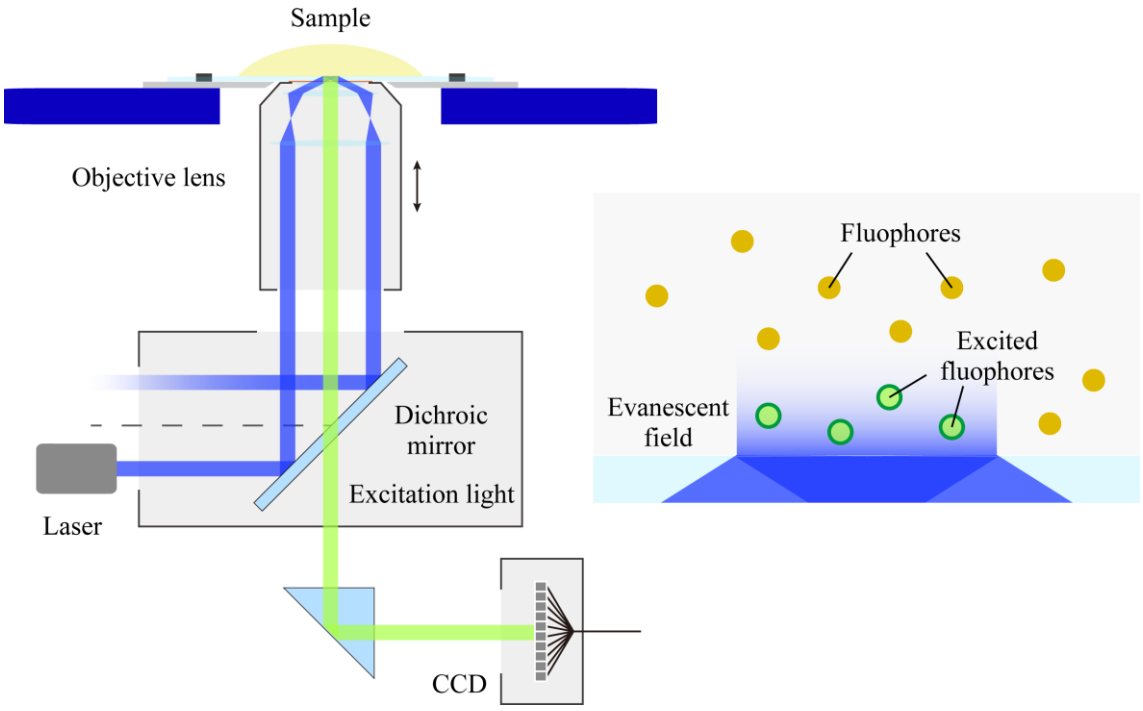

Figure 1-8: Schematics of TIRFM imaging. The laser with shifted light path is totally reflected because of the difference in the refractive index. The excited light from fluophores only in the evanescent field is observed by high-sensitive CCD camera.

1.5 Thesis outline

In Chapter 2, we investigated the mechanical behaviors of β-catenin by employing AFM nano-tensile testing to understand how this molecule contributes to the architectural flexibility of adherens junctions. As the loading condition should be various at adherens junctions depending on the interaction between cadherin and β-catenin, a whole and a part structure of β-catenin have been loaded under tension. β-Catenin molecules chemically modified on the coverslip were directly loaded by AFM probe.

In Chapter 3, we explored the mechanical behaviors and the structures of α-catenin with the objective to reveal how α-catenin retains its activated state under tension to await vinculin. By employing AFM nano-tensile testing, we examined the mechanical behaviors of wild type, mutated, and segmented α-catenin fragments to understand the effect of intramolecular interaction on the mechanical behaviors. The conformations of wild type and mutated α-catenin fragments were examined by AFM structural imaging. In addition, we mechanically activated wild type α-catenin by using the holding method to reveal the mechanical behaviors of its activated state.

In Chapter 4, we developed a novel TIRFM-combined AFM system to investigate the change in vinculin affinity of α-catenin as a result of mechano-adaptive conformational change. In this experiment, we mechanically activated wild type α-catenin by AFM and simultaneously observed their association/dissociation with fluorescent dye-labeled full-length vinculin in a solvent by TIRFM. In addition, we analyzed the mechanical behaviors of α-catenin in the presence and absence of characteristic signals in TIRFM caused by vinculin association, to reveal how the vinculin association alters the mechanical behaviors of α-catenin.

Finally, in Chapter 5, we highlighted the main results, draw conclusions and outline the future prospects of this study.

References

Abe, K. & Takeichi, M. EPLIN mediates linkage of the cadherin–catenin complex to F-actin and stabilizes the circumferential actin belt. *Proc. Natl. Acad. Sci. U. S. A.* **105,** 13–19 (2008).

Adachi, T., Aonuma, Y., Tanaka, M., Hojo, M., Takano-Yamamoto, T. & Kamioka, H. Calcium response in single osteocytes to locally applied mechanical stimulus: Differences in cell process and cell body. *J. Biomech.* **42,** 1989–1995 (2009).

Ando, T., Uchihashi, T., Kodera, N., Yamamoto, D., Taniguchi, M., Miyagi, A. & Yamashita, H. High-speed atomic force microscopy for observing dynamic biomolecular processes. Journal of molecular recognition. *JMR* **20,** 448–458 (2007).

Axelrod, D. Cell-substrate contacts illuminated by total-internal reflection fluorescence. *J. Cell Biol.* **89,** 141–145 (1981).

Bakolitsa, C., Cohen, D. M., Bankston, L. A ., Bobkov, A. A., Cadwell, G. W., Jennings, L., Critchley, D. R., Craig, S. W. & Liddington, R. C. Structural basis for vinculin activation at sites of cell adhesion. *Nature* **430,** 583–586 (2004).

Benjamin, J. M. & Nelson, W. J. Bench to bedside and back again: molecular mechanisms of α-catenin function and roles in tumorigenesis. *Semin. Cancer Biol.* **18,** 53–64 (2008).

Brugués, A., Anon, E., Conte, V., Veldhuis, J. H., Gupta, M., Colombelli, J., Muñoz, J. J., Brodland, G. W., Ladoux, B. & Trepat, X. Forces driving epithelial wound healing. *Nat. Phys.* **10,** 683–690 (2014).

Bustamante, C., Rivetti, C. & Keller, D. J. Scanning force microscopy under aqueous solutions. *Curr. Opin. Struc. Biol.* **7,** 709–716 (1997).

Bustamante, J. O. Liepins, A., Prendergast, R. A., Hanover, J. A. & Oberleithner, H. Membrane biology patch clamp and atomic force microscopy demonstrate TATA-binding protein (TBP) interactions with the nuclear pore complex. *J. Membrane Biol.* **272,** 263–272 (1995).

Chang, K. C. Chiang, Y. W., Yang, C. H. & Liou, J. W. Atomic force microscopy in biology and biomedicine. *TCMJ* **24,** 162–169 (2012).

References

Choi, H. J. Pokutta, S., Cadwell, G. W., Bobkov, A. A., Bankston, L. A., Liddington, R. C. & Weis, W. I. αE-catenin is an autoinhibited molecule that coactivates vinculin. *Proc. Natl. Acad. Sci. U. S. A.* **109,** 8576–8581 (2012).

Drake, B. Prater, C. B., Weisenhorn, A. L., Gould, S. A., Albrecht, T. R., Quate, C. F., Cannell, D. S., Hansma, H. G. & Hansma, P. K. Imaging crystals, polymers, and processes in water with the atomic force microscope. *Science* **243,** 1586–1589 (1989).

Eiraku, M., Takata M., Ishibashi, H., Kawada, K., Sakakura, E., Okuda, S., Sekiguchi, K., Adachi, T. & Sasai Y. Self-organizing optic-cup morphogenesis in three-dimensional culture. *Nature* **472,** 51–56 (2011).

Engel, A. Biological applications of scanning probe microscopes. *Annu. Rev. Biophys. Biophys. Chern.* **20,** 79–108 (1991).

Engler, A. J., Sen, S., Sweeney, H. L. & Discher, D. E. Matrix elasticity directs stem cell lineage specification. *Cell* **126,** 677–689 (2006).

Fristrom, D. The cellular basis of epithelial morphogenesis. A review. Tissue and Cell, **20,** 645–690 (1988).

Funatsu, T., Harada, Y., Tokunaga, M., Saito, K. & Yanagida, T. Imaging of single fluorescent molecules and individual ATP turnovers by single myosin molecules in aqueous solution. *Nature* **374,** 555–559 (1995).

Haase, K., Pelling, A. E. & Haase, K. Investigating cell mechanics with atomic force microscopy. *J. R. SOC. Interface* **12,** 20140970 (2015).

Häberle, W., Hörber, J. K. H., Ohnesorge, F., Smith, D. P. E. & Binnig, G. In situ investigations of single living cells infected by viruses. *Ultramicroscopy* **42–44,** 1161–1167 (1992).

Hannezo, E., Dong, B., Recho, P., Joanny, J. F. & Hayashi, S. Cortical instability drives periodic supracellular actin pattern formation in epithelial tubes. *Proc. Natl. Acad. Sci. U. S. A.* **112,** 8620-8625 (2015).

Harris, A. R., Daeden, A. & Charras, G. T. Formation of adherens junctions leads to the emergence of a tissue-level tension in epithelial monolayers. *J. Cell Sci.* **127,** 2507–2517 (2014).

Harris, T. Adherens junctions: from molecular mechanisms to tissue development and

disease. *Springer,* Netherlands, 434 pp. (2012)

Harris, T. J. & Tepass, U. Adherens junctions: from molecules to morphogenesis. *Nat. Rev. Mol. Cell Biol.* **11,** 502–514 (2010).

Heisenberg, C. P. & Bellaïche, Y. Forces in tissue morphogenesis and patterning. *Cell* **153,** 948–962 (2013).

Hellen, E. H. & Axelrod, D. Kinetics of epidermal growth factor/receptor binding on cells measured by total internal reflection/fluorescence recovery after photobleaching. *J. Fluoresc.* **1,** 113–128 (1991).

Hoffmann, T. & Dougan, L. Single molecule force spectroscopy using polyproteins. *Chem. Soc. Rev.* **41,** 4781–4796 (2012).

Hutson, M. S., Tokutake, Y., Chang, M. S., Bloor, J. W., Venakides, S. Kiehart, D. P. & Edwards, G. S. Forces for morphogenesis investigated with laser microsurgery and quantitative modeling. *Science* **145,** 145–149 (2008).

Ishiyama, N., Tanaka, N., Abe, K., Yang, Y. J., Abbas, Y. M., Umitsu, M., Nagar, B., Bueler, S. A., Rubinstein, J. L., Takeichi, M. & Ikura, M. An autoinhibited structure of α-catenin and its implications for vnculin recruitment to adherens junctions. *J. Biol. Chem.* **288,** 15913–15925 (2013).

Jalili, N. & Laxminarayana, K. A review of atomic force microscopy imaging systems: application to molecular metrology and biological sciences. *Mechatronics* **14,** 907‑945 (2004).

Janovjak, H., Kessler, M., Oesterhelt, D., Gaub, H. & Müller, D. J. Unfolding pathways of native bacteriorhodopsin depend on temperature. *EMBO J.* **22,** 5220–5229 (2003).

Johnson, R. P . & Craig, S. W. An intramolecular association between the head and tail domains of vinculin modulates talin binding. *J. Biol. Chem.* **269,** 12611–12619 (1994).

Joo, C., Balci, H., Ishitsuka, Y., Buranachai, C. & Ha, T. Advances in single-molecule fluorescence methods for molecular biology. *Annu. Rev. Biochem.* **77,** 51–76 (2008).

Kobielak, A. & Fuchs, E. α-Catenin: at the junction of intercellular adhesion and actin dynamics. *Nat. Rev. Mol. Cell Biol.* **5,** 614–625 (2004).

Kodera, N., Yamamoto, D., Ishikawa, R. & Ando, T. Video imaging of walking myosin V by high-speed atomic force microscopy. *Nature* **468,** 72–76 (2010).

Lecuit, T., Lenne, P. F. & Munro, E. Force generation, transmission, and integration during cell and tissue morphogenesis. *Annu. Rev. Cell Dev. Biol.* **27,** 157–184 (2011).

Lekka, M. & Laidler, P. Applicability of AFM in cancer detection. *Nat. Nanotech.* **4,** 72–73 (2009).

Levayer, R. & Lecuit, T. Oscillation and polarity of E-Cadherin asymmetries control actomyosin flow patterns during morphogenesis. *Dev. Cell* **26,** 162–175 (2013).

Li, J., Newhall, J., Ishiyama, N., Gottarge, C., Ikura M., Leckband, D. E. & Tajkhorshid, E. Structural determinants of the mechanical stability of α-catenin. *J. Biol. Chem.* **290,** 18890–18903 (2005).

Lim, C. T., Zhou, E. H., Li, A., Vedula, S. R. K. & Fu, H. X. Experimental techniques for single cell and single molecule biomechanics. *Mat. Sci. Eng. C* **26,** 1278–1288 (2006).

Lindsay, S. M. Biological scanning probe microscopy comes of age. *Biophys. J.* **67,** 2134–2135 (1994).

Liphardt, J., Onoa, B., Smith, S. B., Tinoco, I. Jr. & Bustamante, C. Reversible unfolding of single RNA by mechanical force. *Science* **292,** 733–737 (2014).

Liu, R., Garcia-Manyes, S., Sarkar, A., Badilla, C. L. & Fernández, J. M. Mechanical characterization of protein L in the low-force regime by electromagnetic tweezers/evanescent nanometry. *Biophys. J.* **96,** 3810–3821 (2009).

Maiden, S. L. & Hardin, J. The secret life of α-catenin: moonlighting in morphogenesis. *J. Cell Biol.* **195,** 543–552 (2011).

Malone, A. M. D., Anderson, C. T., Tummala, P. Kwon, R. Y., Johnston, T. R., Stearns, T. & Jacobs, C. R. Primary cilia mediate mechanosensing in bone cells by a calcium-independent mechanism. *Proc. Natl. Acad. Sci. U. S. A.* **105,** 13325–13330 (2007).

Marti, O., Elings, V., Haugan, M., Bracker, C. E., Schneir, J., Drake, B., Gould, A. C., Gurley, J., Hellemans, L., Shaw, K., Weisenhorn, A. L., Zasadzinski, J. & Hansma, P. K. Scanning probe microscopy of biological samples and other surfaces. *J.*

Microsc. **152,** 803–809 (1988).

Martin, A. C., Gelbart, M., Fernandez-Gonzalez, R., Kaschube, M. & Wieschaus, E. F. Integration of contractile forces during tissue invagination. *J. Cell Biol.* **188,** 735–749 (2010).

Matsushita, S., Adachi, T., Inoue, Y., Hojo, M. & Sokabe, M. Evaluation of extensional and torsional stiffness of single actin filaments by molecular dynamics analysis. *J. Biomech.* **43,** 3162–3167 (2010).

Mattheyses, A. L., Simon, S. M. & Rappoport, J. Z. Imaging with total internal reflection fluorescence microscopy for the cell biologist. *J. Cell Sci.* **123,** 3621–3628 (2010).

Meng, W., Mushika, Y., Ichii, T. & Takeichi, M. Anchorage of microtubule minus ends to adherens junctions regulates epithelial cell-cell contacts. *Cell* **135,** 948–959 (2008).

Milos Spasic, Koichiro Maki, Florian A. Herzog & Christopher R. Jacobs, "Effects of Mechanical Stress on Cells", Comprehensive biomaterials – Edition II, in press.

Mitsui, K., Hara, M. & Ikai, A. Mechanical unfolding of α2-macroglobulin atomic force microscope. *FEBS Lett.* **385,** 29–33 (1996).

Miyoshi, H. & Adachi, T. Topography design concept of a tissue engineering scaffold for controlling cell function and fate through actin cytoskele*t*al modulation. *Tissue Eng. Part B Rev.* **20,** 609–627 (2014).

Neuman, K. K. C. & Nagy, A. Single-molecule force spectroscopy: optical tweezers, magnetic tweezers and atomic force microscopy. *Nat. Methods* **5,** 491–505 (2008).

Nishimura, T., Honda, H. & Takeichi, M. Planar cell polarity links axes of spatial dynamics in neural-tube closure. *Cell* **149,** 1084–1097 (2012).

Okuda, S., Inoue, Y., Eiraku, M., Sasai, Y. & Adachi, T. Reversible network reconnection model for simulating large deformation in dynamic tissue morphogenesis. *Biomech. Model. Mechan.* **12,** 627–644 (2013).

Pappas, D. J. & Rimm, D. L. Direct interaction of the C-terminal domain of alpha-catenin and F-actin is necessary for stabilized cell-cell adhesion. *Cell. Commun. Adhes.* **13,** 151–170 (2006).

Pittet, P., Lee, K., Kulik, A. J., Meister, J. J. & Hinz, B. Fibrogenic fibroblasts increase intercellular adhesion strength by reinforcing individual OB-cadherin bonds. *J. Cell Sci.* **121,** 877–886 (2008).

Popa, I., Kosuri, P., Alegre-Cebollada, J., Garcia-Manyes, S. & Fernández, J. M. Force dependency of biochemical reactions measured by single-molecule force-clamp spectroscopy. *Nat. Protoc.* **8,** 1261–1276 (2013).

Rangarajan, E. S. & Izard, T. The cytoskeletal protein α-catenin unfurls upon binding to vinculin. *J. Biol. Chem.* **287,** 18492–18499 (2012).

Rauzi, M., Lenne, P. F. & Lecuit, T. Planar polarized actomyosin contractile flows control epithelial junction remodelling. *Nature* **468,** 1110–1114 (2010).

Reck-Peterson, S. L., Derr, N. D. & Stuurman, N. Imaging single molecules using total internal reflection fluorescence microscopy (TIRFM). *Cold Spring Harb Protoc.* **5,** 1–12 (2010).

Rief, M., Gautel, M., Oesterhelt, F., Fernandez, J. M. & Gaub, H. E. Reversible unfolgind of individual titin immunoglobulin domains by AFM. *Science* **276,** 1109–1112 (1997).

Sheikh, F., Chen, Y., Liang, X., Hirschy, A., Stenbit, A. E., Gu, Y., Dalton, N. D., Yajima, T., Lu, Y., Knowlton, K. U., Peterson, K. L., Perriard, J. C. & Chen, J. αE-catenin inactivation disrupts the cardiomyocyte adherens junction, resulting in cardiomyopathy and susceptibility to wall rupture. *Circulation* **114,** 1046–1055 (2006).

Shibata, M., Yamashita, H., Uchihashi, T., Kandori, H. & Ando, T. High-speed atomic force microscopy shows dynamic molecular processes in photoactivated bacteriorhodopsin. *Nat. Nanotech.* **5,** 208–212 (2010).

Sokabe, M., Sachs, F. & Jing, Z. Q. Quantitative video microscopy of patch clamped membranes stress, strain, capacitance, and stretch channel activation. *Biophys. J.* **59,** 722–728 (1991).

Stirnemann, G., Giganti, D., Fernandez, J. M. & Berne, B. J. Elasticity, structure, and relaxation of extended proteins under force. *Proc. Natl. Acad. Sci. U. S. A.* **110,** 3847–3852 (2013).

Takeichi, M. Dynamic contacts: rearranging adherens junctions to drive epithelial

remodelling. *Nat. Rev. Mol. Cell Biol.* **15,** 397–410 (2014).

Takeichi, M. The cadherins: cell-cell adhesion molecules controlling animal morphogenesis. *Development* **102,** 639–655 (1988).

Taniguchi, K., Maeda, R., Ando, T., Okumura, T., Nakazawa, N., Hatori, R., Nakamura, M., Hozumi, S., Fujiwara, H. & Matsuno, K. Chirality in planar cell shape contributes to left-right asymmetric epithelial morphogenesis. *Science* **333,** 339–341 (2011).

Uchihashi, T., Iino, R., Ando, T. & Noji, H. High-speed atomic force microscopy reveals rotary catalysis of rotorless F1-ATPase. *Science* **333,** 755–758 (2011).

Valle-Orero, J., Eckels, E. C., Stirnemann, G., Popa, I., Berkovich, R. & Fernandez, J. M. The elastic free energy of a tandem modular protein under force. *Biochemical and Biophysical Research Communications* **460,** 434-438 (2015).

Vasioukhin, V., Bauer, C., Degenstein, L., Wise, B. & Fuchs, E. Hyperproliferation and defects in epithelial polarity upon conditional ablation of α-catenin in skin. *Cell* **104,** 605–617 (2001).

Wang, Y. C., Khan, Z., Kaschube, M. & Wieschaus, E. F. Differential positioning of adherens junctions is associated with initiation of epithelial folding. *Nature* **484,** 390–393 (2012).

Waterman-Storer, C. M., Salmon, W. C. & Salmon, E. D. Feedback interactions between cell-cell adherens junctions and cytoskeletal dynamics in newt lung epithelial cells. *Mol. Biol. Cell* **11,** 2471–2483 (2000).

Wen, K. K., Rubenstein, P. A. & DeMali, K. A. Vinculin nucleates actin polymerization and modifies actin filament structure. *J. Biol. Chem.* **284,** 30463–30473 (2009).

Yamada, S., Pokutta, S., Drees, F., Weis, W. I. & Nelson, W. J. Deconstructing the cadherin-catenin-actin complex. *Cell* **123,** 889–901 (2005).

Yap, A. S., Gomez, G. A. & Parton, R. G. Perspective adherens junctions revisualized: organizing cadherins as nanoassemblies. *Dev. Cell* **35,** 12–20 (2015).

Yildiz, A., Tomishige, M., Vale, R. D. & Selvin, P. R. Kinesin walks hand-over-hand. *Science* **303,** 676–678 (2004).

Yonemura, S. A mechanism of mechanotransduction at the cell-cell interface:

Emergence of α-catenin as the center of a force-balancing mechanism for morphogenesis in multicellular organisms. *BioEssays* **33,** 732–736 (2011).

Yonemura, S., Wada, Y., Watanabe, T., Nagafuchi, A. & Shibata, M. α-Catenin as a tension transducer that induces adherens junction development. *Nat. Cell Biol.* **12,** 533–542 (2010).

Zhong, Q., Inniss, D., Kjoller, K. & Elings, V. B. Fractured polymer/silica fiber surface studied by tapping mode atomic force microscopy. *Surf. Sci.* **290,** 688–692 (1993).

Zhuang, X. & Rief, M. Single-molecule folding. *Curr. Opin. Struc. Biol.* **13,** 88–97 (2003).

Chapter 2

β-Catenin as a Tension Transmitter

2.1 Introduction

Adherens junctions form a link between cytoskeletal actin filaments in adjacent cells and transmit the intercellular force (Tepass, 2002; Harris and Tepass, 2010). Component molecules, such as cadherin (a transmembrane protein involved with cell–cell adhesion), β-catenin, α-catenin (a cytoplasmic protein that plays a role as a tension-sensor in maturation of adherens junctions (Yonemura *et al*., 2010)), and EPLIN (Cherbin-Petinot *et al*., 2012), directly bind together serially in this order to interact with the force-generating actin cytoskeleton. The intercellular tension frequently fluctuates depending on the cell arrangement within the tissue and myosin activities within individual cells. Therefore, adherens junctions and their component molecules are frequently exposed to high tension between cells (Miyake *et al*., 2006; Thiery *et al*., 2012). To control unbalanced forces, α-catenin at adherens junctions adaptively matures (Yonemura *et al*., 2010), and during this process, mechanical behaviors of components of adherens junctions would be a key factor in determining the characteristics of this mechano-feedback mechanism (Kobielak and Fuchs, 2004; Choi *et al*., 2012).

2.1 Introduction

β-Catenin, another important component of adherens junctions, functions as a direct linker between cadherin and α-catenin and contains armadillo (ARM) repeats in its central region (138–664 amino acids) forming a superhelical spiral structure (Xing *et al*., 2008; Huber and Weis, 2011). Such unique spiral structures play a role as tension transmitters and are found in Ankyrin (ANK) repeats with a similar superhelical spiral protein in hair cells, exhibiting low stiffness under low tension and high stiffness under high tension for mechanotransduction (Lee *et al*., 2006). A previous single-molecule experiment showed a high mechanical stability of β-catenin when subjected to a high force (Ritco-Vonsovici *et al*., 2007), while the other experiment suggested that β-catenin unfolds under tension with low mechanical stability (Valbuena *et al*., 2012). Therefore, we considered that it is possible that the mechanical behaviors of β-catenin vary in experimental conditions such as solvent compounds, pH, and temperature.

In the present study, we aimed to elucidate the mechanical behaviors of β-catenin as a possible tension transmitter at adherens junctions (Maki *et al,* 2015). We employed AFM nano-tensile testing by directly loading single molecules (Rief al., 1997). We adopted a similar rate of loading as that used in previous studies (Ritco-Vonsovici *et al*., 2007; Valbuena *et al*., 2012) for comparison, although the rate would not necessarily match up with the *in vivo* condition. We performed two types of experiments, in which a part and a whole structure of β-catenin were loaded under tension. To apply the force to a part of β-catenin, single-tagged (N-terminus GST-tagged) β-catenin was introduced to experiments, where N-terminus GST-tag and solvent-exposed amine residues widely dispersed in ARM repeats were targeted. In addition, to load the full component of β-catenin by both its ends, double-tagged [N-terminus GST-tagged and C-terminus His-tagged] β-catenin was introduced.

2.2 Materials and Methods

2.2.1 Materials

The N-terminal domain of β-catenin directly associates with α-catenin, and the central ARM repeats interact with the cytoplasmic domain of cadherin, as shown in Fig. 2-1a. To analyze the mechanical behavior of β-catenin as a tension transmitter at adherens junctions, we used two types of β-catenin fusion proteins, i.e., single-tagged and double-tagged human full-length β-catenin. Single-tagged β-catenin, as shown in Fig. 2-1b, purchased from Abnova Corporation, was used in the AFM nano-tensile testing, where the GST tag and the solvent-exposed lysine residues were targeted. Using single-tagged β-catenin, we targeted 26 lysines in the whole structure, of which 20 lysines were widely dispersed in ARM repeats. In addition, double-tagged β-catenin, as shown in Fig. 2-1c, was used in nano-tensile testing, where GST and His tags at both termini were targeted for modification processes of the AFM tip and the substrate. The plasmid DNA of double-tagged β-catenin was cloned into pGex6pl-7his and transformed into *E-coli* BL21-D3-pLysS. Double-tagged β-catenin was expressed overnight using 0.1 mM isopropyl β-D-1-thiogalactopyranoside (IPTG) induction at 20°C and purified with GST bulk kit (GE Healthcare Biosciences). Using double-tagged β-catenin, we were able to load full-length β-catenin including, all 12 ARM repeats.

For chemical modification of silicon nitride AFM tips and cover slips, surface treatment agents, i.e., (3-aminopropyl) triethoxysilane (APTES; Sigma-Aldrich Co., LLC) (Madox and Jenkins, 1987) and (3-mercaptopropyl)-trimethoxy-silane (MPTMS; Sigma-Aldrich Co., LLC) were utilized. N-hydroxylsuccinimide-polyethylene glycol-N-hydroxylsuccinimide (NHS-PEG-NHS, NANOCS Inc.; M.W., 3.4 kDa), maleimide-polyethylene glycol-N-hydroxylsuccinimide (Mal-PEG-NHS, NANOCS Inc.; M.W., 3.4 kDa) and N-(6-maleimidocaproyloxy)sulfosuccinimide (Sulfo-EMCS, DOJINDO Lab.) were also utilized.

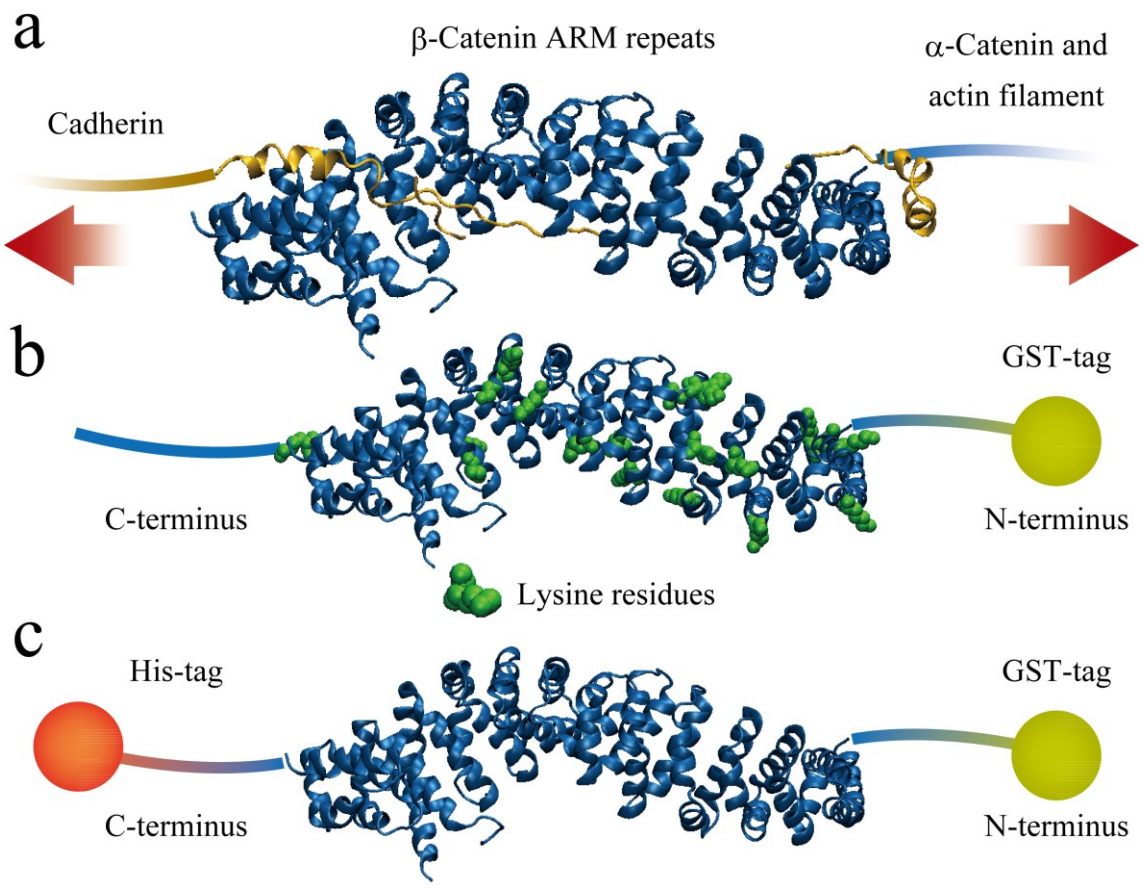

Figure 2-1: Schematic of β-catenin subjected to intercellular tension and β-catenin fusion proteins. **a.** The interaction condition between the cytoplasmic domain of cadherin and β-catenin. The N-terminus of β-catenin directly interacts with α-catenin and is exposed to tension generated by the actomyosin contraction. **b.** Single-tagged [N-terminus GST-tagged] β-catenin with lysine residues (green) exposed to the solvent. The yellow sphere indicates the GST tag. **c.** Double-tagged [N-terminus glutathione-S-transferase (GST)-tagged and C-terminus His-tagged] full-length β-catenin. The orange sphere indicates the His tag.

2.2.2 Chemical modification

For AFM nano-tensile testing of β-catenin in the two loading methods, as illustrated in Fig. 2-2, AFM tip and cover slips were chemically modified for each experiment. The silicon nitride AFM cantilever (OMCL-TR400PSA-1, Olympus Co.; spring constant, 0.02 N/m) was used for measuring piconewton order small forces (Popa *et al*., 2013). The AFM tip was washed with Milli-Q water (EMD Millipore Co.), oxidized using ozone cleaner, and treated with 2% APTES in 99.5% ethanol for 15 min. It was then treated with 5 mM NHS-PEG-Mal ester for 30 min and with 10 mM glutathione for 1 h. β-Catenin (1 μg/mL) was modified on the AFM tip using glutathione-GST affinity binding (Habig *et al*., 1974) for 2 h. Finally, the unreacted maleimide groups were blocked using 0.1% ethanethiol (Sigma-Aldrich Co., LLC) in phosphate-buffered saline (PBS) for 5 min. All reactions were performed at 27ºC.

To modify the substrate, a cover glass was washed with Milli-Q water, oxidized, and treated with 2% MPTMS in 99.5% ethanol for 15 min. In single-tagged β-catenin experiments (left panel in Fig. 2-2), the APTES cover slip was treated with 5 mM NHS-PEG-NHS for 30 min and washed with PBS. In double-tagged β-catenin experiments (right panel in Fig. 2-2), the substrate was treated with 0.4 mM maleimide-C3-NTA (Mal-C3-NTA; DOJINDO Lab.) for 1 h, with 10 mM $NiCl_2$ (Wako Pure Chemical Industries) for 30 min, followed by washing with PBS.

In our experimental settings, there could be nonspecific linkages between 1) the AFM tip and the substrate and 2) the PEG linker and the substrate. To distinguish the force responses of β-catenin with nonspecific linkages, we performed control experiments 1) without β-catenin and 2) without PEG linker. For experiments without β-catenin, we modified the AFM tip and the substrate in the same process, except without β-catenin. For the experiment without PEG linker, we used 1 mM Sulfo-EMCS instead of Mal-PEG-NHS for modifying the AFM tip.

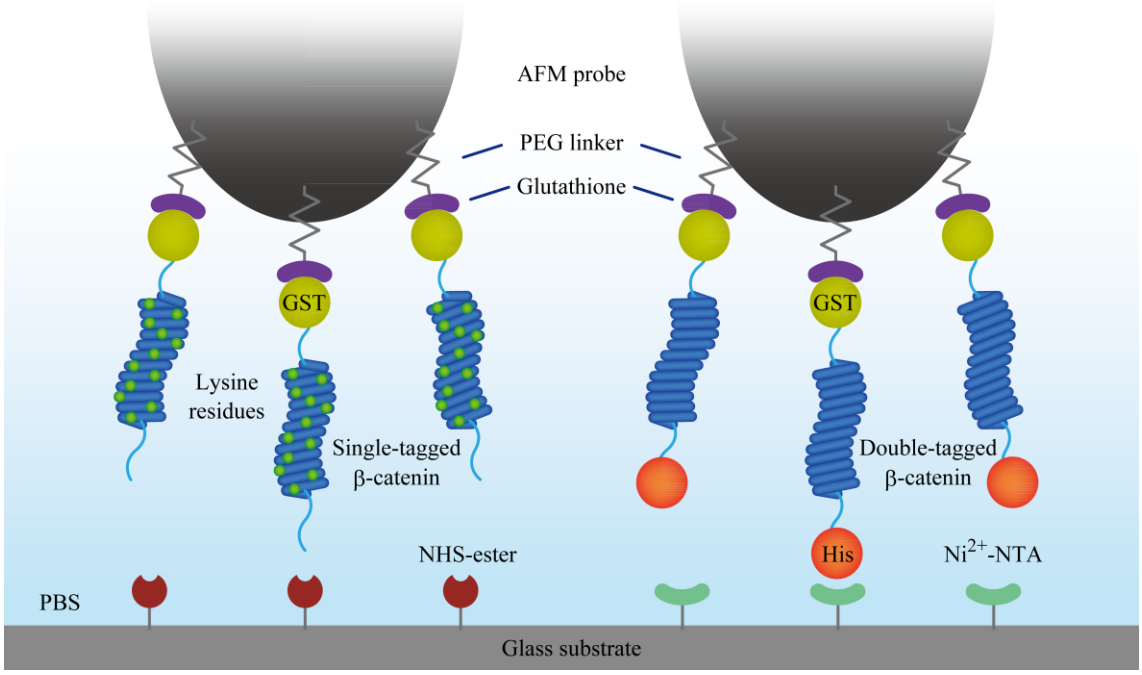

Figure 2-2: Schematics of AFM nano-tensile testing. Single-tagged (left) and double-tagged (right) β-catenin molecules modified on the AFM tip by the interaction between glutathione and the GST tag at the N-terminus. The AFM tip was then placed in contact with the substrate to allow interaction between 1) lysine residues and NHS-ester for single-tagged β-catenin and 2) the His tag at the C-terminus and Ni^{2+}-NTA for double-tagged β-catenin. Finally, the AFM tip was moved upward and the β-catenin molecules were directly loaded.

2.2.3 AFM nano-tensile testing for β-catenin

Mechanical behaviors of a part or a whole structure of β-catenin molecules were examined by AFM using a Nanowizard III BioAFM (JPK Instruments, Berlin, Germany) was used for the β-catenin nano-tensile testing. The spring constant of each

AFM cantilever was calibrated using the energy equipartition theorem. The AFM nano-tensile testing of β-catenin was conducted in PBS (pH 7.4). The double-tagged β-catenin-modified AFM tip was approached at a speed of 0.2 μm/s and it was in contact with the cover slip for 5 s to facilitate the binding of the C-terminus histidine tag of β-catenin and the substrate Ni^{2+} nitrilotriacetic acid (Ni^{2+}-NTA). The single-tagged β-catenin-modified AFM tip was approached in the same manner to facilitate binding of the external amino group of β-catenin with the NHS ester. We targeted 20 lysine residues, which were exposed to the solvent in ARM repeats (Ying *et al*., 2008) (green spheres, left panel in Fig. 2-2) and applied tensile force to various numbers of ARM-repeats. The tip was then retracted at the same speed. To verify the elasticity of β-catenin under low tension, we performed a loading–unloading experiment. The retraction of β-catenin from the substrate was prevented by a gradual reduction of the piezo-moving distance (d) to 50, 30, and 20 nm until the appearance of the unloading curve, taking into account the retract extension observed from results in the loading experiment. Force (F) versus d curves were obtained and converted into F versus β-catenin extension ΔL curves, referred to as the force curves, by subtracting the cantilever deflection from d.

2.2.4 Spring constants analysis

To quantify the mechanical properties of β-catenin under tension, we estimated the β-catenin spring constants k from the force curves. The spring constant k was determined as the average value of the tangent stiffness [$dF/d(\Delta L)$] (first-order derivatives of the force curve) in the specified linear region, as described below. Initially, the base line of the applied force was determined as the average value of force points after unbinding, and the base line of extension was determined where the smoothed force is 0 pN. Next the first- and second-order derivatives of the force curves [$dF/d(\Delta L)$ and $d^2F/d(\Delta L)^2$], respectively, were calculated. In the derivation process, each curve was smoothed using a simple moving average, where the number of datum points for the average was determined as 25 before and after the averaging point. Subsequently, the

linear region was specified, where the second order derivatives take values within the determined range of $-1 < d^2F/d(\Delta L)^2 < 1$. All parameters for calculation, such as the data points for the moving average and the second order derivatives range to determine linear regions, were set based on the correlation coefficient ($R^2 > 0.95$) between the force and linear regression curves. Finally, we calculated the spring constants k as the average of the first-order differentiated force in the linear region.

2.2.5 Statistical analysis

To confirm that the spring constants k of single-tagged and double-tagged β-catenin have different values, we used an F test, which verifies the hypothesis that two distributions have the same standard deviations σ_1 and σ_2. The spring constants of single-tagged (n = 66) and double-tagged (n = 34) β-catenin were compared by the F test ($p < 0.001$).

2.2.6 Polymer chain models

In our study, we analyzed the mechanical behaviors of β-catenin under high tension by fitting three polymer chain models to force curves: 1) freely jointed chain (FJC) model (Smith *et al*., 1992), 2) worm-like chain (WLC) model (Marco *et al*., 1995), and 3) two-state WLC model (Haverkamp *et al*., 2007).

The FJC model describes the relationship between the applied force F and extension ΔL expressing the entropy elasticity as

$$\Delta L = L\left[\coth\left(\frac{F \cdot b}{k_B T}\right) - \frac{k_B T}{F \cdot b}\right], \tag{2.1}$$

where k_B is the Boltzmann constant, T is temperature, b is the Kuhn length and L is the fully extended length.

The WLC model also describes the relationship between force and extension considering the bending energy of polymer chain as

$$F = \frac{k_{\mathrm{B}}T}{p}\left[\frac{1}{4}\left(1-\frac{\Delta L}{L_{\mathrm{c}}}\right)^{-2}+\frac{\Delta L}{L_{\mathrm{c}}}-\frac{1}{4}\right], \tag{2.2}$$

where p is the persistent length and L_{c} is the contour length.

Two-state WLC model is an advanced model of WLC considering the conformational transition of local structures from initial state to the other state. The force F is given by

$$F = \frac{k_{\mathrm{B}}T}{p}\left[\frac{1}{4}\left(1-\frac{\Delta L}{L_{\mathrm{c}}'}\right)^{-2}+\frac{\Delta L}{L_{\mathrm{c}}'}-\frac{1}{4}\right], \tag{2.3}$$

where L_{c}' is the contour length of two-state WLC model which extends under force F. The contour length L_{c}' is given by

$$L_{\mathrm{c}}' = L_{\mathrm{c0}} + n \cdot \Delta L_{\mathrm{s}} \cdot \gamma(F), \tag{2.4}$$

where L_{c0} is the contour length at initial state, n is the number of local structures, ΔL_{s} is the increase in extension for each local structure, and $\gamma(F)$ is the possibility of conformational transition of local structure that is given by

$$\gamma(F) = \left[1+\exp\left(\frac{\Delta G_{\mathrm{s}} - F \cdot \Delta L_{\mathrm{s}}}{k_{\mathrm{B}}T}\right)\right]^{-1}, \tag{2.5}$$

where ΔG_{s} is the free-energy change in conformational transition and the local structure breaks under the transition force F_{t}, which corresponds to the value of $\Delta G_{\mathrm{s}}/\Delta L_{\mathrm{s}}$. Force curves obtained in our experiments for single-tagged β-catenin were fitted by these three polymer chain models in least-square analysis.

2.3 Results

2.3.1 Nonlinear elastic behavior

As shown in Figs. 2-3a and 2-3b, the force curves obtained in AFM nano-tensile testing for single-tagged (green lines) and double-tagged (orange lines) β-catenin showed nonlinear behaviors during the loading process. Interestingly, the force curves showed linear regions initial extension, as shown in Fig. 2-3c. Nonspecific tethers with small rupture force F_R (<50 pN) were observed in the experiment without β-catenin, whereas specific tethers (F_R > 100 pN) were observed in the experiment without a PEG linker. These results indicated that our results were caused by β-catenin behaviors. Unlike double-tagged β-catenin, single-tagged β-catenin exhibited various spring constants k in linear regions caused by the variation of reacted amine residues of β-catenin. Under high tension, β-catenin behaved as a rather rigid material and was not fully unfolded, which was confirmed by the force curves without any tension relaxation before unbinding of the tip from the substrate and by the fact that maximum extensions were much shorter than the estimated extended full length of β-catenin (310 nm). In addition, nonlinear behavior was observed in the loading–unloading experiments using both single-tagged and double-tagged β-catenin, in which the loading (orange line) and unloading (blue line) curves were fully reversible, as shown in Fig. 2-3d. These results suggest that β-catenin plays a role as a nonlinear elastic material under tension.

2.3.2 Number of loaded molecules

To confirm that single β-catenin molecules were loaded, we evaluated the rupture force F_R, which was the peak value of F in the force curves, as shown in Fig. 2-3c. As shown in Fig. 2-4, the histogram of F_R in the single-tagged β-catenin experiment (green bar) exhibited two peaks (Odorico *et al*., 2007; Han *et al*., 2011). We fitted the histogram with a weighted mixture Gaussian distribution, where the number of distributions was

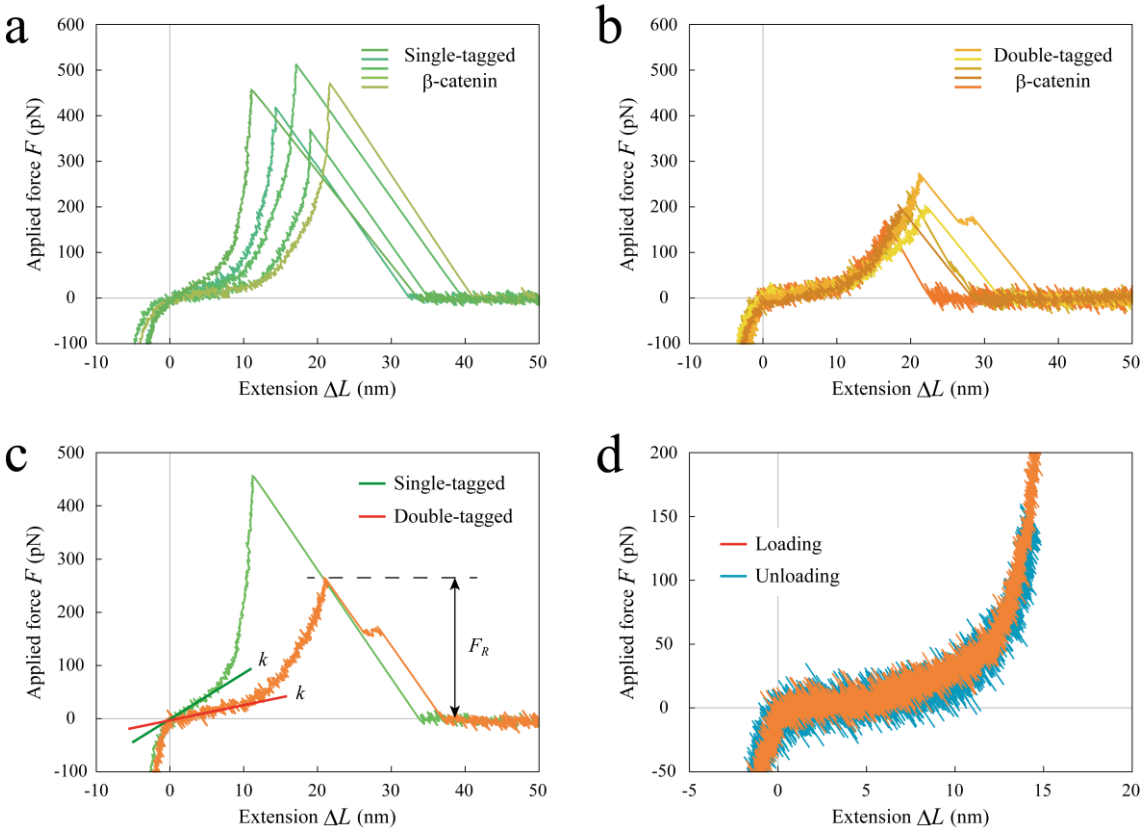

Figure 2-3: Results of AFM nano-tensile testing for β-catenin. **a and b.** Force curves for single-tagged (**a**, green line) and double-tagged (**b**, orange line) β-catenin. **c.** The rupture force F_R and initial spring constant k were analyzed. The orange and green linear lines indicate the linear regression curves in initial linear regions. **d.** Force curve obtained in loading (orange) and unloading (blue) double-tagged β-catenin experiments.

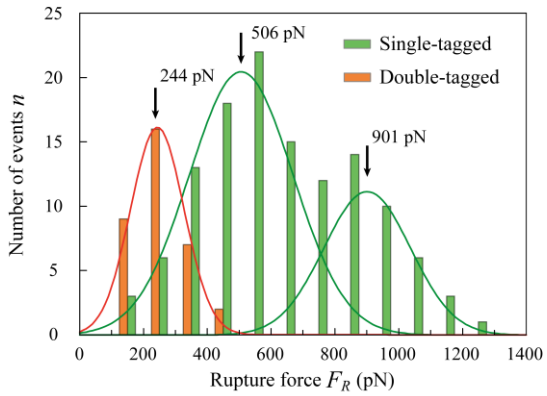

Figure 2-4: Histogram of F_R for single-tagged and double-tagged β-catenin.

determined so as to minimize the residual sum of squares with the condition that each constitutive distribution has a weight larger than 10%. The two peaks of the histogram indicated that the force curves were caused by single molecule (506 ± 163 (Mean ± S.D.) pN) and double molecule (901 ± 136 pN) β-catenin. The double-molecule force curves with high rupture force did not show significant increases in extension compared to single-molecule force curves, because they were bound to the substrate in a parallel way. In contrast, as depicted in Fig. 2-4, the histogram depicting F_R in the double-tagged β-catenin experiment (orange bar) exhibited a single peak representing the unbinding of a single NTA-Ni^{2+}-His bond, whereas a previous study suggested that the histogram exhibited three maximal peaks corresponding to single, double, and triple bonds because the His_6-tag contains up to three binding sites for NTA-Ni^{2+} (Verbelen *et al*., 2007). In our results, the force curves would reflect the mechanical behaviors of single molecule double-tagged β-catenin.

2.3.3 Spring constants

To quantify the mechanical properties of β-catenin, spring constants k in linear regions of the force curves were calculated. The force curves of single-tagged β-catenin were extracted, and the value of F_R was found to be 506 ± 192 pN (half width at half maximum of first peak) to evaluate the mechanical properties of single molecules. Spring constant k of the linear region was found to be 6.5 ± 3.0 pN/nm for single-tagged β-catenin and rather smaller values 3.9 ± 1.3 pN/nm for double-tagged β-catenin. The dispersion for single-tagged β-catenin (n = 66) was significantly larger than the corresponding dispersion for double-tagged β-catenin (n = 34) [F test ($p < 0.001$)], which was caused from the variation in reacted amines of single-tagged β-catenin, in other words, variation in the number of ARM repeats directly loaded. This result indicates that the spring constant k of β-catenin decreases according to the increasing number of ARM repeats. Such a property as a “nanospring” has been reported by Lee *et al*. (2006) on ANK repeats that form the same superhelical structure as ARM repeats.

2.3.4 Mechanical properties as a polymer chain

For analyzing the β-catenin behaviors under high tension, we fitted polymer chain models to the force curves of single-tagged β-catenin as shown in Fig. 2-5. Force curves (green line) were better explained by the simple WLC model (purple long-dashed line) than the FJC model (blue short-dashed line). In addition, we found that the two-state WLC model (red solid line), which considers the increase in the contour length caused by conformational transition from the initial state to the other state, showed the best fits to the force curves. The conformational transition from the initial state (red dotted line) occurred at high tension (F_t > 150 pN), whereas the increase in the contour length, ΔL_c, was 1–2 nm (from red dashed line to solid line, Fig. 2-5). These results indicated that β-catenin underwent minor conformational transition to more rigid state under high tension. The extended lengths in our experiments (~25 nm) were significantly shorter than the expected fully extended length (~304 nm), considering that the contour length of each amino acid is 0.4 nm. Our result indicated that β-catenin undergoes minor conformational transition and is not fully unfolded with high mechanical stability.

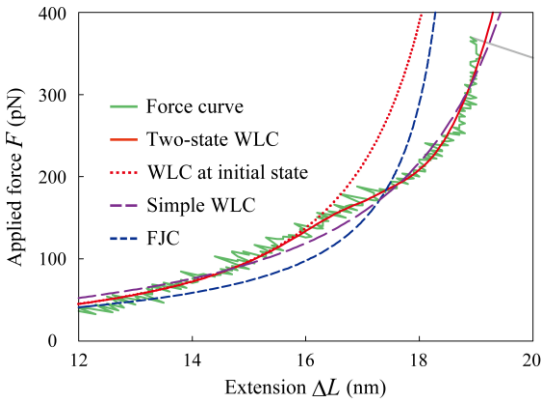

Figure 2-5: Results of curve fittings. Force curves (green line) were fitted by the two-state WLC model (red solid line), simple WLC model (purple long-dashed line), and FJC model (blue short-dashed line). The WLC curve at the initial state (red dotted line) was estimated from the result of fitting by the two-state WLC model.

2.4 Discussion

2.4.1 β-Catenin as a tension transmitter

Our experiments using AFM revealed the mechanical behaviors of β-catenin under tension at the molecular level. β-Catenin behaved as a nonlinear elastic material under tension with a linear response under low tension and a rather rigid response under high tension. In addition, such a nonlinear elastic behavior of β-catenin would correspond to the in vivo situation because the tension applied to β-catenin in our experiments is in the same range as the tension exerted on single actin filaments (Ishijima *et al*., 1996). We accordingly suggest that β-catenin functions as a flexible component that preserves links between constitutive molecules at adherens junctions under low tension, though acting as a rigid tension transmitter with high mechanical stability under high tension. Thus, β-catenin would contribute to regulating the intercellular force balance as a tension transmitter.

2.4.2 Mechanical behaviors of terminal regions

Here, we discuss the mechanical contribution of non-ARM domains to the function of β-catenin. The N-terminal domain (1–137 amino acids) of β-catenin directly associates with α-catenin, and the C-terminal domain (665–781 amino acids) does not interact with cadherin. Because both N- and C-terminal regions are unable to form stable structure by themselves (Huber *et al*., 1997; Huber and Weis, 2011), it is assumed that the non-ARM domains make no contribution in increasing the tension during the loading process. Moreover, in experiments using double-tagged β-catenin, we infrequently obtained the force curves that showed a certain extension without an increase in tension, caused by unstable non-ARM domains before load-bearing region with nonlinear behaviors. This result suggested that non-ARM domains exhibit extension, but do not play a significant mechanical role of β-catenin as a tension transmitter

2.4.3 Effects of environment on mechanical behaviors

In our study, AFM nano-tensile testing was performed for isolated β-catenin fusion proteins under slightly different conditions from physiological ones. For example, a previous report by Valbuena *et al*. suggested that the interaction between β-catenin and cadherin is essential for β-catenin to transmit intercellular tension with high mechanical stability. To examine the mechanical stability of β-catenin itself, we performed experiments for single-tagged β-catenin in 8 M urea–PBS, a protein solubilizing agent. The resulting force curves showed linear regions under low tension and rigid regions under high tension without tension relaxation, which corresponded well with the curves obtained in experiments without urea. This result is in agreement with the report (Huber *et al*., 1997) that showed ARM repeats structure of β-catenin conserved in 2.4 M urea. Furthermore, the report (uploaded to the Protein Data Bank under the PDB code 4EVT) showed that β-catenin treated by 8.3 M urea retains its ARM repeats structure. Therefore, experiments in urea confirmed the high mechanical stability of β-catenin.

The force range of molecular behaviors remains to be discussed. For the main results, the experiment was performed with a loading rate of 4000 pN/s. We also performed the experiments at a lower loading rate of 1000 pN/s, a rate similar to that in Valbuena's experiments, but unfolding events were not observed. Although we could not determine the exact reasons for the discrepancy in the results with the report, it could be because of the differences in the solvent compounds and testing temperature. The solvent compounds could affect the mechanical behaviors of proteins (Popa *et al*., 2013). In Valbuena's experiments, PBS buffer containing 5 mM dithiothreitol (DTT), which avoids aggregation, was used for 0.3–0.4 mg/mL β-catenin. In contrast, we used PBS buffer without any additional compounds for a lower concentration (1 μg/mL) of β-catenin. In addition, the testing temperature could affect the helix content of protein and its unfolding force (Law *et al*., 2003). Nevertheless, it is possible that there are undiscovered molecular mechanisms that clearly explain the discrepancy in the results. For example, a previous report (Ritco-Vonsovici *et al*., 2007) suggested that β-catenin

has various conformations in equilibrium. Obviously, other experimental methods that enable a low-loading-rate experiment, such as magnetic tweezers (Yao *et al*., 2014), are required to estimate the molecular behaviors under physiological conditions. In our study, we report one aspect of the function of β-catenin as a tension transmitter at adherens junctions.

2.4.4 Future prospects

In the present study, we showed the mechanical behaviors of β-catenin as a tension transmitter at intercellular adherens junctions, employing the method of AFM nano-tensile testing. This direct measurement of molecular behavior can offer new insights into force-induced dynamical mechanisms in multicellular systems. The high mechanical stability as exhibited by β-catenin could be a common mechanical property for some proteins, which also work under inter- or intracellular force. Since α-catenin, another component molecule, is activated to expose the cryptic signal binding site under tension, the high mechanical stability would be important to sustain the activated state.

2.5 Conclusion

In this chapter, we successfully examined the mechanical behaviors of β-catenin by employing AFM. We performed two types of experiments, in which a part and a whole structure of β-catenin were loaded under tension. The results of nano-tensile testing indicated that β-catenin behaves as a nonlinear elastic material under tension, i.e., a mechanical component with low stiffness under low tension and high stiffness under high tension. The nonlinear elastic behavior exhibited in our experiment suggests a mechanical function of β-catenin to serve as a tension transmitter at adherens junctions: 1) preserving links between component molecules under low tension and 2) transmitting high tension with high mechanical stability.

References

Chervin-Pétinot, A., Courçon, M., Almagro, S., Nicolas, A., Grichine, A., Grunwald, D., Prandini, M.H., Huber, P. & Gulino-Debrac, D. Epithelial protein lost in neoplasm (EPLIN) interacts with α-catenin and actin filaments in endothelial cells and stabilizes vascular capillary network in vitro. *J. Biol. Chem.* **287,** 7556–7572 (2012).

Choi, H. J., Pokutta, S., Cadwell, G. W., Bobkov, A. A., Bankston, L. A., Liddington, R. C. & Weis, W. I. αE-catenin is an autoinhibited molecule that coactivates vinculin. *Proc. Natl. Acad. Sci. U. S. A.* **109,** 8576–8581 (2012).

Habig, H. W., Pabst, J. M. & Jakoby, B. W. Glutathione S-Transferase: The first enzymatic step in mercapturic acid formation, *J. Biol. Chem.* **249,** 7130–7139 (1974).

Han, S. W., Mieda, S., Nakamura, C., Kihara, T., Nakamura, N. & Miyake, J. Successive detection of insulin-like growth factor-II bound to receptors on a living cell surface using an AFM. *J. Mol. Recogn.* **24,** 17–22 (2011).

Harris, T. J. C. & Tepass, U. Adherens junctions: from molecules to morphogenesis. *Nat. Rev. Mol. Cell Biol.* **11,** 502–514 (2010).

Huber, A. H., Nelson, W. J. & Weis, W. I. Three-dimensional structure of the armadillo repeat region of β-catenin. *Cell* **90:**871–882 (1997).

Huber, A. H. & Weis, W. I. The structure of the β-catenin/E-cadherin complex and the molecular basis of diverse ligand recognition by β-catenin. *Cell* **105,** 391–402 (2011).

Ishijima, A., Kojima, H., Higuchi, H., Harada, Y., Funatsu, T. & Yanagida, T. Multiple- and single-molecule analysis of the actomyosin motor by nanometer-piconewton manipulation with a microneedle: unitary steps and forces. *Biophys. J.* **70,** 383–400 (1996).

Kobielak, A. & Fuchs, E. α-Catenin: at the junction of intercellular adhesion and actin dynamics. *Nat. Rev. Mol. Cell Biol*. **5,** 614–625 (2004).

Law, R., Liao, G., Harper, S., Yang, G., Speicher, D. W. & Discher, D. E. Pathway Shifts and Thermal Softening in Temperature-Coupled Forced Unfolding of

Spectrin Domains. *Biophys. J.* **85,** 3286–3293 (2003)

Lee, G., Abdi, K., Jiang, Y., Michaely, P., Bennett, V. & Marszalek, P. E. Nanospring behaviour of ankyrin repeats. *Nature* **440,** 246–249 (2006).

Madox, H. P. & Jenkins, D. 3-Aminopropyltriethoxysilane (APES): a new advance in section adhesion, tissue patterns and morphogenesis, *J. Clin. Pathol.* **40,** 1256–1260 (1987)

Maki, K., Han, S. W. & Adachi, T. β-catenin as a tension transmitter revealed by AFM nanomechanical testing, *Cell Mol. Bioeng.* **8**, 14-21 (2015).

Marko, J. F. & Siggia, E. D. Stretching DNA. *Macromolecules* **28,** 8759–8770 (1995).

Miyake, Y., Inoue, N., Nishimura, K., Kinoshita, N., Hosoya, H. & Yonemura, S. Actomyosin tension is required for correct recruitment of adherens junction components and zonula occludens formation. *Exp. Cell Res.* **312,** 1637–1650 (2006).

Odorico, M., Teulon, J. M., Bessou, T., Vidaud, C., Bellanger, L., Chen, S. W., Quenmeneur, E., Parot, P. & Pellequer, J. L. Energy landscape of chelated uranyl: antibody interactions by dynamic force spectroscopy. *Biophys. J.* **93,** 645–654 (2007).

Popa, I., Kosuri, P., Alegre-Cebollada, J., Garcia-Manyes, S. & Fernandez, J. M. Force dependency of biochemical reactions measured by single-molecule force-clamp spectroscopy. *Nat. Protoc.* **8,** 1261–1276 (2013).

Rief, M., Gautel, M., Oesterhelt, F., Fernandez, J. M. & Gaub, H. E. Reversible unfolding of individual titin immunoglobulin domains by AFM. *Science* **276,** 1109–1112 (1997).

Ritco-Vonsovici, M., Ababou, A. & Horton, M. Molecular plasticity of β-catenin: New insights from single-molecule measurements and MD simulation. *Protein Sci.* **16,** 1984–1998 (2007).

Smith, S. B., Finzi, L. & Bustamante, C. Direct mechanical measurements of the elasticity of single DNA molecules by using magnetic beads. *Science* **258,** 1122–1126 (1992).

Haverkamp, R. G., Marshall, A. T. & Williams, M. A. K. Model for stretching elastic biopolymers which exhibit conformational transformations. *Phys. Rev. E* **95,**

021907 (2007).

Tepass, U. Adherens junctions: new insight into assembly, modulation and function. *BioEssays* **24,** 690–695 (2002).

Thiery, J. P., Engl, W., Viasnoff, V. & Dufour, S. Biochemical and biophysical origins of cadherin selectivity and adhesion strength. *Curr. Opin. Cell Biol.* **24,** 614–619 (2012).

Valbuena, A., Vera, A. M., Oroz, J., Menéndez, M. & Carrión-Vázquez, M. Mechanical properties of β-catenin revealed by single-molecule experiments. *Biophys. J.* **103,** 1744–1752 (2012).

Verbelen, C., Gruber, H. J. & Dufre, Y. F. The NTA–His_6 bond is strong enough for AFM single-molecular recognition studies. *J. Mol. Recogn.* **20,** 490–494 (2007).

Xing, Y., Takemaru, K. I., Liu, J., Berndt, J. D., Zheng, J. J., Moon, R. T. & Xu, W. Crystal structure of a full-length β-catenin. *Structure* **16,** 478–487 (2008).

Yao, M., Qiu, W., Liu, R., Efremov, A., Cong, P., Seddiki, R., Payre, M., Lim, C. T., Ladoux, B., Mège, R-M. & Yan, J. Force-dependent conformational switch of α-catenin controls vinculin binding, *Nat. Commun.* **5,** 4525 (2014).

Yonemura, S., Wada, Y., Watanabe, T., Nagafuchi, A. & Shibata, M. α-Catenin as a tension transducer that induces adherens junction development. *Nat. Cell Biol.* **12,** 533–542 (2010).

Chapter 3

Mechano-adaptive Conformational Change of α-Catenin

3.1 Introduction

A combination of contractile forces in individual cells drives tissue dynamics such as morphogenesis (Martin *et al*., 2010; Eiraku *et al*., 2011; Lecuit *et al*., 2011) and wound healing (Tamada *et al*., 2007). The cadherin-based adherens junctions function as direct links between the contractile actomyosin cytoskeletons of different cells (Harris and Tepass, 2010; Meng and Takeichi, 2009). Adherens junctions balance the intercellular tensions by the adaptive assembly of the cytoskeletal actin filaments (Miyake *et al*., 2006; Levayer, and Lecuit, 2013; Engl *et al*., 2014; Sato *et al*., 2015). In this mechano-adaptive mechanism, α-catenin, a tension-sensing component of adherens junctions, is critical regulator of vinculin (Lecuit, 2010; Yonemura, 2011; Kim *et al*., 2015), which recruits another actin filament to adherens junctions (Grashoff *et al*., 2010; Huvenerrs *et al*., 2012).

3.1 Introduction

The molecular mechanisms of the vinculin regulation by α-catenin have been investigated using various approaches. The molecular and cellular study of Yonemura *et al*. (2010) has revealed that α-catenin under intercellular tension exposes the cryptic VBS. The process is triggered by the release of the autoinhibited conformation caused by an intramolecular interaction between its M1 domain (residues 277-393) containing VBS (residues 325–360) and the vinculin-inhibitory M2-M3 domain (residues 391-631). The autoinhibited conformation has been determined in the crystallized α-catenin [PDB code: 4K1N] (Ishiyama *et al*., 2013), where the vinculin-binding surface of VBS is buried in the helix bundle of MI domain that is structurally stabilized by M2-M3 helix bundles. Single-molecule experiments using magnetic tweezers have suggested that the disruption of M1/M2-M3 interaction requires only approximately 5-pN tension (Yao *et al*., 2014), which is close to the range of forces generated by a single myosin molecule (Finer *et al*., 1994). Thereby, the M1/M2-M3 interaction holds the key to the mechanical activation of α-catenin, recruiting vinculin under tension.

However, α-catenin mechanically activated under tension faces a critical problem common to all tension-sensing proteins. Usually, an external force acts as a biomolecule denaturant (Obenhauser *et al*., 2001; Popa *et al*., 2013). A study (Liu *et al*., 2009) using AFM has reported a complete unfolding of a protein in approximately 30 s under low tension of approximately 13 pN. Furthermore, α-helical proteins such as α-catenin have lower mechanical stabilities than other β-sheet proteins (Hoffmann and Dougan, 2012). During the tension-sensing process, the helical conformation of VBS should be conserved to associate with vinculin (Choi *et al*., 2012). Thus, the most significant question is how does α-catenin, one of the tension-sensing proteins, retain its activated state while avoiding the successive unfolding under denaturing tension.

In Chapter 2, we revealed that β-catenin, another component of adherens junctions, exhibit extremely high mechanical stability to stably transmit intercellular tension. In this chapter, our objective is to verify a hypothesis that α-catenin under tension also exhibit high mechanical stability to sustain the activated intermediate state

(Maki *et al*., 2016). We investigated the mechanical behaviors of α-catenin by AFM nano-tensile testing (Lv *et al*., 2014; Goldmann *et al*., 2015; Maki *et al*., 2015). To compare the mechanical behaviors of α-catenin before and after the conformational change, we employes following two types of loading conditions: (A) direct loading and (B) loading with a holding period to wait for mechanical activation (Maki *et al*., 2016). We also compared the mechanical behaviors of α-catenin with that of talin, which is a well-known tension-sensor protein at focal adhesions (Maki *et al*., 2016).

3.2 Materials and Methods

3.2.1 Protein purification

DNA fragments of mouse wild type (WT) αE-catenin M1-M3 domain, mutated (MT) M1-M3 domain, M1 domain, and M2-M3 domain, as shown in Fig. 3-1a, were amplified by PCR and cloned into the pGEX6P-3 vector (GE Healthcare). The MT fragment, in which autoinhibiting M1/M2-M3 interaction is disrupted, behaved as an activated α-catenin that interacts with vinculin under no tension, as illustrated in Fig. 3-1b. The weakened M1/M2-M3 interaction causes a change in the angle between helix bundles M2 and M3 (Ishiyama *et al*., 2013) and the destabilization of helix bundle M1 (Li *et al*., 2015). All plasmids were verified by DNA sequencing and transformed into *E-coli* strain BL21Star (DE3) (Invitrogen) cells. Proteins were expressed at 20°C in Luria–Bertani medium containing 0.1 mM isopropyl-β-D-thiogalactopyranoside. Cells expressing αE-catenin were suspended in 20 mM Tris-HCl buffer (pH 8.0) containing 150 mM NaCl and disrupted by sonication. After ultracentrifugation, the supernatant was applied onto a Glutathione Sepharose 4B column (GE Healthcare). Eluted proteins were further purified by anion-exchange (HiTrap Q HP, GE Healthcare) and gel filtration (Superdex 200 pg, GE Healthcare) chromatography.

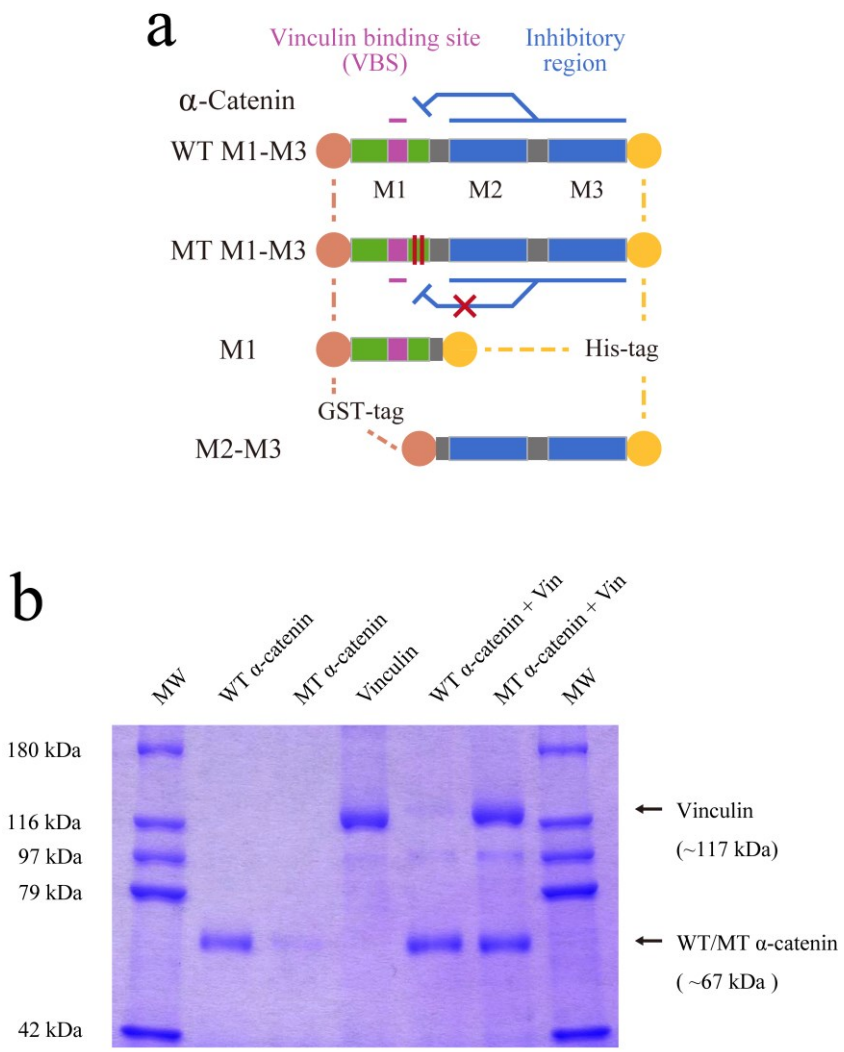

Figure 3-1: α-Catenin fragments and vinculin used in AFM nano-tensile testing. **a.** WT M1-M3 (residues 276–634), MT M1-M3 (M319G and R326E), M1 (residues 276–393), and M2-M3 (residues 385–634). **b.** Pull-down assay for α-catenin samples with vinculin. WT and MT (M319G and R326E) α-catenin M1-M3 fragments and full-length vinculin were mixed and incubated in solution and were applied to GST SpinTrap (GE Healthcare). After two times washing, α-catenin and vinculin were eluted together. Autoinhibited WT α-catenin did not show vinculin affinity. In contrast, vinculin associated with MT α-catenin, indicating that the mutations disrupted the autoinhibiting M1/M2-M3 interaction while conserving the vinculin binding affinity.

3.2.2 Chemical modification

For AFM nano-tensile testing a cover slip and AFM tip were treated using a chemical modification process (Popa *et al*., 2013). The cover slip was modified with α-catenin at its C-terminus and AFM tip was modified with glutathione, which interacts with N-terminal GST-tag of α-catenin. The cover slip was oxidized and treated with 2% MPTMS/ethanol for 15 min. The substrate was then treated with 2 mM maleimide-C3-NTA (Mal-C3-NTA; DOJINDO Lab.) /PBS for 30 min, with 10 mM $NiCl_2$ (Wako Pure Chemical Industries) /Milli-Q for 30 min, and washed with PBS. α-Catenin fragments (10 μM for each fragment) were modified by NTA-Ni^{2+}-His_6 affinity binding for 1 h and finally washed with working buffer (10 mM HEPES, 150 mM NaCl, pH 7.2). For the AFM nano-tensile testing of vinculin-associated α-catenin fragments, the α-catenin-modified substrate was further incubated with 1 μM full-length vinculin/PBS for 30 min and washed with working buffer. Silicon nitride AFM tip (OMCL-TR400PSA-1; spring constant, 0.02 N/m, Olympus Co.) was first oxidized using ozone cleaner and treated with 2% APTES/ethanol for 15 min. The tip was then treated with 1.5 mM Mal-PEG-NHS ester/PBS for 30 min and with 10 mM glutathione/PBS for 1 h. The remaining maleimide was quenched with 50 mM 2-mercaptoethanol/HEPES and finally washed with working buffer.

3.2.3 AFM nano-tensile testing for α-catenin

α-Catenin fragments modified on the cover slip at the C-terminus exploiting NTA-Ni^{2+}-His_6 affinity were loaded at the N-terminus using GST-GSH affinity. As shown in Fig. 3-2a, the autoinhibited WT M1-M3 fragment was examined in the following two types of loading conditions: (A) direct loading (orange line) and (B) loading with a holding period (magenta line) to wait for mechanical activation. As a result, we obtained force curves with multiple saw-tooth patters, as depicted in Fig. 3-2b, which are caused by multiple conformational transitions of α-catenin fragments during

unfolding process under tension. Based on the force curves, we calculated contour length L_c to identify intermediate states during unfolding and the measured peak unfolding force F_u to estimate the mechanical stabilities of the abovementioned α-catenin fragments.

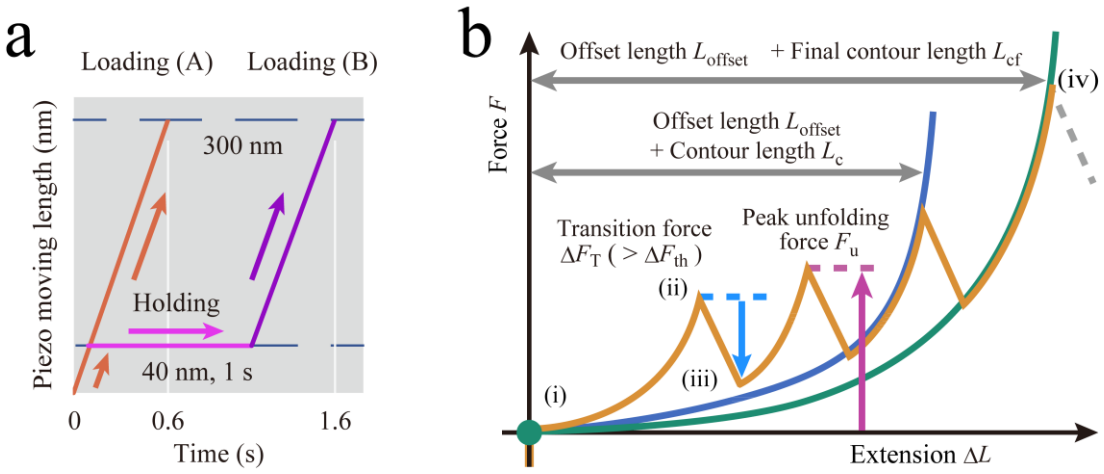

Figure 3-2: Methods for two types of loading and force curve analysis. **a.** Loading conditions (A) and (B). The piezo-actuator was moved upward by 300 nm at a constant speed of 500 nm/s ("Loading (A)" in this study, orange line). To analyze the mechanical behavior of WT M1-M3 after mechanical activation, we introduced a holding time of 1 s at 40 nm of constant piezo-moving length ("Loading (B)," orange (initial loading), magenta (holding), and purple (further loading)). **b.** Force curve analysis. First, the force curves with saw-tooth patterns [state (i) to (iv), orange curve] caused by single-molecule behaviors were identified, with the rupture force and final stiffness in the last peak [state (iv)]. Next, the offset length L_{offset} was determined by WLC-model fitting to the last peak (green curve) with the fixed final contour length L_{cf} [143.2 nm (WT/MT M1-M3), 46.8 nm (M1), and 99.6 nm (M2-M3)]. Finally, we measured the contour length L_c and peak unfolding force F_u at each force peak with transition force ΔF_T [state (ii) to (iii)] greater than the threshold ΔF_{th}.

3.2.4 Force curve analysis

In this chapter, we analyzed the force curves to understand the unfolding pathway of α-catenin molecules. The force curves corresponding to the single α-catenin molecules were extracted and their characteristics were analyzed using the in-house software, as illustrated in Fig. 3-2b. First, we extracted the force curves for completely extended single α-catenin molecules, based on the thresholds of force and stiffness at the rupture event, assuming an 85%-extended WLC model (Bustamante *et al*., 1994),

$$F(\Delta L) = \frac{k_{\mathrm{B}}T}{l_{\mathrm{pf}}}\left[\frac{1}{4}\left(1-\frac{\Delta L}{L_{\mathrm{cf}}}\right)^{-2}+\frac{\Delta L}{L_{\mathrm{cf}}}-\frac{1}{4}\right], \tag{3.1}$$

where k_{B} is the Boltzmann constant, T is temperature [300 K], l_{pf} is the final persistence length [0.4 nm] based on a previous report (Carrion-Vazquez *et al*., 1999). The final contour length L_{cf} was estimated as 143.2 nm (WT/MT M1-M3 domain), 46.8 nm (M1 domain), and 99.6 nm (M2-M3 domain) based on the number of residues. The threshold of the stiffness excluded the curves with low stiffness for aggregated molecules. For the extracted curves, we determined the length of offset L_{offset}, corresponding to PEG length (approximately 45 nm) and the tip curvature radius, by fitting WLC model allowing baseline offset as

$$F(\Delta L) = \frac{k_{\mathrm{B}}T}{l_{\mathrm{pf}}}\left[\frac{1}{4}\left(1-\frac{\Delta L}{L_{\mathrm{cf}}+L_{\mathrm{offset}}}\right)^{-2}+\frac{\Delta L}{L_{\mathrm{cf}}+L_{\mathrm{offset}}}-\frac{1}{4}\right], \tag{3.2}$$

to the final peak at the rupture event (green line in Fig. 3-2b), where L_{offset} was a fitting parameter. Finally, we identified the intermediate force peaks with the transition force ΔF_{T} (cyan arrow in Fig. 3-2b) based on the threshold ΔF_{th} (40 pN) and calculated the contour length L_{c} and the persistence length l_{p} by fitting WLC model with the determined L_{offset} to the force peaks as follows:

$$F(\Delta L) = \frac{k_{\mathrm{B}}T}{l_{\mathrm{p}}}\left[\frac{1}{4}\left(1 - \frac{\Delta L}{L_{\mathrm{c}} + L_{\mathrm{offset}}}\right)^{-2} + \frac{\Delta L}{L_{\mathrm{c}} + L_{\mathrm{offset}}} - \frac{1}{4}\right], \qquad (3.3)$$

by considering that the PEG linker, without any substructures, can be fully unfolded at each intermediate state. To analyze the mechanical stabilities for intermediate states, we measured peak unfolding force F_{u} (magenta arrow in Fig. 3-2b). We adopted lower ΔF_{th} (20 pN) to detect the force peaks caused by unfolding of unstable substructures.

3.2.5 Number density of force peaks

Based on scatter plots of peak unfolding force F_{u} versus contour length L_{c}, we evaluated the number density n_{d} (L_{c}, F_{u}) of force peaks per curve by taking the product of the average number of force peaks per one curve N and the probability density P (L_{c}, F_{u}) calculated using two-variable Gaussian distribution function as

$$P(L_{\mathrm{c}}, F_{\mathrm{u}}) = \frac{\sum_k g(L_{\mathrm{c}}, F_{\mathrm{u}}, L_{ck}, F_{\mathrm{u}k})}{\sum_k [\iint g(L_{\mathrm{c}}, F_{\mathrm{u}}, L_{ck}, F_{\mathrm{u}k}) dL_{\mathrm{c}} dF_{\mathrm{u}}]}, \qquad (3.4)$$

where

$$g = \frac{1}{2\pi\sigma_L\sigma_F}\exp\left\{-\frac{1}{2}\left[\frac{(L_{\mathrm{c}} - L_{ck})^2}{{\sigma_L}^2} + \frac{(F_{\mathrm{u}} - F_{\mathrm{u}k})^2}{{\sigma_F}^2}\right]\right\}, \qquad (3.5)$$

in which the summation for k meant the summation for all scattered data points.

3.2.6 AFM structural imaging

Molecular conformations of α-catenin fragments and vinculin were examined by AFM structural imaging. We employed the tapping mode by using AFM cantilevers with high resonance frequency (BL-AC40TS-C2; spring constant, 0.1 N/m; resonance frequency,

110 kHz; radius of tip, < 7 nm; Olympus Co.). Below are the methods for sample preparation, AFM imaging, and data analysis.

The fresh mica surface was achieved by cleaving the top surface of Muscovite mica disc (φ, 9.5 mm; ALLIANCE Biosystems) by tape and washed by 20 mM Tris-HCl buffer (pH 8.0). α-Catenin and vinculin (1 nM) in the working buffer were placed on the mica for 1 h at room temperature. The solution were removed and gently washed by the working buffer for three times. Finally, we placed the 50 μL of working buffer. The AFM structural imaging was conducted by the tapping mode for soft protein samples. We performed the measurement with the drive frequency of ~26 kHz for the scan range of 1 μm x 1 μm (512 pixels x 512 pixels). The obtained images were first processed by the JPK SPM Data Processing Software. The tilt of mica was calibrated by subtracting the polynomial line fitting from each scan line, in which we used the data of which height are in bottom 70 % so that molecular aggregates with extraordinary large height are not considered for fitting. The height values between pixels were finally interpolated by a bicubic method.

3.3 Results

3.3.1 Mechano-adaptive conformational change

WT M1-M3 domain in loading (A) unfolded each domain under tension. To analyze the stochastic unfolding trajectories from obtained force curves as shown in Fig. 3-3a, we evaluated the number density of force peaks, n_d (L_c, F_u) on the basis of scatter plots of F_u versus L_c. The contour map of the number density n_d showed three wide horizontal regions with similar intervals, as shown in Fig. 3-3b. The low n_d in the initial region (green line) indicated that the weak helix bundle of M1 unfolded easily, with infrequent force peaks. However, the last two regions (blue lines) with high n_d, i.e., with

frequent force peaks, corresponded to two stable helix bundles of M2-M3 domain. These results indicated that M1-M3 domain unfolding depended on the mechanical stability of their helix bundles under direct loading.

However, WT M1-M3 domain in loading (B) showed force peaks within a rather greater force range, as depicted in Fig. 3-3c, and the contour map of n_d showed greater peak unfolding force F_u, as shown in Fig. 3-3d, than those in loading (A) (Fig. 3-3b). This result indicated that the conformation of M1-M3 domain changed to another intermediate state that required higher tension for further unfolding. As the peak unfolding force F_u increased along the entire contour length L_c (Fig. 3-3d), the conformational change must have occurred at all three helix bundles M1-M3. The contour map showed a specific peak at L_c of approximately 45.4 nm (arrow in Fig. 3-3d); the net extension was approximately 19.0 nm, <40% of completely extended length of M1 domain. This observation suggested that VBS in M1 domain was conserved in this region. During the holding time, the force relaxation curve showed stepwise relaxations (Fig. 3-4a), implying dynamic transitions in the M1-M3 conformation. The force distribution at the beginning (0 s) of the holding time settled into a narrow distribution approximately 10 pN at the end of this period as shown in Fig. 3-4b, showing that the M1-M3 conformation finally equilibrated under low tension. We suggest that M1/M2-M3 interaction was partly diminished during the holding time; the average extension of approximately 2.8 nm in the holding period was longer than the reported extension (Li *et al*., 2015) that was approximately 1.0 nm for the mechanical activation of M1-M3 domain. The probability density of the force peaks in loading (B) in the initial extension was lower than that in loading (A), as shown in Fig. 3-4c, which supported this suggestion. Thus, we revealed that M1-M3 domain of α-catenin adaptively changes the conformation to another stable state under low tension, with weakened M1/M2-M3 interaction.

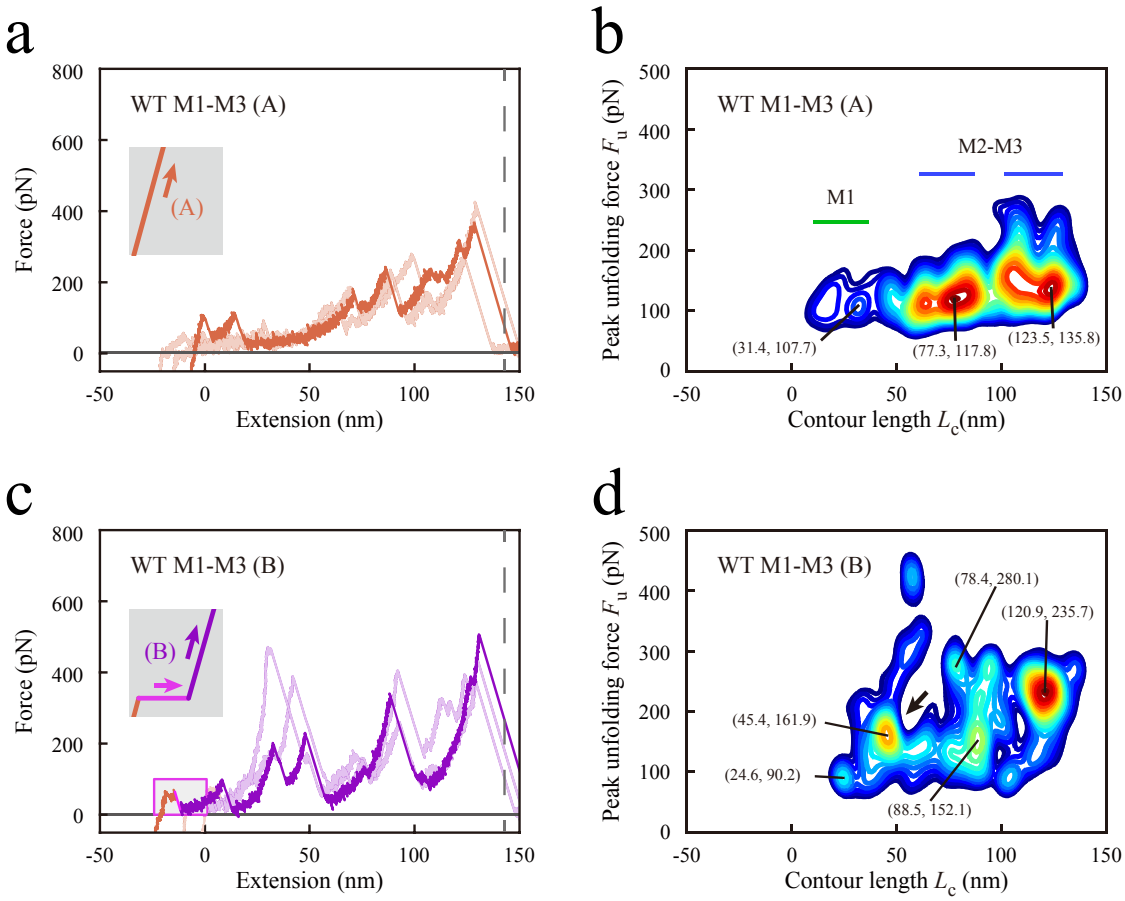

Figure 3-3: Results of AFM nano-tensile testing for WT M1-M3 domain in loading (A) and (B). **a.** Force curves for WT M1-M3 fragment in loading (A). The force curves are shifted to the left by the offset length L_{offset}. **b.** Contour map of number density n_d of force peaks in loading (A) based on 797 force curves. Color contours are set from the maximum value of n_d (red) to 0.4 × the value (blue). **c.** Force curves in loading (B). **d.** Contour map in loading (B) based on 514 force curves.

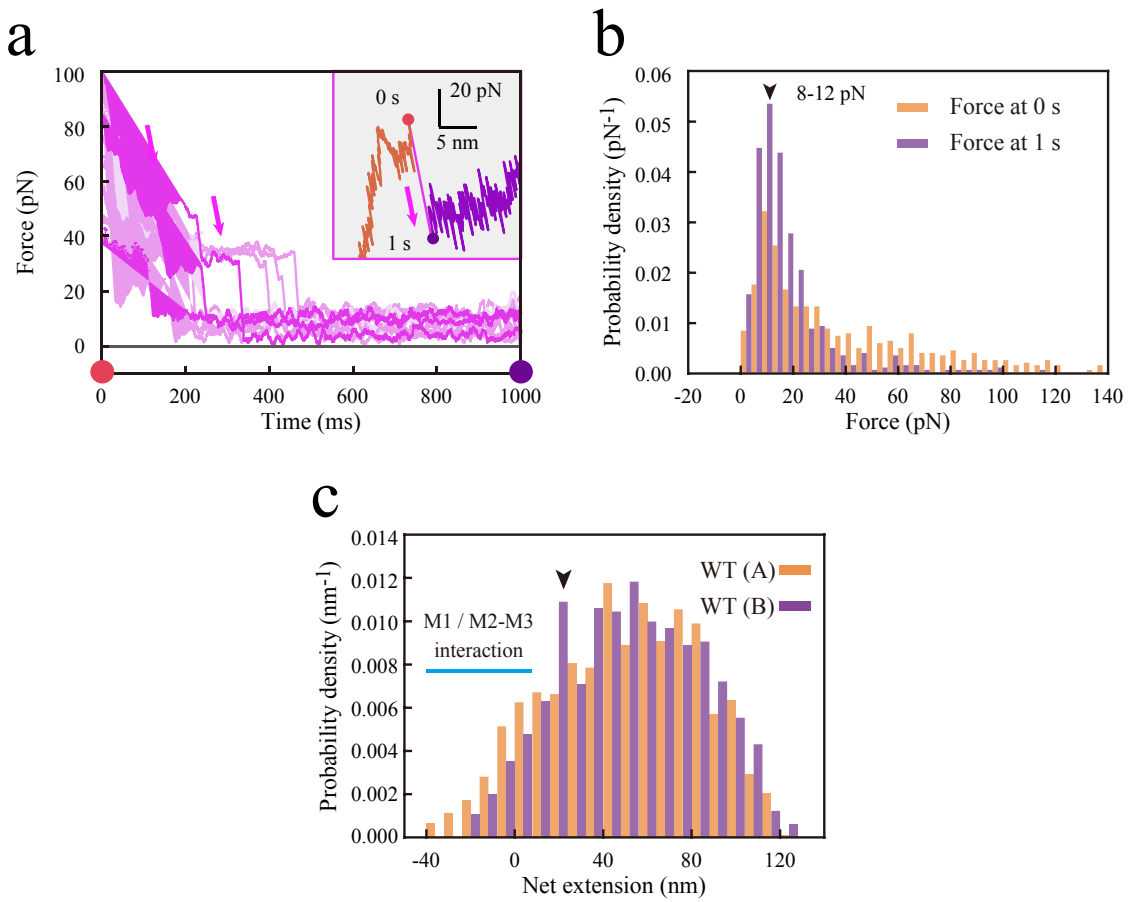

Figure 3-4: Conformational change in holding time. **a.** Force relaxation curve during the holding time. **b.** The probability density of force at 0 s (orange bars) and 1 s (purple bars) during the holding time. **c.** Histograms of the net extension of WT M1-M3 in loading (A) (orange bars) and loading (B) (purple bars). The arrowhead shows the salient peak in loading (B) corresponding to the peak indicated in the contour map. In the initial extension, the probability density in loading (B) was lower than that in loading (A), indicating that the M1/M2-M3 interaction was partly diminished during the holding time in loading (B).

3.3.2 Intramolecular interaction as a molecular switch

To elucidate the conformational changes in the M1-M3 domain with weakened M1/M2-M3 interaction, we examined the MT M1-M3 fragment, of which force curves are shown in Fig. 3-5a. The contour map for MT M1-M3 domain showed two specific regions (L_c = 19.4 nm and 37.6 nm, arrowheads in Fig. 3-5b). The regions had greater peak unfolding forces F_u (146.8 pN and 141.0 pN) than those for WT in loading (A), as shown in Fig. 3-5c. Moreover, the number densities n_d in these regions were higher than those in WT (arrowheads, the side view of n_d distribution in Fig. 3-5c). Furthermore, in the later region (50 nm < L_c < 150 nm), two separate regions observed in WT M1-M3 domain (blue lines, upper part of Fig. 3-5c) fused into one broad region in MT (lower part). This observation indicated that M2-M3 domain changed its conformation because of weakened M1/M2-M3 interaction. The result for MT M1-M3 domain indicated that weakened M1/M2-M3 interaction triggers the changes in M1-M3 conformation.

Individual M1 and M2-M3 domains, of which force curves are shown in Figs. 3-6a and 3-6b, exhibited one and two regions in the contour maps, as shown in Fig. 3-6c. As depicted in Fig. 3-6d, the n_d values were higher than those for M1-M3 fragments, indicating that M1 and M2-M3 domains settled into an innate stable state without interacting with each other. In particular, the peak unfolding force for the M1 domain (155.9 pN, Fig. 3-6c) was approximately 50% greater than that for the corresponding region of WT M1-M3 in loading (A) (107.7 pN, Fig. 3-3b). This result indicated that the weak helix bundle M1 changed the conformation to another state with higher mechanical stability without the interaction with M2-M3 domain. To compare the mechanical stabilities of α-catenin fragments, we analyzed the number of force peaks N per curve, as shown in Fig. 3-7. The stacked bar graphs display N values, with color intensity illustrating the range of transition force ΔF_T for force peaks (Fig. 3-2b). The greater ΔF_T values correspond to more stable substructures. For WT M1-M3 fragment (orange and purple bars), N values at large ΔF_T (>100 pN, associated with a stable substructure) increased in loading (B) compared with that in loading (A). On the other

hand, the value of N at small ΔF_T (20 pN to 40 pN, associated with unstable substructure) decreased in loading (B). This result supported our idea that the conformation of WT M1-M3 changed to a more stable state with weakened M1/M2-M3 interaction under tension. In addition, the sum of the N values for M1 (green bar, Fig. 3-7) and M2-M3 (blue bar) was greater than that for WT M1-M3 in loading (A). This result suggested that the M1/M2-M3 interaction destabilized the M1 and M2-M3 conformations under no force. On the basis of the results for mutated and segmented α-catenin fragments, we determined that M1/M2-M3 interaction acted as a molecular switch to induce the mechano-adaptive conformational change of M1-M3 domain.

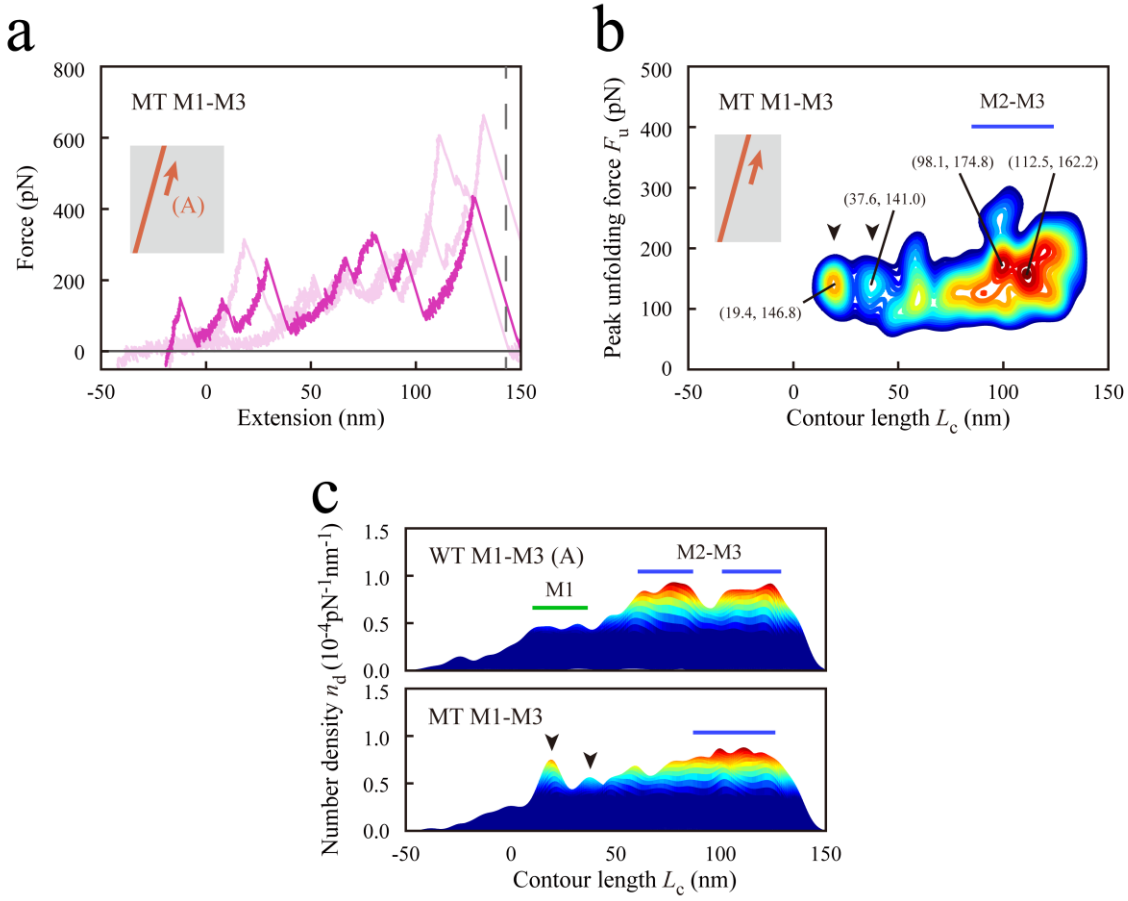

Figure 3-5: Results of nano-tensile testing for MT M1-M3 fragment. **a.** Force curves for MT M1-M3 domain. **b.** Contour map for MT M1-M3 fragment based on 576 force curves. **c.** Comparison of the number density nd in contour maps from a side view in WT and MT M1-M3 fragments.

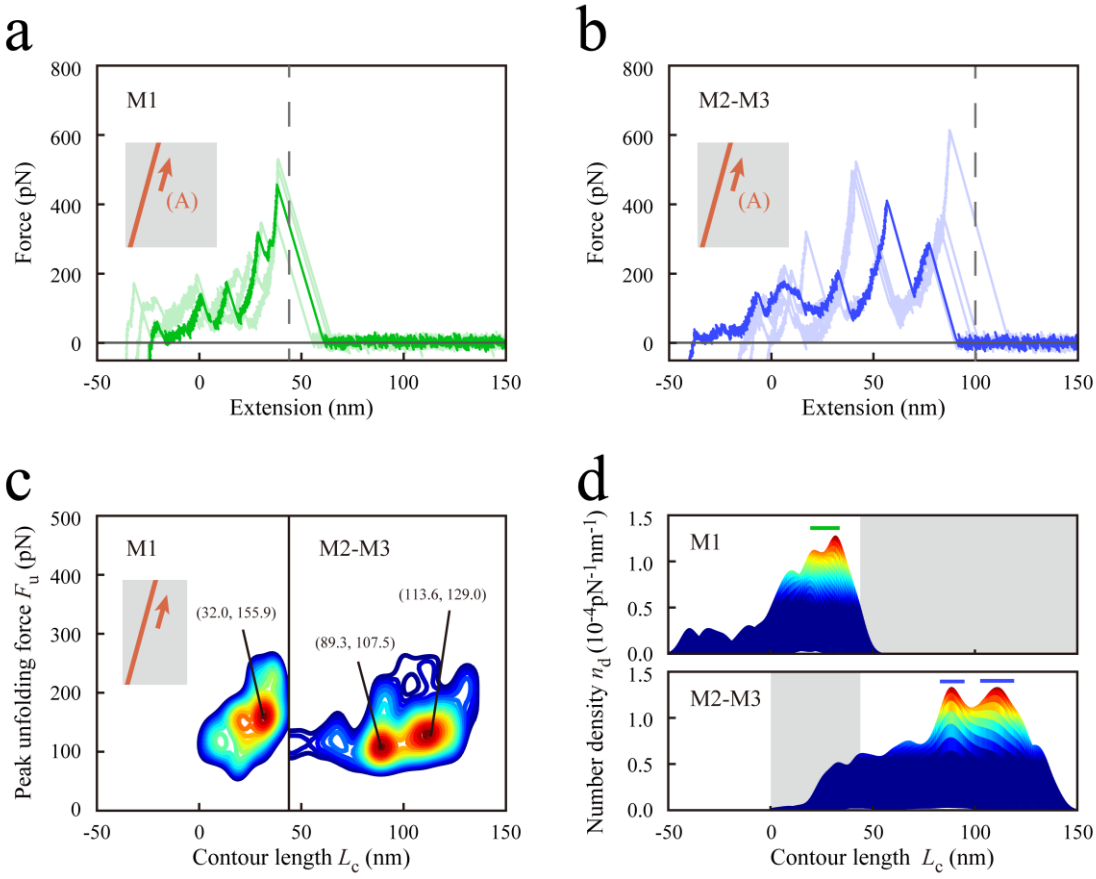

Figure 3-6: Results for segmented M1 and M2-M3 fragments. **a and b.** Force curves. **c.** Contour maps for M1 and M2-M3 fragments based on 181 and 785 force curves, respectively. The contour map for M2-M3 fragment is shifted to the right by 46.8 nm, which corresponds to the fully-extended length of M1 domain. **d.** Comparison of the number density n_d in contour maps against contour length L_c from a side view.

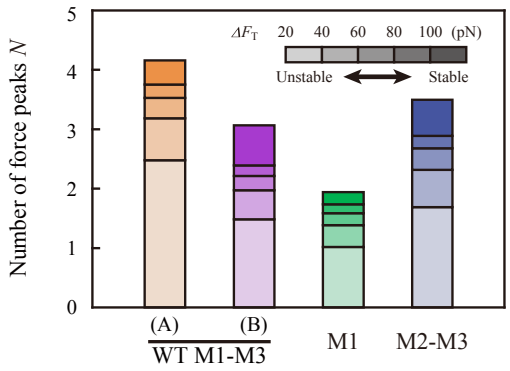

Figure 3-7: The average number of force peaks N per curve. The stacked bar graphs display N values, with color intensity illustrating the range of transition force ΔF_T. The substructure stability increases with the increasing ΔF_T values.

3.3.3 Conformational switch observed by structural imaging

To reveal conformational change of α-catenin caused by the disruption of M1/M2-M3 interaction, we performed AFM structural imaging. As shown in Figs. 3-8a and 3-8b, we obtained three dimensional images of WT and MT M1-M3 domain. Figs. 3-8c and 3-8d show the magnified and smoothed images. For WT M1-M3 domain, we found the three regions corresponding with three helix bundles (Fig. 3-8c), while MT M1-M3 domain showed a different conformation with one region, as shown in Fig. 3-8d, which corresponds to one helix bundle, and another larger region, which can be caused by overlapped two helix bundles. Without helix bundle M1, helix bundles M2-M3 are known to take a compact conformation to interact closer each other. This suggested that the larger region in AFM image corresponds to helix bundles M2-M3 and the smaller region corresponds to helix bundle M1.

Interestingly, in the obtained images, we found many molecules aligned to one direction. As the adhesion between α-catenin molecule and mica surface is mediated by outside hydrophobic sites of α-catenin, the alignment could be caused by rotation of molecules around such a specific site as a pivot point under flow during the sample preparation. As shown in Figs. 3-9a and 3-9b, we simply named the three domains in WT as A, B, and C domains and two domains in MT as X and Y domains. The analysis for the height of each region revealed that, as depicted in Fig. 3-9c, three helix bundles in wild type exhibit similar heights (orange bars), such as 1.65 ± 0.29 (Mean ± S.D.) nm, 1.66 ± 0.28 nm, and 1.57 ± 0.31 nm. In contrast, the larger region in the MT M1-M3 domain showed significantly larger height of 1.91 ± 0.36 nm than that of the smaller region, 1.49 ± 0.18 nm (magenta bars). This analysis supported the larger region in MT M1-M3 domain could be caused by overlapped M2 and M3 domains. As MT M1-M3 domain associated with vinculin while wild type did not, this conformational change could be important in vinculin affinity as well as the mechanical stabilities.

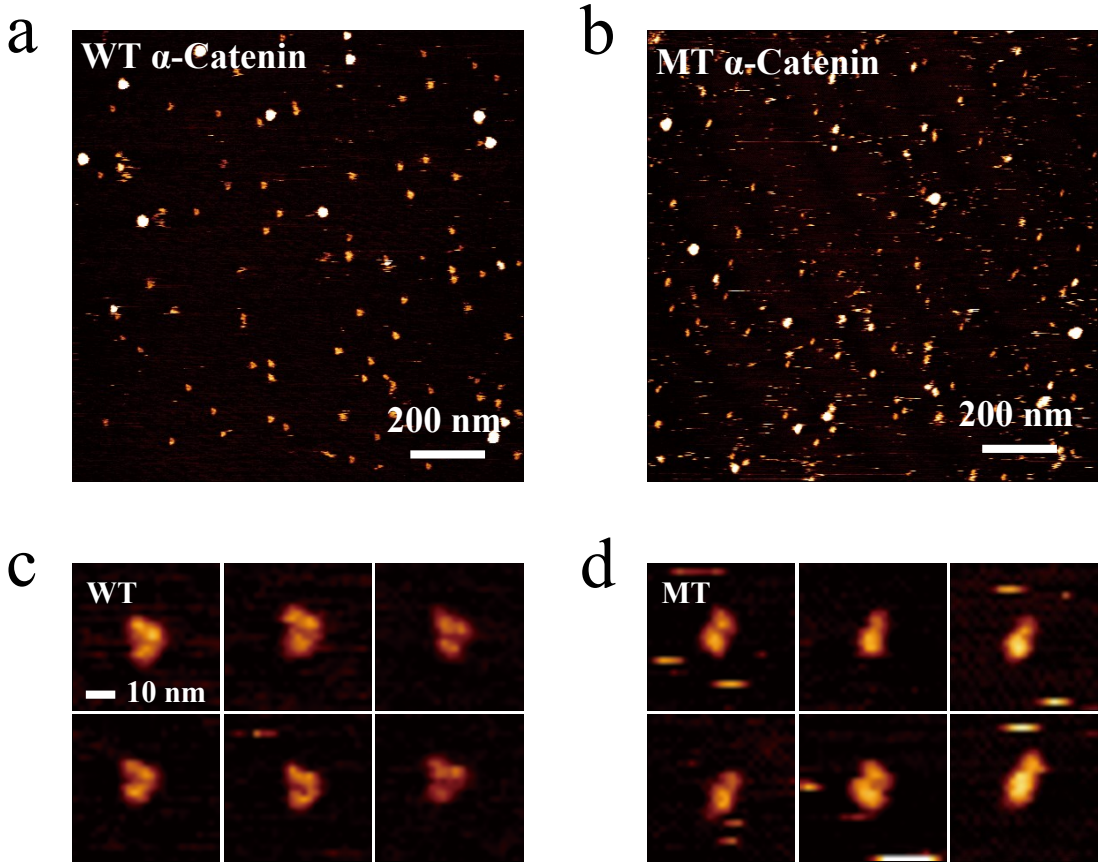

Figure 3-8: Results of AFM structural imaging for WT and MT M1-M3 fragments. **a and b.** Obtained structural images of WT and MT M1-M3 fragments. Color contours are set from 3 nm (white) to 0 nm (black). **c and d.** Smoothed images.

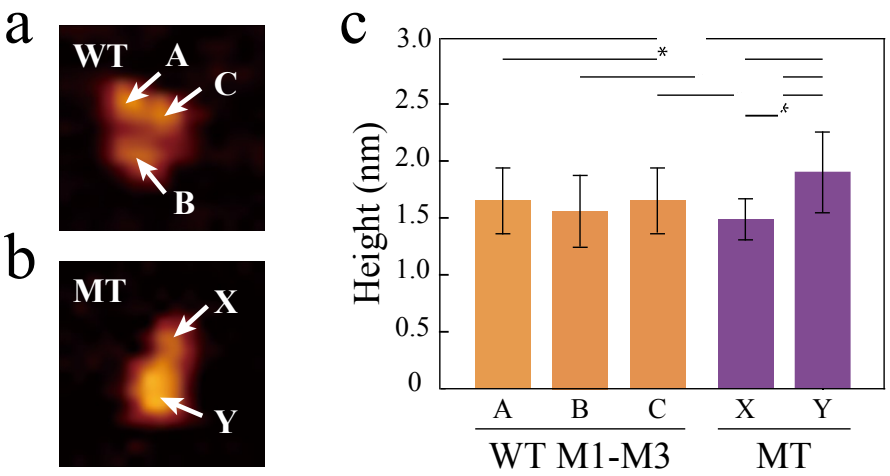

Figure 3-9: Analysis of the height of intramolecular domains. The statistical difference in mean values was analyzed using *t*-test (*, $p < 0.01$)

3.3.4 Comparison with mechanical behaviors with talin

To understand how the changes in mechanical behaviors of tension-sensor proteins alter their tension-sensitivities in *in vivo* conditions, we examined talin molecules, a well-known tension-sensor protein in focal adhesions (Izard and Vonrhein, 2004; Roberts and Critchley, 2009), by nano-tensile testing. Focal adhesion is a molecular complex (Kanchanawong *et al*., 2010), which connects intercellular actin cytoskeleton and extracellular matrix such as fibronectin and collagen. At focal adhesion, talin directly links actin filament and integrin, a transmembrane protein associated with a variety of extracellular matrix. As similarly as α-catenin, talin associates with vinculin under tension to promote a stable molecular complex by positively remodeling actin cytoskeleton (Hytönen and Vogel, 2008; Golji and Mofrad, 2010; Grashoff *et al*., 2010). The tension-sensing domain of talin, as shown in Fig. 3-10a, forms 62 α-helices (gray and magenta ellipses). These helices further form 11 helix bundles (purple, cyan and green boxes), some of which include VBS (magenta ellipses). Patel *et al.* (2006) has suggested that structural stabilities of VBS-containing helix bundles determine their tension-sensitivities under tension, while little is known about the mechanical behaviors of each helix bundle. In this chapter, we compared the mechanical behaviors of helix bundles in talin, which exhibit high and low tension-sensitivities in *in vivo* conditions.

In this experiment, as shown in Fig. 3-10b, the mechanical behaviors of talin 486-654 residues a helix bundle (Papagrigoriou *et al*., 2004) with low tension-sensitivity, and talin 754-889 residues, a helix bundle (Fillingham *et al*., 2005) with high tension-sensitivity, were examined by nano-tensile testing. 486-654 residues and 754-889 residues of talin molecules were directly loaded with the constant piezo moving speed of 500 nm/s. The force curves were similarly analyzed as in Chapter 3.

As a result of nano-tensile testing, we observed the significant difference in mechanical behaviors of 486-654 residues and 754-889 residues of talin. Fig. 3-10c shows the histogram of total unfolding energy E_{tot}. The total unfolding energy E_{tot} of

talin 486-654 residues showed symmetrical distribution, which was quite similar as the histogram for α-catenin 276-393 residues, which also forms one helix bundle. In contrast, the histogram for talin 754-889 residues showed right-skewed distribution with lower mode value than that for talin 486-654 residues and α-catenin 276-393 residues. The samples of E_{tot} for 486-654 residues and 754-889 residues of talin were not achieved by the same population, as tested by the Mann-Whitney U test ($p < 0.001$). Based on the analysis for each force peak during unfolding, we also observed that the peak unfolding force F_u of 486-654 residues, 215.1 ± 91.9 (Mean ± S.D.) pN, was larger than that of 754-889 residues (189.2 ± 85.5 pN). In addition, the persistence length l_p of talin 754-889 residues, 0.19 ± 0.14 (Mean ± S.D.) nm, was significantly larger than talin 486-654 residues (0.12 ± 0.08 nm) and α-catenin 276-393 residues (0.12 ± 0.07 nm) (T test, $P < 0.001$). This result indicated that the intermediate state of talin 754-889 residues exhibit low tensile stiffness. These results suggest that talin 754-889 residues is more easy to unfold under tension than talin 486-654 residues, which was consistent with the difference in their tension-sensitivities in cells. In addition, the results suggested that the mechano-adaptive conformational change of α-catenin contributes to its robust tension-sensing at adherens junctions.

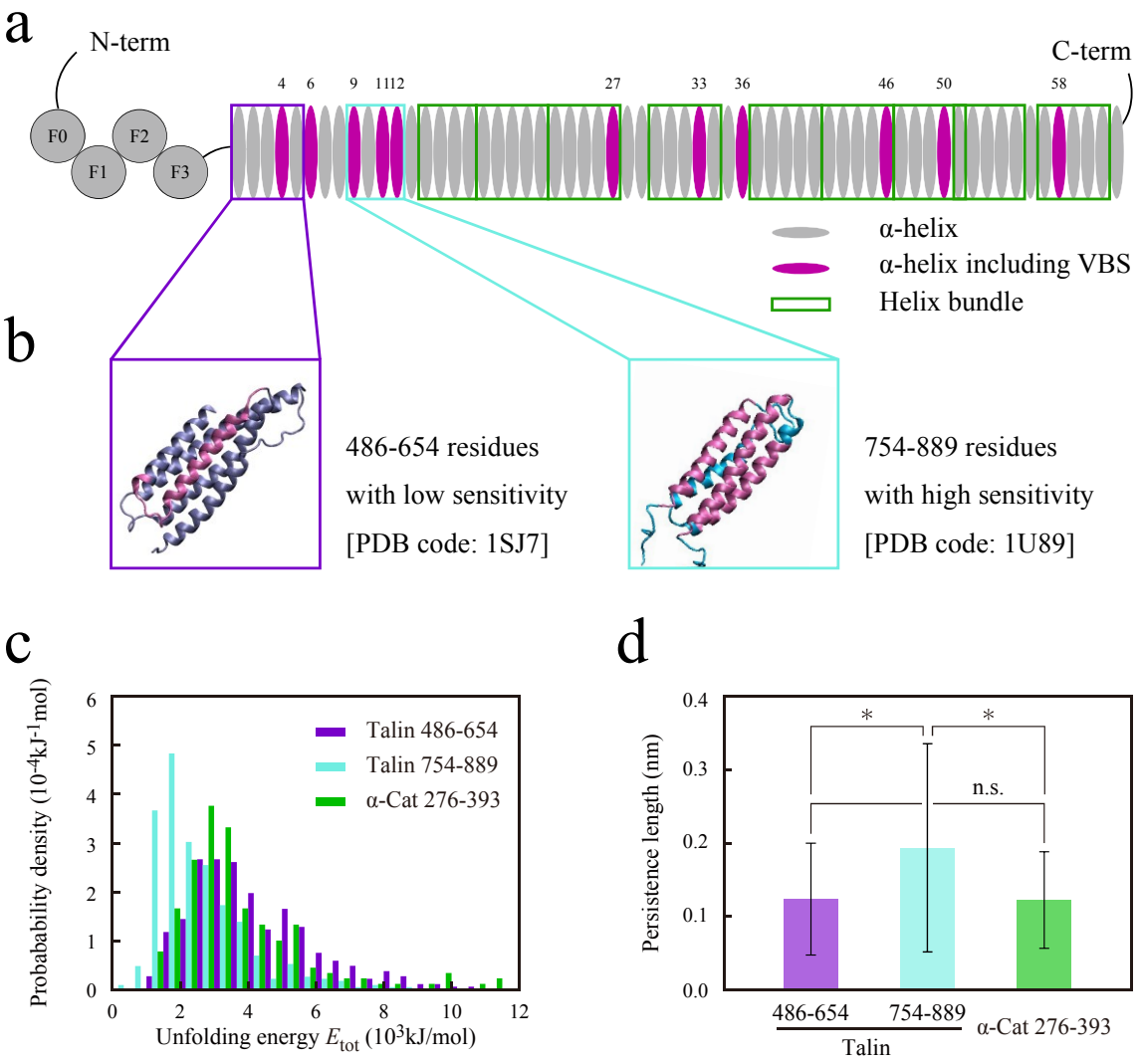

Figure 3-10: Nano-tensile testing for talin. **a.** Schematics of functional domains of talin. α-Helices are shown in ellipses and Helix bundles are shown in box. **b.** Crystal structures of a helix bundle with low tension-sensitivity (left, 486-654 residues, PDB code: 1SJ7) and that with high tension-sensitivity (right, 754-889 residues, PDB code: 1U89). was caused by the detachment of the AFM probe from the surface of coverslip. **c.** Histogram of the total unfolding energy E_{tot} for 486-654 residues (purple bars) and 754-889 residues (cyan bars) of talin and 276-393 residues of α-catenin (green bars). **d.** Bar chart of the persistence length l_p. The statistical difference in mean values was analyzed using *t*-test (*, $p < 0.001$)

3.3.5 Effects of vinculin association on mechanical behaviors

To elucidate how vinculin binding affects the mechanical behavior of α-catenin, we examined α-catenin fragments after vinculin treatment. The contour map of n_d for vinculin-associated MT M1-M3 domain, of which force curves are shown in Fig. 3-11a, showed characteristic regions (L_c = 29.4 nm and 37.3 nm; arrows in Fig. 3-11b) at a greater peak unfolding force F_u (154.7 pN and 248.5 pN) than that for MT M1-M3 without vinculin (Fig. 3-5b). This result indicated that M1-M3 domain was reinforced by vinculin association. In contrast to MT M1-M3 domain, vinculin-associated M1, of which force curves are shown in Fig. 3-11c, exhibited the contour map, as shown in Fig. 3-10d, with two regions at smaller F_u (99.7 pN and 96.7 pN) than M1 without vinculin (155.9 pN, Fig. 3-6c). Vinculin-associated M1 showed one region at a rather greater F_u (195.8 pN, Fig. 3-11d). This result indicated that the conformation of vinculin-associated M1 comprised a stable helix of VBS and two unstable substructures.

Comparing the results for MT M1-M3 and M1 fragments, we concluded that M2-M3 domain stabilized the unstable vinculin-associated M1 domain. Thus, the number of force peaks N at large ΔF_T (>100 pN) for MT M1-M3, as shown in Fig. 3-12a, was increased by vinculin association (red bar), with a decrease in N at small ΔF_T (20 pN–40 pN). The number of force peaks for M1 did not change significantly (cyan bar). The stabilizing role of M2-M3 domain was further confirmed in the analysis of total energy E_{tot} for completely unfolding, as depicted in Fig. 3-12b. The total energy E_{tot} for M1, as shown in Fig. 3-12c, decreased after vinculin association (cyan bar) that was caused by greater decrease in unfolding energy for two unstable substructures than the increase in unfolding energy for stable VBS helix. However, MT M1-M3 increased after vinculin association (red bar). These results revealed that M1-M3 domain was reinforced by association with vinculin at the head domain, as illustrated in Fig. 3-12d, with M2-M3 domain stabilizing the conformation of vinculin-associated M1 domain.

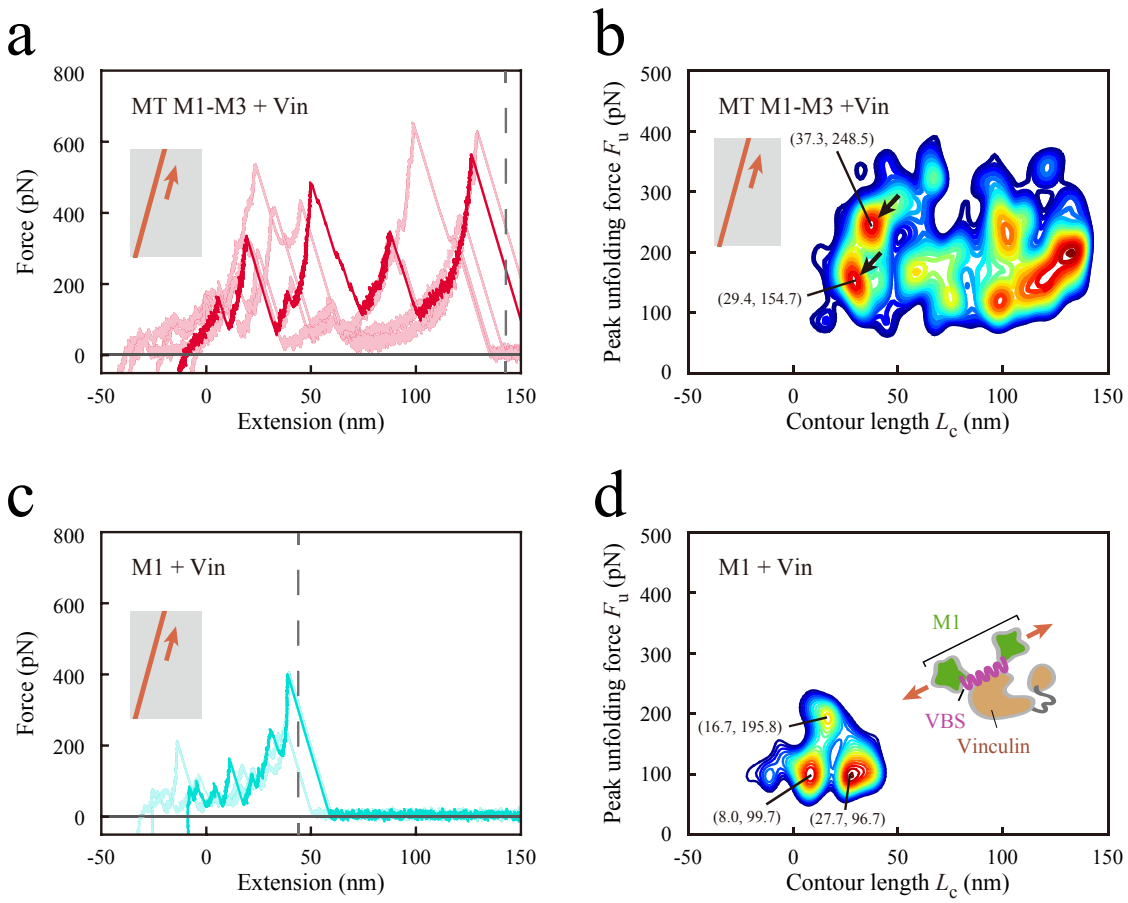

Figure 3-11: Effects of vinculin association on mechanical behaviors. **a and c.** Force curves for MT M1-M3 and M1 fragments associated with full-length vinculin. **b and d.** Contour maps MT M1-M3 and M1 fragments associated with full-length vinculin based on 571 and 111 force curves, respectively.

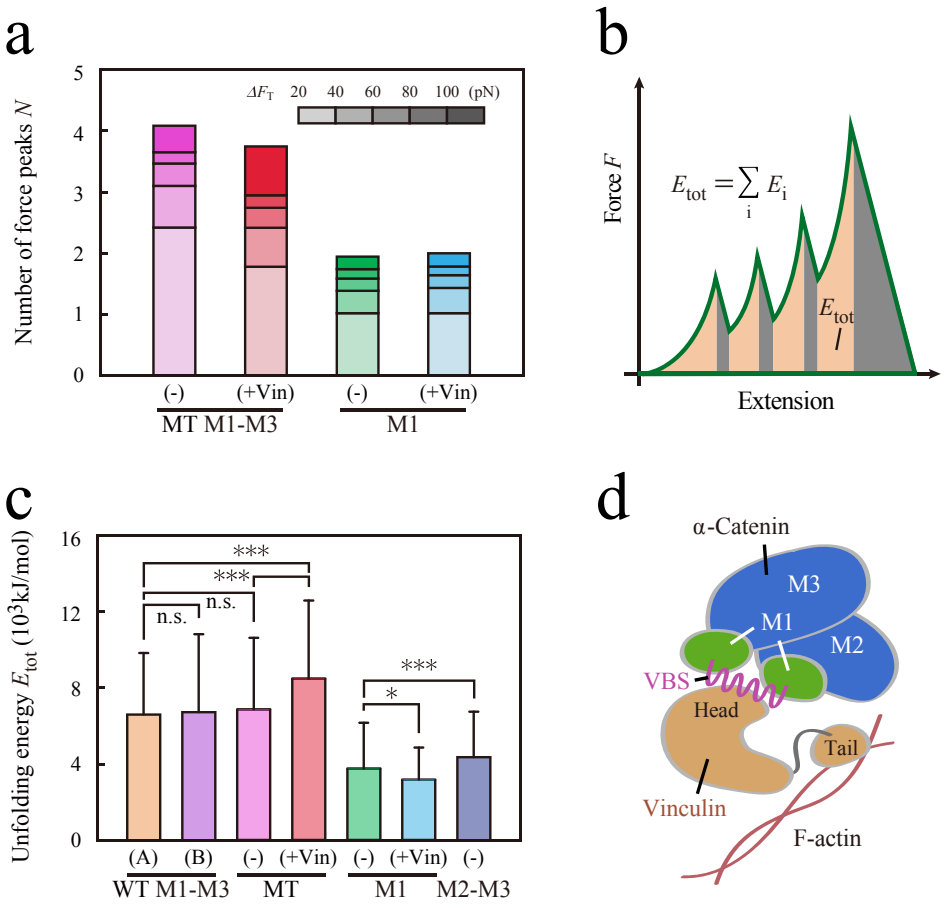

Figure 3-12: Analysis of the number of force peaks and unfolding energy. **a.** Changes in the average number of force peaks N caused by vinculin binding. Conformational change in holding time. **b.** Schematic of the analysis of the total unfolding energy E_{tot}. The total unfolding energy E_{tot} (orange area) was calculated by subtracting the cantilever bending energy (gray area) from the piezo-moving energy (green-enclosed area). **c.** *n* the bar chart of E_{tot} for examined fragments, the statistical significance of the differences was analyzed using *t*-test (*, $p < 0.05$ and ***, $p < 0.005$). E_{tot} for MT M1-M3 fragment significantly was increased by vinculin association, while no significant differences were observed for WT and MT M1-M3 fragments without vinculin association. **d.** Schematic of the molecular complex consisting of α-catenin, vinculin, and actin filament (F-actin).

3.3.6 Changes in persistence length

To examine the changes in α-catenin as a polymer chain, we analyzed persistence length l_p, as shown in Fig. 3-13a. In the initial extension (0 nm < L_c ≤ 72 nm, the left plot), the persistence length l_p for WT M1-M3 in loading (B) (purple bar) was greater than in loading (A) (orange bar), indicating that tensile force required to a certain amount of extension was decreased by mechanical activation. No significant differences were observed in the later extension (72 nm < L_c ≤ 144 nm, the right plot). After vinculin association, l_p settled to a smaller value in the entire extension (red bars), implying that M1-M3 was immobilized due to conformational reinforcement by vinculin. Here, the increase in l_p of M1-M3 by mechanical activation was consistent with the increase in the peak unfolding force F_u. As illustrated in Fig. 3-13b, we can postulate the same energy barrier E_b for the next intermediate state in M1-M3 before and after the activation on the basis of total unfolding energy E_{tot}. Further, the activated M1-M3 (B), with greater l_p, should be extended more to overcome the energy barrier E_b than M1-M3 (A), with smaller l_p, resulting in a larger F_u. Thus, M1-M3 domain of α-catenin under tension changes the conformation to an intermediate state with a larger persistence length, and finally settles into the immobilized state caused by vinculin association.

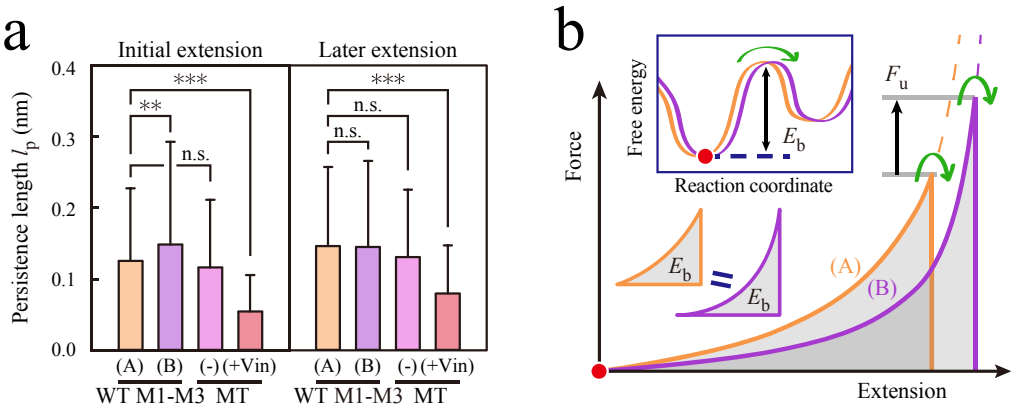

Figure 3-13: Persistence length analysis. **a.** Persistence lengths l_p. Error bars show standard deviations. Statistical significance in mean values was analyzed using *t*-test (**, $p < 0.01$; ***, $p < 0.005$). **b.** Effect of persistence length on peak unfolding force.

3.4 Discussion

3.4.1 α-Catenin as an adaptive tension sensor

On the basis of our single-molecule experiments, we revealed the mechano-adaptive sensory mechanism of α-catenin. Under physiologically possible low tension, α-catenin adaptively changed the conformation to a stable intermediate state. Such mechano-adaptive conformational changes enable α-catenin at adherens junctions to retain the activated state under tension, without successive unfolding, to function as a robust tension-sensor. Our findings could be one solution to a paradox. The tension-sensing proteins require mechanical forces for their activation; however, they have to be stable under such conditions because the mechanical forces function as basic protein denaturants. Furthermore, we revealed that the association with vinculin reinforces α-catenin conformation; the stable α-catenin-vinculin complex contributes to the tight anchoring of adhesive molecules at adherens junctions (Thomas *et al*., 2013) by recruiting another actin filament. Therefore, we suggest that the mechano-adaptive sensory ability of α-catenin arises from its molecular plasticity in response to both mechanical and biochemical cues.

3.4.2 Role of tension in the conformational change

Our results for mutated (MT M1-M3) and segmented (M1, M2-M3) α-catenin revealed that the M1/M2-M3 interaction acts as a conformational switch to the intermediate state, where M1 and M2-M3 domains change to the conformations with increased stability. Our results are consistent with the previous reports that the helix bundle M1 requires the structural stabilization by M2-M3 domain (Li *et al*., 2013) and that helix bundles M2-M3 are approximately 180°-rotated in conformation without M1 domain (Pokutta *et al*., 2002; Yang *et al*., 2001). However, there were some discrepancies between the results for MT M1-M3 without mechanical activation and those for WT M1-M3 in

loading (B) with mechanical activation. Thus, we should consider both the importance of tension for the drastic conformational changes and the conformational switch caused by M1/M2-M3 interaction.

3.4.3 Association of α-catenin with full-length vinculin

In our experiments, the full-length vinculin firmly associated with MT M1-M3 fragment, with an increase in peak unfolding force F_u and a decrease in the persistence length l_p. The full-length vinculin assumes an autoinhibited conformation for α-catenin (Cohen *et al*., 2005). Our results suggested that the VBS exposed in the mechanically-activated α-catenin opens the autoinhibited conformation of vinculin to make a stable α-catenin–vinculin complex. Our data supported the previous reports (Choi *et al*., 2012: Peng *et al*., 2012) that α-catenin and vinculin are "co-activated" for interacting with each other under tension. This type of a force-induced vinculin-activation mechanism of α-catenin could be conserved in talin and α-actinin that are similar adhesive proteins constituting a molecular complex with vinculin and actin filament (Bois *et al*., 2006).

3.4.4 Utility of the holding method by AFM

The loading rate used here was appropriate for the qualitative analysis of the mechanical behavior of α-catenin. Our results for WT M1-M3 domain in loading (A) were in agreement with the results of the experiments (performed using magnetic tweezers) using a low loading rate (approximately 4 pN/s) (Yao *et al*., 2014). Moreover, the "holding" method utilized in our study allowed us to analyze the conformational changes under physiologically possible low tension of approximately 10 pN. Thus, by introducing the holding time into fast loadings, we succeeded in analyzing the conformational changes of α-catenin molecules under low tension while efficiently exploring their unfolding trajectories.

3.4.5 Relationship between persistence length and subcomponents

The persistence length L_p appeared in this study was smaller than that reported (approximately 0.4 nm) for titin molecules (Carrion-Vazquez *et al*., 1999). This discrepancy may be related to the secondary structures of molecules. A previous study (Stirnemann *et al*., 2013) employing molecular dynamics simulation revealed that a protein with high φ dihedral potential shows a small persistence length of 0.19 nm. This suggests that α-helical proteins such as α-catenin, of which φ dihedral angle is more constrained than β-sheet proteins such as titin, exhibit smaller persistence length. In addition, subcomponents in α-catenin molecules, such as helix bundles, could decrease the persistence length L_p.

3.4.6 New concept of mechano-adaptive molecules

Based on our study, we propose a novel concept of "mechano-adaptive" molecules that fulfill their innate functions by adapting to the cellular forces. Under these forces, biomolecules such as proteins and nucleic acids may change their conformations, mechanical behaviors, and chemical properties. Such molecular-scale changes under mechanical forces could affect force-induced phenomena at cellular and tissue level. We believe that our study may be the basis for future studies investigating the concept of mechano-adaptive sensory mechanism.

3.5 Conclusion

In this chapter, we revealed how α-catenin retains its activated state while avoiding unfolding under tension. Using single-molecule force spectroscopy employing AFM, we found that mechanically activated α-catenin fragment had higher mechanical stability than a non-activated fragment. The results of our experiments using mutated and segmented fragments showed that the key intramolecular interactions acted as a conformational switch. The drastic conformational change of α-catenin was observed by AFM structural imaging, suggesting the change in its vinculin affinity. We also found that the conformation of α-catenin was reinforced by association with vinculin. We demonstrate that α-catenin adaptively changes its conformation under tension to a stable intermediate state and finally settles into a more stable state reinforced by association with vinculin. Our data suggest that the plastic characteristics of α-catenin, revealed in response to both mechanical and biochemical cues, enable the functional-structural dynamics at the cellular and tissue levels.

References

Bois, P. R., O'Hara, B. P., Nietlispach, D., Kirkpatrick, J. & Izard, T. The vinculin binding sites of talin and α-actinin are sufficient to activate vinculin. *J. Biol. Chem.* **281,** 7228–7236 (2006).

Bustamante, C., Marco, J. F., Siggia, E. D. & Smith, S. Entropic elasticity of lambda-phage DNA. *Science* **265,** 1599–1600 (1994).

Carrion-Vazquez, M., Oberhauser, A. F., Fowler, S. B., Marszalek, P. E., Broedel, S. E., Clarke, J. & Fernandez, J. M. Mechanical and chemical unfolding of a single protein: a comparison. *Proc. Natl. Acad. Sci. U. S. A.* **96,** 3694–3699 (1999).

Choi, H. J., Pokutta, S., Cadwell, G. W., Bobkov, A. A., Bankston, L. A., Liddington, R. C. & Weis, W. I. αE-catenin is an autoinhibited molecule that coactivates vinculin. *Proc. Natl. Acad. Sci. U. S. A.* **109,** 8576–8581 (2012).

Cohen, D. M., Chen, H., Johnson, R. P., Choudhury, B. & Craig, S. W. Two distinct head-tail interfaces cooperate to suppress activation of vinculin by talin. *J. Biol. Chem.* **280,** 17109–17117 (2005).

Eiraku, M., Takata M., Ishibashi, H., Kawada, K., Sakakura, E., Okuda, S., Sekiguchi, K., Adachi, T. & Sasai Y. Self-organizing optic-cup morphogenesis in three-dimensional culture. *Nature* **472,** 51–56 (2011).

Engl, W., Arasi, B., Yap, L. L., Thiery, J. P. & Viasnoff, V. Actin dynamics modulate mechanosensitive immobilization of E-cadherin at adherens junctions. *Nat. Cell Biol.* **16,** 584–591 (2014).

Fillingham, I. J., Gingras, A. R., Papagrigoriou, E., Patel, B., Emsley, J., Critchley, D. R., Roberts, G. C. K. & Barsukov, I. L. A vinculin binding domain from the talin rod unfolds to form a complex with the vinculin head. *Structure* **13,** 65-74 (2005).

Finer, J. T., Simmons, R. M. & Spudich, J. A. Single myosin molecule mechanics: piconewton forces and nanometre steps. *Nature* **368,** 113–119 (1994).

Goldman, D. H., Kaiser, C. M., Milin, A., Riqhini, M., Tinoco, I. J. & Bustamante, C. Mechanical force releases nascent chain-mediated ribosome arrest in vitro and in vivo. *Science* **348,** 457–460 (2015).

Golji, J. & Mofrad, M. R. K. A Molecular dynamics investigation of vinculin activation. *Biophys. J.* **99,** 1073-1081 (2010).

Grashoff, C., Hoffmann, B. D., Brenner, M. D., Zhou, R., Parsons, M., Yang, M. T., McLean, M. A., Sliger, S. G., Chen, C. S., Ha, T. & Schwartz, M. A. Measuring mechanical tension across vinculin reveals regulation of focal adhesion dynamics. *Nature* **466,** 263–266 (2010).

Harris, T. J. C. & Tepass, U. Adherens junctions: from molecules to morphogenesis. *Nat. Rev. Mol. Cell Biol.* **11,** 502–514 (2010).

Hoffmann, T. & Dougan, L. Single molecule force spectroscopy using polyproteins. *Chem. Soc. Rev.* **41,** 4781–4796 (2012).

Huveneers, S., Oldenburg, J., Spanjaard, E. G., Krogt, G., Grigoriev, I., Akhmanova, A., Rehmann, H. & Rooij, J. Vinculin associates with endothelial VE-cadherin junctions to control force-dependent remodeling. *J. Cell Biol.* **196,** 641–652 (2012).

Hytönen, V. & Vogel, V. How force might activate talin's vinculin binding sites: SMD reveals a structural mechanism. *PLoS comp. Biol.* **4:**e24 (2008).

Ishiyama, N., Tanaka, N., Abe, K., Yang, Y. J., Abbas, Y. M., Umitsu, M., Nagar, B., Bueler, S. A., Rubinstein, J. L., Takeichi M. & Ikura M. An autoinhibited structure of α-catenin and its implications for vinculin recruitment to adherens junctions. *J. Biol. Chem.* **288,** 15913–15925 (2013).

Izard, T. & Vonrhein, C. Structural basis for amplifying vinculin activation by talin. *J. Biol. Chem.* **279,** 27667-27678 (2004).

Kanchanawong, P., Shtengel, G., Pasapera, A. M., Ramko, E. B., Davidson, M. W., Hess, H. F. & Waterman, C. M. A. Nanoscale architecture of integrin-based cell adhesions. *Nature* **468,** 580–584 (2010).

Kim, T. J., Zheng, S., Sun, J., Muhamed, J., Wu, J., Lei, L., Kong, X., Leckband, D. E. & Wang, Y. Dynamic visualization of α-catenin reveals rapid, reversible conformation switching between tension states. *Curr. Biol.* **25,** 218–224 (2015).

Lecuit, T. α-Catenin mechanosensing for adherens junctions. *Nat. Cell Biol.* **12,** 522–524 (2010).

Lecuit, T., Lenne, P. F. & Munro, E. Force generation, transmission, and integration during cell and tissue morphogenesis. *Annu. Rev. Cell Dev. Biol.* **27,** 157–184 (2011).

Levayer, R. & Lecuit, T. Oscillation and polarity of E-cadherin asymmetries control actomyosin flow patterns during morphogenesis. *Dev. Cell* **26,** 162–175 (2013).

Li, J., Newhall, J., Ishiyama, N., Gottarge, C., Ikura, M., Leckband, D. E. & Tajkhorshid, E. Structural determinants of the mechanical stability of α-catenin. *J. Biol. Chem.* **290,** 18890–18903 (2015).

Liu, R., Garcia-Manyes, S., Sarkar, A., Badilla, C. L. & Fernández, J. M. Mechanical characterization of protein L in the low-force regime by electromagnetic tweezers/evanescent nanometry. *Biophys. J.* **96,** 3810–3821 (2009).

Lv, C., Gao, X., Li, W., Xue, B., Qin, M., Butrick, L. D., Zhou, H., Cao, Y., Robinson, R. C. & Wang, W. Single-molecule force spectroscopy reveals force-enhanced binding of calcium ions by gelsolin. *Nat. Commun.* **5,** 4623 (2014).

Maki, K., Han, S. W. & Adachi, T. β-Catenin as a tension transmitter revealed by AFM nanomechanical testing. *Cell. Mol. Bioeng.* **8,** 14–21 (2015).

Maki, K., Han, S. W., Hirano, Y., Yonemura, S., Hakoshima, T. & Adachi, T. Mechano-adaptive sensory mechanism of α-catenin under tension. *Sci. Rep.* **6,** 24878, (2016).

Maki, K., Nakao, N. & Taiji Adachi, "Nano-mechanical characterization of tension-sensitive helix bundles in talin rod", *Biochemical and Biophysical Research Communications*, (2017).

Martin, A. C., Gelbart, M., Fernandez-Gonzalez, R., Kaschube, M. & Wieschaus, E. F. Integration of contractile forces during tissue invagination. *J. Cell Biol.* **188,** 735–749 (2010).

Meng, W. & Takeichi, M. Adherens junction: molecular architecture and regulation. *Cold Spring Harb. Perspect. Biol.* **1,** a002899 (2009).

Miyake, Y., Inoue, N., Nishimura, K., Kinoshita N., Hosoya, H. & Yonemura, S. Actomyosin tension is required for correct recruitment of adherens junction components and zonula occludens formation. *Exp. Cell Res.* **312,** 1637–1650 (2006).

Oberhauser, A. F., Hansma, P. K., Carrion-Vazquez, M. & Fernández, J. M. Stepwise unfolding of titin under force-clamp atomic force microscopy. *Proc. Natl. Acad. Sci. U. S. A.* **98,** 468–472 (2001).

Patel, B., Gingras, A. R., Bobkov, A. A., Fujimoto, M., Zhang, M., Liddington, R. C., Mazzeo, D., Emsley, J., Roberts, G. C. K., Barsukov, I. L. & Critchley, D. R. The activity of the vinculin binding sites in talin is influenced by the stability of the helical bundles that make up the talin rod. *Structure* **13,** 65-74 (2006).

Papagrigoriou, E., Gingras, A. R., Barsukov, I. L., Bate, N., Fillingham, I. J., Patel, B., Frank, R., Ziegler, W. H., Roberts, G. C. K., Critchley, D. R. & Emsley, J. Activation of a vinculin-binding site in the talin rod involves rearrangement of a five-helix bundle. *EMBO J.* **23,** 2942-2951 (2004).

Peng, X., Maiers, J. L., Choudhury, D., Craig, S. W. & DeMali, K. A. α-Catenin uses a novel mechanism to activate vinculin. *J. Biol. Chem.* **287,** 7728–7737 (2012).

Pokutta, S., Drees, F., Takai, Y., Nelson, W. J. & Weis, W. I. Biochemical and structural definition of the l-afadin- and actin-binding sites of α-catenin. *J. Biol. Chem.* **277,** 18868–18874 (2002).

Popa, I., Kosuri, P., Alegre-Cebollada, J., Garcia-Manyes, S. & Fernández, J. M. Force dependency of biochemical reactions measured by single-molecule force-clamp spectroscopy. *Nat. Protoc.* **8,** 1261–1276 (2013).

Roberts, G. C. K. & Critchley, D. R. Structural and biophysical properties of the integrin-associated cytoskeletal protein talin. *Biophys. Rev.* **1,** 61-69 (2009).

Stirnemann, G., Giganti, D., Fernández, J. M. & Berne, B. J. Elasticity, structure, and relaxation of extended proteins under force. *Proc. Natl. Acad. Sci. U. S. A.* **110,** 3847–3852 (2013).

Tamada, M., Perez, T. D., Nelson, W. J. & Sheetz, M. P. Two distinct modes of myosin assembly and dynamics during epithelial wound closure. *J. Cell Biol.* **176,** 27–33 (2007).

Thomas, W. A., Boscher, C., Chu, Y. S., Cuvelier, D., Martinez-Rico, C., Sddiki, R., Heysch, J., Ladoux, B., Thiery, J. P., Mege, R. M. & Dufour, S. α-Catenin and vinculin cooperate to promote high E-cadherin-based adhesion strength. *J. Biol. Chem.* **288,** 4957–4969 (2013).

Sato, K., Ogawa, Y., Ito, S., Fujisawa, S. & Minami, K. Strain magnitude dependent intracellular calcium signaling response to uniaxial stretch in osteoblastic cells. *J. Biomech. Sci. Eng.* **10,** 15-00242 (2015).

Yang, J., Dokurno, P., Tonks, N. K. & Barford, D. Crystal structure of the M-fragment of α-catenin: implications for modulation of cell adhesion. *EMBO J.* **20,** 3645–3656 (2001).

Yao, M., Qiu, W., Liu, R., Efremov, A. K., Cong, P., Seddiki, R., Payre, M., Lim, C. T., Ladoix, B., Mege, R. M. & Yan, J. Force-dependent conformational switch of α-catenin controls vinculin binding. *Nat. Commun.* **5,** 4525 (2014).

Yonemura, S., Wada, Y., Watanabe, T., Nagafuchi, A. & Shibata, M. α-Catenin as a tension transducer that induces adherens junction development. *Nat. Cell Biol.* **12,** 533–542 (2010).

Yonemura, S. A mechanism of mechanotransduction at the cell-cell interface: emergence of α-catenin as the center of a force-balancing mechanism for morphogenesis in multicellular organisms. *Bioessays* **33,** 732–736 (2011).

Chapter 4

Mechano-guided Association of α-Catenin with Vinculin

4.1 Introduction

Adhesive interaction between neighboring cells contributes to the mechanical maintenance of morphogenetic changes in embryos (Eiraku *et al*., 2011; Okuda *et al*., 2016; Lecuit and Yap, 2015) as well as homeostasis in mature tissues. Cadherin-based adherens junctions connect the actin cytoskeleton between cells and dynamically change the strength of adhesion in response to intercellular tension (DuFort *et al*., 2011; Levayer and Lecuit *et al*., 2013; Takeichi, 2014; Engl *et al*., 2014). During the maturation process of adherens junctions, α-catenin and vinculin cooperate to remodel the actin cytoskeleton (Yonemura *et al*., 2010; Maiden *et al*., 2011). α-Catenin participates in the cadherin–catenin complex (CCC), where cadherin, β-catenin, and α-catenin serially associate together. (Kobielak *et al*., 2004; Yap *et al*., 2015). The CCC interacts with actin filaments via α-catenin (Cavey *et al*., 2008; Wickline *et al*., 2016) in

the cytoplasmic region of adherens junctions to transmit intercellular tension generated by the actomyosin cytoskeleton. Under intercellular tension, α-catenin becomes associated with vinculin (Yonemura *et al*., 2010). Vinculin is another key protein in the architecture of adherens junctions. The C-terminus of vinculin interacts with monomeric and filamentous actin to initiate the formation of bundled actin filaments and to remodel existing filaments (Wen *et al*., 2009). α-Catenin and vinculin thereby induce local remodeling of the actin cytoskeleton at adherens junctions to increase the strength of adhesion, which stably transmits intercellular tension.

The association between α-catenin and vinculin is surprising as these proteins form autoinhibited structures that prevent their association. The autoinhibition of α-catenin against vinculin association is formed by interaction between the α-catenin M1 domain, which includes VBS, and the M2–M3 domain (Rangarajan *et al*., 2013; Ishiyama *et al*., 2013). Similarly, the autoinhibition of vinculin against α-catenin association is formed by interaction between the vinculin head domain, which includes the α-catenin binding site, and the tail domain (Johnson and Craig, 1994; Bacolitsa *et al*., 2004; Cohen *et al*., 2005).

While the autoinhibition of α-catenin and vinculin must be unlocked to allow their association, the molecular mechanism underlying this process is still unclear. A previous study indicates that the M1–M2 domain of α-catenin with an exposed VBS does not interact with autoinhibited full-length vinculin, while both of these molecules co-precipitate with actin filaments (Choi *et al*., 2012). This result suggests that the autoinhibition of vinculin is disrupted by simultaneous interaction with the open-form α-catenin and actin filament. In this possible mechanism, α-catenin and full-length vinculin at least weakly/transiently associate with each other before forming a stable complex with actin filaments (Choi *et al*., 2012). In Chapter 3, we found that the mechanical disruption of α-catenin autoinhibition causes an adaptive conformational change that increases mechanical stability, while mutational disruption promotes its affinity to full-length vinculin (Maki *et al*., 2016). Therefore, we hypothesized that the

mechanically induced conformational change of α-catenin alters its affinity to vinculin head domain, which enables α-catenin to associate with vinculin by secondarily unlocking its autoinhibition.

To reveal the association mechanism of mechanically activated α-catenin with full-length vinculin, we developed a system TIRFM-combined AFM. Other studies have used TIRFM-based molecular observation combined with DNA cutting/pasting (Kufer *et al*., 2009) and structural imaging experiment (Brown *et al*., 2009) to provide a strong tool for investigating the biochemical and structural aspects of biomechanical phenomena at the molecular level. By using the TIRFM-combined AFM system, we mechanically activated α-catenin molecules modified on a coverslip by AFM and simultaneously observed the dynamics of full-length vinculin molecules dissolved in solvent using TIRFM.

4.2 Materials and Methods

4.2.1 TIRFM-combined AFM

As illustrated in Fig.4-1, we mechanically activated α-catenin using AFM while observing the dynamics of vinculin TIRFM. The piezo in AFM was controlled in the following three steps, as shown in Fig. 4-2: (1) initial extension (from 1.60 s to 1.68 s; piezo moving speed υ, 500 nm/s), shown in a magenta line, to mechanically activate α-catenin, (2) holding with a constant piezo height of 40 nm for 2 s (from 1.68 s to 3.68 s), shown in a yellow line, to keep α-catenin under tension awaiting vinculin, and (3) later extension (from 3.68 s to 4.20 s, υ, 500 nm/s), shown in a cyan line, to examine the mechanical behaviors of α-catenin after vinculin association. During the nano-tensile testing, we simultaneously observed Alexa 488-labeled full-length vinculin in the working buffer using TIRFM.

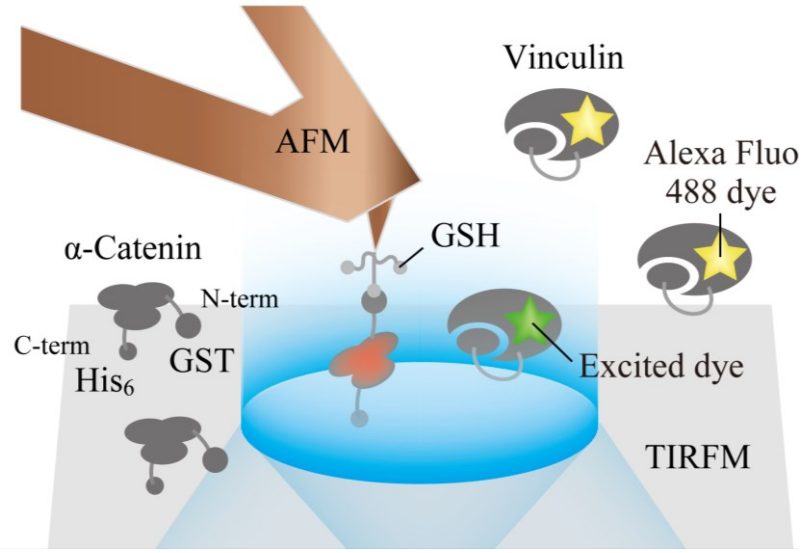

Figure 4-1: Schematic of an experiment using TIRFM-combined AFM. α-Catenin molecules on coverslips were mechanically activated by AFM; simultaneously, full-length vinculin molecules in solvent were observed by TIRFM. Vinculin molecules were illuminated when they appear in an evanescent field (cyan region).

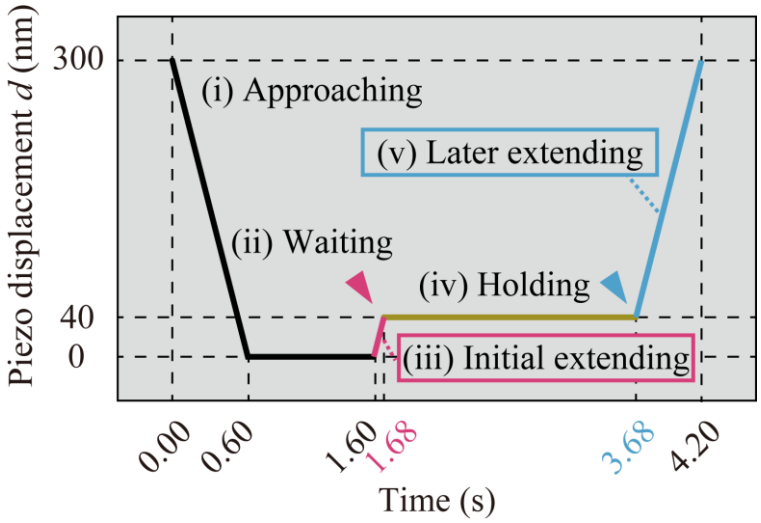

Figure 4-2: Programmed piezo displacement for AFM nano-tensile testing.

4.2.2 Protein purification

α-Catenin and vinculin were expressed and purified as reported in Chapter 3. DNA fragments of mouse αE-catenin M1–M3 (residues 276–634) and M2–M3 (residues 385–634) were amplified by PCR and cloned into the pGEX6P-3 vector (GE Healthcare). A DNA fragment of mouse full-length vinculin (residues 1–1066) was cloned into the pET-6b (+) vector (Novagen). These plasmids were verified by DNA sequencing and transformed into Escherichia coli strain BL21Star (DE3) cells (Invitrogen). α-Catenin and vinculin molecules were expressed at 20°C in Luria–Bertani medium with 0.1 mM isopropyl-β-D-thiogalactopyranoside. BL21Star cells expressing α-catenin and vinculin were suspended in 20 mM Tris-HCl buffer (pH 8.0) containing 150 mM NaCl and disrupted by sonication. The supernatant after ultracentrifugation was applied to a Glutathione Sepharose 4B column (GE Healthcare). Proteins eluted from the column were further purified by anion exchange (HiTrap Q HP, GE Healthcare) and gel filtration (Superdex 200 pg, GE Healthcare) chromatography. N-terminal His_6 tags on vinculin molecules were then cleaved using human rhinovirus 3C protease.

4.2.3 Chemical modification

The coverslips were cleaned in a plasma cleaner, sonicated in 1 M KOH for 15 min, and sonicated in ethanol for 15 min. After cleaning, the coverslips were thoroughly washed in MilliQ-treated water (EMD Millipore, Hayward, CA, USA). For modification with α-catenin molecules, the coverslips were treated with 2% MPTMS/ethanol for 15 min and then treated with 2 mM maleimide-C3-NTA (Mal-C3-NTA; DOJINDO Laboratories, Kumamoto, Japan) in 20 mM Tris-HCl buffer for 30 min. The NTA-modified coverslips were then treated with 10 mM NiCl2 (Wako Pure Chemical Industries, Osaka, Japan)/MilliQ water for 30 min and further washed with MilliQ water and 20 mM Tris-HCl buffer. Using NTA-Ni^{2+}-His_6 affinity binding, 500-μM α-catenin fragments in 20 mM Tris-HCl buffer were modified on the coverslips. The coverslips

were finally washed with 20 mM Tris-HCl buffer.

AFM tips were first cleaned up in a plasma cleaner and then treated with 2% APTES/MilliQ for 15 min. The tips were then treated with 6 mM Mal-PEG-NHS ester/20 mM Tris-HCl buffer for 30 min and with 10 mM glutathione/20 mM Tris-HCl buffer for 1 h. The remaining maleimide groups were quenched with 50 mM 2-mercaptoethanol/MilliQ water and washed with 20 mM Tris-HCl buffer.

4.2.4 Fluorescent labeling of vinculin

Full-length vinculin molecules were labeled using the Alexa Fluor 488 Protein Labeling Kit (Thermo Fisher Scientific, Waltham, MA, USA), in which primary amines of vinculin molecules formed covalent bonds with Alexa 488 dye. Full-length vinculin molecules and Alexa 488 dye were conjugated at 1:1 ratio at room temperature. Alexa-488–labeled vinculin molecules were purified using size exclusion chromatography. For each measurement using TIRFM-combined AFM, Alexa 488-labeled vinculin molecules were dissolved at a concentration of 10 nM in working buffer (pH 8.0; 20 mM Tris-HCl, 1 mM DTT, and 2 mM Trolox). DTT was added to the working buffer to prevent aggregation of vinculin molecules caused by disulfide bonds, and Trolox, a reducing agent, was used to sustain the fluorescence of the Alexa 488 dye by maintaining reducing conditions in the working buffer.

4.2.5 Vinculin observation by TIRFM

To observe vinculin molecules by TIRFM, we controlled the penetration depth of the evanescent field as 150 nm, which is the length of a fully extended αE-catenin M1–M3 fragment (~144 nm). We used 100X objective lens for TIRFM (UAPON 100XOTIRF; NA, 1.49; Olympus Co.). The power of the 488-nm laser (OBIS 488 LS; Coherent, Inc., Santa Clara, CA, USA) was decreased to 2.97 W/cm^2 by ND filter to avoid photobleaching. The exposure time was 50 ms and the final frame rate was 14.76

frames/s. We synchronized the TIRFM observation with the AFM nano-tensile testing using the pulse signal output from the AFM controller that externally controlled the EM-CCD camera (iXon Ultra 888; Andor Technology Ltd., Belfast, UK). Finally, the square region (15 x 15 pixels) around the tip position were cropped and analyzed.

4.3 Results

4.3.1 Mechanical activation of α-catenin under tension

As a result of AFM nano-tensile testing for α-catenin M1–M3 domain (residues 276–634), as shown in Fig. 4-3a, we obtained force curves (force F versus extension ΔL). A maximum force amplitude threshold of 50 pN was used in obtaining nano-tensile testing. This threshold was large enough to identify molecular responses since the force amplitude caused by thermal fluctuations is ~13 pN. Over the time course of force during the holding time, as depicted in Fig. 4-3b, the force curve shows stepwise tension relaxations caused by conformational changes of α-catenin under tension as shown in Chapter 3 (Maki *et al*., 2016). As indicated in Fig. 4-3c, Force at the beginning of the holding time with broad distribution (magenta bars) was equilibrated to ~10 pN with a rather narrow distribution at the end (cyan bars); the force range at the end of holding time corresponds to the force generated by couples of myosin molecules (Finer *et al*., s1994). These results indicate that α-catenin changes its conformation in response to tension.

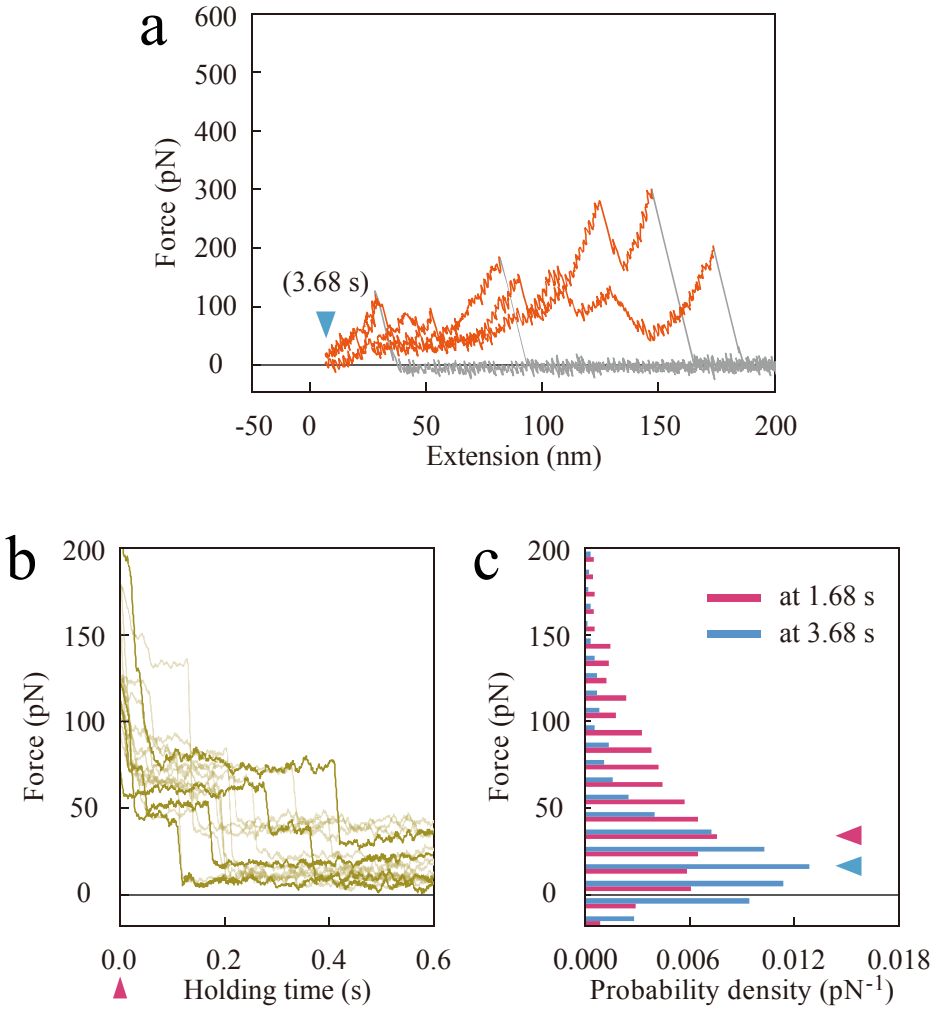

Figure 4-3: The results of AFM nano-tensile testing. **a.** The force versus extension curves with force responses of α-catenin were identified on the basis of the maximum force amplitude. Force curves for later extension after 3.68 s (cyan arrowhead) in force measurement are shown. **b.** Time course of force in the holding time after 1.68 s (magenta arrowhead) in force measurement. Initial time course for 0.6 s is shown. **c.** Force distributions at the beginning (magenta bars) and end (cyan bars) of holding time (at 1.68 and 3.68 s in force measurement).

4.3.2 Association of mechanically activated α-catenin with vinculin

The dynamics of full-length vinculin molecules were observed by TIRFM simultaneously with the AFM nano-tensile testing. In the time courses of fluorescent intensity in the movies obtained in conjunction with α-catenin responses in force curves, we observed a square pulse in the intensity with a possibility of 0.71%, as shown in Fig. 4-4a, in which the intensity increased during the holding time and then decreased at the beginning of later extension. This result indicates that vinculin associates with α-catenin under tension and dissociates upon further extension of α-catenin. Similar square pulses were observed with a possibility of 0.10% in the movies obtained without α-catenin responses in force curves, while the timing of the decrease in the intensity was not synchronized with the nano-tensile testing. The unsynchronized square pulses could be caused by transient association/dissociation of vinculin with α-catenin in autoinhibited conformation under no tension.

In the time courses of fluorescent intensity in the movies obtained with and without α-catenin responses, we observed a different type of signal, i.e., a step increase in the intensity with a possibility of 0.67%, as shown in Fig. 4-4b, in which the intensity increased independently of the holding time and sustained until the nano-tensile testing was completed. We determined that the step increases resulted from nonspecific vinculin association with the surface of coverslip, not to α-catenin molecules, as the step increases were observed on the coverslips on which we did not modify α-catenin molecules. The square pulses, which were caused by specific vinculin association with the α-catenin M1–M3 domain, were not observed for the M2–M3 domain (residues 385–634) lacking the M1 domain. This result indicates that vinculin associates with α-catenin M1 domain but not to any linker components nor the M2–M3 domain. Based on these results, we propose that the conformational change of α-catenin under tension allows its M1 domain, which contains the VBS, to associate with full-length vinculin.

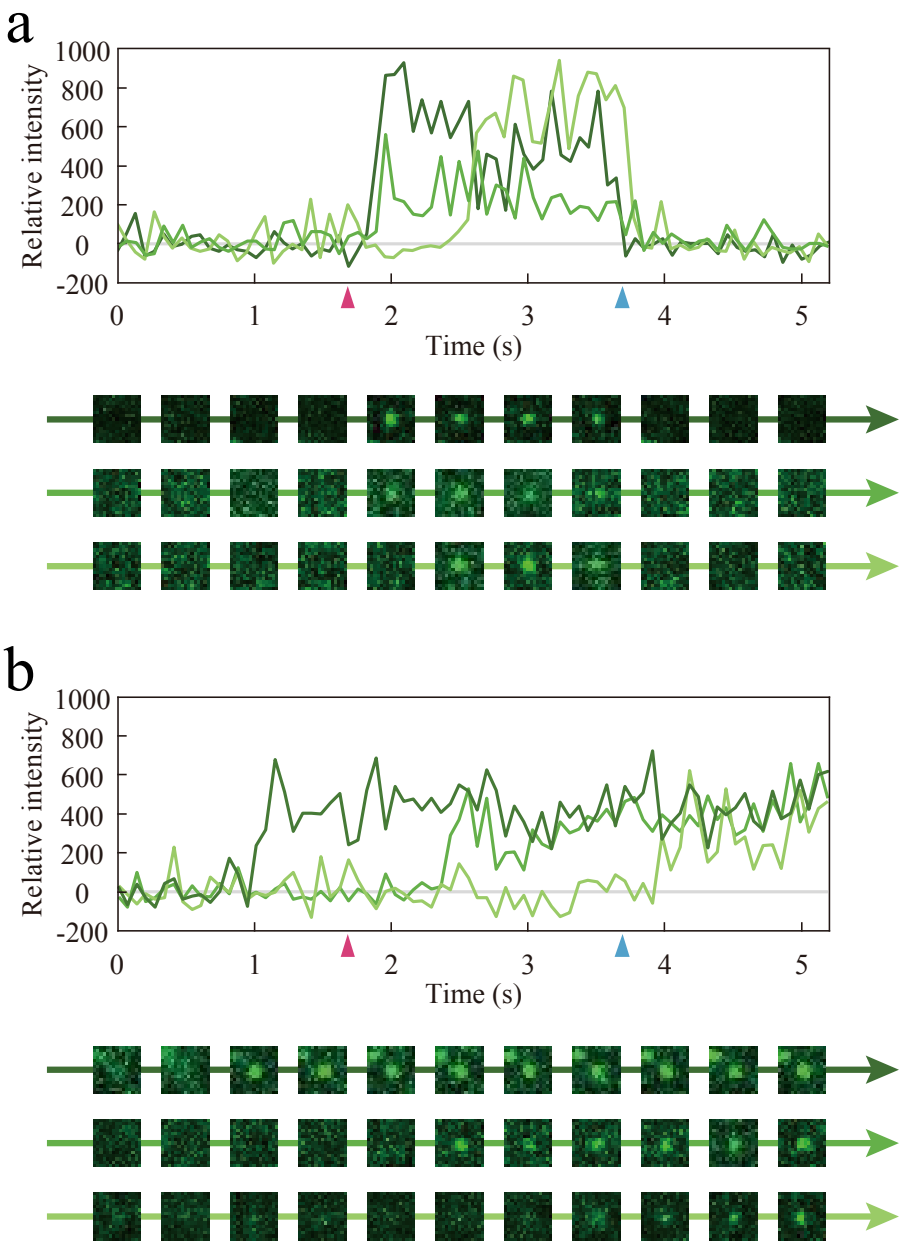

Figure 4-4: The results of TIRFM observation. **a.** Square pulses with increase in intensity after 1.68 s (magenta arrow head), representing vinculin association with mechanically activated α-catenin and decrease at 3.68 s (cyan arrow head), representing vinculin dissociation caused by further α-catenin extension. Time courses of images are shown in the lower panel. **b.** Step increases in intensity, independent of the timing of nano-tensile testing, caused by vinculin interaction with the surface of coverslip.

4.3.3 Reinforcement of α-catenin by vinculin association

To explore how the mechanical behavior of α-catenin changes by association with vinculin, we analyzed force curves in conjunction with the step increases observed in TIRFM, as shown in Fig. 4-5a. As shown in Fig. 4-5b, the unfolding force F_u was measured at every peak in the force curves except the last peak, which is caused by the detachment of the AFM probe from α-catenin. The histogram of the unfolding force F_u for the force curves without square pulse, as shown in Fig. 4-5c, showed right skewed distribution with mode value of ~100 pN. The high unfolding force F_u of more than 600 pN, which we did not observe in Chapter 3 (Maki *et al*., 2016), could be caused by parallel loading of several α-catenin molecules; we used a 50-fold higher concentration of α-catenin than in the experiments in Chapter 3 to increase the loading possibility. In contrast to force curves in the absence of a square pulse, those in the presence of a square pulse showed rather symmetric distributionwith a higher mode value (~150 pN), as shown in Fig. 4-5c. This positive change in mechanical responses indicates that α-catenin is mechanically reinforced by association with vinculin, as illustrated in Fig. 4-5d, which is consistent with the previous observation in Chapter 3 that α-catenin mutationally disrupted in autoinhibition is reinforced by association with full-length vinculin (Maki *et al*., 2016). Thus, we suggest that the mechanically activated α-catenin is reinforced by association with full-length vinculin.

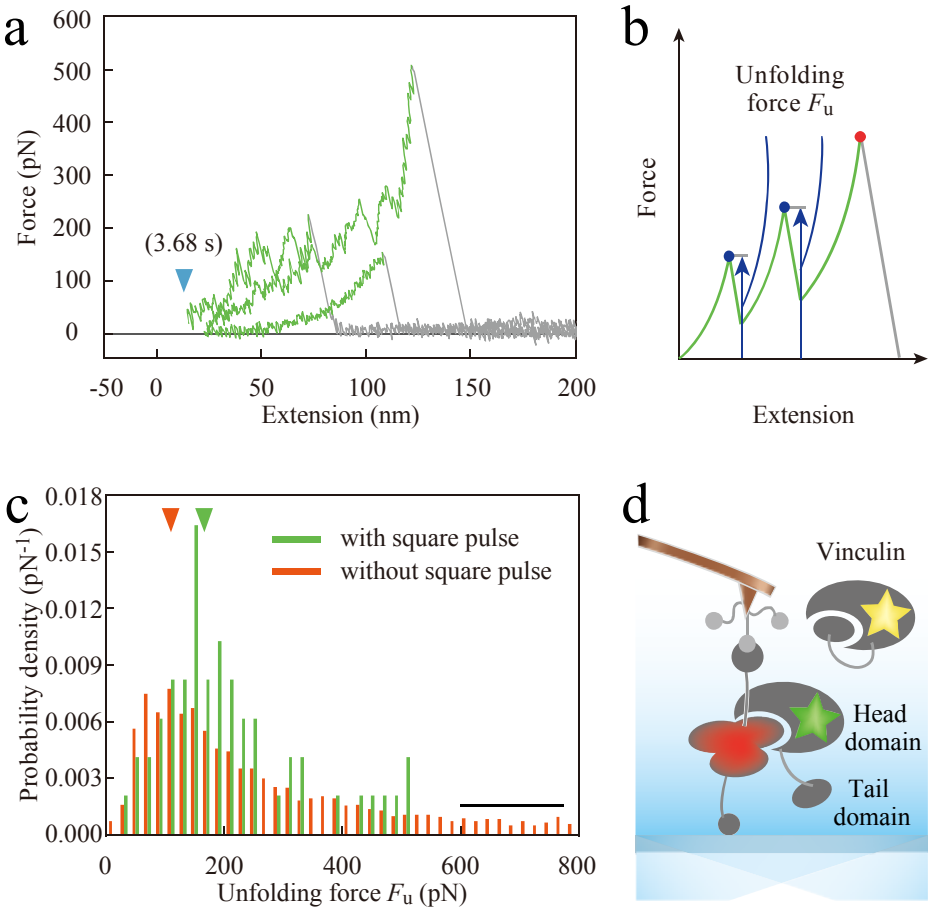

Figure 4-5: Reinforcement of α-catenin by association with vinculin. **a.** Force curves obtained with square pulses (i.e., vinculin association). **b.** Schematics of unfolding force (F_u) analysis. F_u was measured for every peak, blue dot, except the last peak, a red dot, which was caused by the detachment of the AFM probe from the surface of coverslip. **c.** Histogram of F_u for force curves with and without square pulses. High F_u (more than 600 pN, black line) could be caused by parallel loading of several α-catenin molecules. **d.** Association of mechanically activated α-catenin with autoinhibited vinculin. Conformational change of α-catenin under tension increased its affinity to vinculin head domain to form a mechanically stable complex.

4.4 Discussion

4.4.1 Mechano-guided association of α-catenin with vinculin

By using TIRFM-combined AFM, we directly demonstrated that a conformational change in the α-catenin M1–M3 domain under tension alters its affinity for full-length vinculin. Since both the α-catenin M1–M3 domain and full-length vinculin exhibit autoinhibited conformations against each other, how both of these molecules form a complex in mature adherens junctions was enigmatic. Although it has been proved that the α-catenin M1–M2 lacking the M3 domain exhibits higher affinity for the vinculin head domain than does the M1–M3 domain, interaction between the α-catenin M1–M2 domain and full-length vinculin has not been observed (Yonemura *et al*., 2010; Choi *et al*., 2012). Such a unique association mechanism between α-catenin and vinculin would be allowed by the autoinhibited structure of vinculin: the dissociation constant of the autoinhibiting interaction in vinculin between its head and tail domains (~1 nM) (Bacolitsa *et al*., 2004) is smaller than that of the interaction between the isolated α-catenin M1–M2 domain open form and the vinculin head domain (15 nM) (Yonemura *et al*., 2010; Choi *et al*., 2012). In the present study, we directly observed that the α-catenin M1–M3 domain makes a mechanically stable complex with full-length vinculin. This result is consistent with the result in Chapter 3 that the open form of the mutated α-catenin M1–M3 domain forms a mechanically stable complex with full-length vinculin, while the isolated M1 domain does not (Maki *et al*., 2016). Therefore, we suggest that the conformational change of full-length α-catenin involving the M1–M3 domains is crucial for the large increase in vinculin affinity.

Here we suggest a tension-based two-step unlocking mechanism of α-catenin and vinculin; first, intercellular tension unlocks the autoinhibition of the α-catenin M1–M3 domain; second, the overall conformational change drastically alters the vinculin

affinity to unlock the autoinhibition of vinculin, resulting in a stable molecular complex. This “mechano-guided association mechanism” mediated by force would be important for preferential assembly of a well-ordered molecular complex from a variety of adhesive molecules that could potentially associate together in the cytoplasm.

4.4.2 Dissociation of vinculin under high tension

In our results, the dissociating behaviors of vinculin from α-catenin were identified as sudden drops in intensity in square pulses observed in TIRFM. Interestingly, the vinculin dissociating events were observed even in the cases where α-catenin were not fully unfolded, i.e. the maximum extensions of α-catenin were shorter than its fully-extended length of ~143 nm. This result suggests that vinculin could dissociate from α-catenin in the beginning of the later extension. This result is consistent with the result in Chapter 3, in which full-length vinculin-associated α-catenin showed large force peaks in small extensions (~30 nm), suggesting vinculin can dissociate from α-catenin in initial extension. Since the isolated head domain of vinculin dissociates only when the α-catenin M1–M3 domain is almost fully extended (Yao *et al*., 2014), our result suggest that full-length vinculin dissociates more readily from α-catenin VBS than the vinculin head domain does. It is possible that high tension destabilizes the interaction between α-catenin VBS and vinculin head domain so that the vinculin tail domain recovers the head domain. Thus, we suggest that a biphasic association mechanism of α-catenin and vinculin would play a pivotal role in regulating intercellular tension; 1) under ~10 pN tension, α-catenin associates with vinculin to generate larger tension by positively remodeling actomyosin cytoskeleton, and 2) under higher tension threshold, vinculin dissociates from α-catenin to suppress the tension by deconstructing the adhesion structure.

4.5 Conclusion

α-Catenin and vinculin in adherens junctions cooperate to promote adhesion strength by remodeling the actin cytoskeleton. Under intercellular tension, α-catenin changes its conformation to associate with vinculin that nucleates actin polymerization. However, under tension-free conditions, both proteins assume autoinhibited conformations that prevent their association. By employing TIFRM-combined AFM, we mechanically activated α-catenin using AFM while observing vinculin association/dissociation using TIRFM. As a result, we found that mechanically-activated α-catenin unlocks the autoinhibition of vinculin to establish a mechanically stable complex. This mechano-guided association mechanism of autoinhibited proteins would allow for the preferential formation of well-ordered adherens junction architecture from several adhesive molecules. Furthermore, mechanically activated α-catenin was reinforced by the association with vinculin to form the stable molecular complex at adherens junction.

References

Bakolitsa, C. Cohen, D. M., Bankston, L.A., Bobkov, A. A., Cadwell, G.W., Jennings, L., Critchley, D. R., Craig, S. W. & Liddington, R. C. Structural basis for vinculin activation at sites of cell adhesion. *Nature* **430,** 583–586 (2004).

Brown, A. E. X., Hategan, A., Safer, D., Goldman, Y. E. & Discher, D. E. Cross-correlated TIRF/AFM reveals asymmetric distribution of force-generating heads along self-assembled, 'synthetic' myosin filaments. *Biophys. J.* **96,** 1952–1960 (2009).

Cavey, M., Rauzi, M., Lenne, P. F. & Lecuit, T. A two-tiered mechanism for stabilization and immobilization of E-cadherin. *Nature* **453,** 751–756 (2008).

Choi, H. J., Pokutta, S., Cadwell, G. W., Bobkov, A. A., Bankston, L. A., Liddington, R. C. & Weis, W. I. αE-catenin is an autoinhibited molecule that coactivates vinculin. *Proc. Natl. Acad. Sci. U. S. A.* **109,** 8576–8581 (2012).

Cohen, D. M., Chen, H., Johnson, R. P., Choudhury, B. & Craig, S. W. Two distinct head-tail interfaces cooperate to suppress activation of vinculin by talin. *J. Biol. Chem.* **280,** 17109–17117 (2005).

DuFort, C. C., Paszek, M. J. & Weaver, V. M. Balancing forces: architectural control of mechanotransduction. *Nat. Rev. Mol. Cell Biol.* **12,** 308–319 (2011).

Eiraku, M., Takata, M., Ishibashi, H., Kawada, K., Sakakura, E., Okuda, S., Sekiguchi, K., Adachi, T. & Sasai Y. Self-organizing optic-cup morphogenesis in three-dimensional culture. *Nature* **472,** 51–56 (2011).

Engl, W., Arasi, B., Yap, L. L., Thiery, J. P. & Viasnoff, V. Actin dynamics modulate mechanosensitive immobilization of E-cadherin at adherens junctions. *Nat. Cell Biol.* **16,** 584–591 (2014).

Finer, J. T., Simmons, R. M. & Spudich, J. A. Single myosin molecule mechanics: piconewton forces and nanometre steps. *Nature* **368,** 113–119 (1994).

Ishiyama, N., Tanaka, N., Abe, K., Yang, Y. J., Abbas, Y. M., Umitsu, M., Nagar, B., Bueler, S. A., Rubinstein, J. L., Takeichi, M. & Ikura, M. An autoinhibited structure of α-catenin and its implications for vinculin recruitment to adherens junctions. *J. Biol. Chem.* **288,** 15913–15925 (2013).

Johnson, R. P. & Craig, S. W. An intramolecular association between the head and tail domains of vinculin modulates talin binding. *J. Biol. Chem.* **269,** 12611–12619 (1994).

Kobielak, A. & Fuchs, E. α-Catenin: at the junction of intercellular adhesion and actin dynamics. *Nat. Rev. Mol. Cell Biol.* **5,** 614–625 (2004).

Kufer, S. K., Strackharn, M., Stahl, S. W., Gumpp, H., Pichner, E. M. & Gaub, H. E, Optically monitoring the mechanical assembly of single molecules. *Nat. Nanotechnol.* **4,** 45–49 (2009).

Lecuit, T. & Yap, A. S. E-cadherin junctions as active mechanical integrators in tissue dynamics. *Nat. Cell Biol.* **17,** 533–539 (2015).

Levayer, R. & Lecuit, T. Oscillation and polarity of E-Cadherin asymmetries control actomyosin flow patterns during morphogenesis. *Dev. Cell* **26,** 162–175 (2013).

Maiden, S. L. & Hardin, J. The secret life of α-catenin: moonlighting in morphogenesis. *J. Cell Biol.* **195,** 543–552 (2011).

Maki, K., Han, S. W., Hirano, Y., Yonemura, S., Hakoshima, T. & Adachi, T. Mechano-adaptive sensory mechanism of α-catenin under tension. *Sci. Rep.* **6,** 24878, (2016).

Okuda, S., Inoue, Y., Eiraku, M., Adachi, T. & Sasai, Y. Modeling cell apoptosis for simulating three-dimensional multicellular morphogenesis based on a reversible network reconnection framework. *Biomech. Model. Mechanobiol.* **15,** 805–816 (2016).

Rangarajan, E. S. & Izard, T. Dimer asymmetry defines α-catenin interactions. *Nat. Struct. Mol. Biol.* **20,** 188–193 (2013).

Takeichi, M. Dynamic contacts: rearranging adherens junctions to drive epithelial remodelling. *Nat. Rev. Mol. Cell Biol.* **15,** 397–410 (2014).

Wickline, E. D., Dale, I. W., Merkel, C. D., Heier, J. A., Stolz, D. B. & Kwiatkowski, A. V. αT-catenin is a constitutive actin-binding α-catenin that directly couples the cadherin-catenin complex to actin filaments. *J. Biol. Chem.* **291,** 15687–15699 (2016).

Wen, K. K., Rubenstein, P. A. & DeMali, K. A. Vinculin nucleates actin polymerization and modifies actin filament structure. *J. Biol. Chem.* **284,** 30463–30473 (2009).

Yao, M., Qiu, W., Liu, R., Efremov, A. K., Cong, P., Seddiki, R, Payre, M., Lim, C. T, Ladoix, B., Mege, R. M. & Yan, J. Force-dependent conformational switch of α-catenin controls vinculin binding. *Nat. Commun.* **5,** 4525 (2014).

Yap, A. S., Gomez, G. A. & Parton, R. G. Adherens junctions revisualized: organizing cadherins as nanoassemblies. *Dev. Cell* **35,** 12–20 (2015).

Yonemura, S., Wada, Y., Watanabe, T., Nagafuchi, A. & Shibata, M. α-Catenin as a tension transducer that induces adherens junction development. *Nat. Cell Biol.* **12,** 533–542 (2010).

Chapter 5

Conclusion

In the present thesis, based on single-molecule biomechanical experiments using AFM and TIRFM, the mechanical behaviors of constitutive molecules of mechano-sensitive adherens junctions were explored with the objective of understanding how the molecules cooperate to sense the intercellular tension by changing the conformations under tension. Below is a summary of the major findings and observations.

In Chapter 2, the mechanical behaviors of β-catenin under tension were examined by AFM. A part and a whole structure of β-catenin have been loaded under tension since the loading condition could be various at adherens junctions depending on the interaction between cadherin and β-catenin. The results indicated that β-catenin behave as a nonlinear elastic material under tension, i.e., a mechanical component with low stiffness under low tension and high stiffness under high tension. The nonlinear elastic behavior exhibited in our experiment has suggested a mechanical function of β-catenin to serve as a tension transmitter at adherens junctions: 1) preserving links between constitutive molecules at adherens junctions under low tension and 2) transmitting high tension with high mechanical stability.

In Chapter 3, we have revealed how α-catenin retains its activated state while avoiding unfolding under tension. Using single-molecule force spectroscopy employing AFM, we have found that mechanically activated α-catenin fragment had higher mechanical stability than a non-activated fragment. The results of our experiments using mutated and segmented fragments have showed that the key intramolecular interactions acted as a conformational switch. The drastic conformational change of α-catenin has been observed by AFM structural imaging, suggesting the change in its vinculin affinity. We have also found that the conformation of α-catenin was reinforced by association with vinculin. We have demonstrated that α-catenin adaptively changes its conformation under tension to a stable intermediate state, and finally settles into a more stable state reinforced by association with vinculin. Our data have suggested that the plastic characteristics of α-catenin in response to both mechanical and biochemical cues enable the functional-structural dynamics at the cellular and tissue levels.

In Chapter 4, we have examined how the conformational change of α-catenin under tension alters its vinculin affinity. Although α-catenin and vinculin in adherens junctions cooperate to promote adhesion strength by remodeling the actin cytoskeleton, both proteins assume autoinhibited conformations that prevent their association under tension-free conditions. Thereby, it had been mysterious how both molecules are activated to form a molecular complex at adherens junctions. As α-catenin had drastically changed the conformation under tension, we hypothesized that the conformational change alters the vinculin affinity. By employing TIFRM-combined AFM, we mechanically activated α-catenin using AFM while observing vinculin association/dissociation using TIRFM. As a result, we found that mechanically-activated α-catenin unlocks the autoinhibition of vinculin to establish a mechanically stable complex. This mechano-guided association mechanism of autoinhibited proteins would allow for the preferential formation of well-ordered adherens junction architecture from several adhesive molecules. Furthermore, mechanically activated α-catenin was reinforced by the association with vinculin to form the stable molecular complex at adherens junction.

In conclusion, the present thesis has proposed the new molecular mechanisms in intercellular mechanotransduction. We have revealed that the dynamical coupling of force, structure and function originates the tension-sensitivity of α-catenin. The results are a significant progress in elucidating the molecular biomechanics in dynamical and complex multicellular systems. The new concepts emerging from our investigations, i.e., “the mechano-adaptive conformational change” and “the mechano-guided association for autoinhibited molecules” could explain how robust and well-ordered molecular architectures are established and maintained in cells. Furthermore, the structural-functional dynamics presented by α-catenin under tension inspires a powerful molecular machine that dynamically changes its structure to alter its biochemical property, such as signal binding affinity or redox state, and to exert mechanical force for crushing cancer cells or sewing micro injuries. Thus, the present thesis could contribute to the further development of the field of biomechanics, biophysics, and bioengineering.

The vivid activities of cells emerge from various functions of constitutive biomolecules and their kinetic interactions with each other. In addition, as observed in this study, biomolecules exhibit a wide variation in their behaviors under mechanical and chemical conditions, which would contribute to the functional and structural robustness in cells. For exploring the molecular characteristics together with variations, it is required to develop high-through put methods with minimized measurement error and, at the same time, to solidly evaluate the results from a theoretical point of view. Such approaches, based on the sense of mechanical engineering, can be utilized to any research objectives in larger spatial scales. Accordingly, the approaches would become increasingly important in the next stage of life studies to comprehensively understand the multiscale life system in cooperation with other approaches such as molecular biology, structural biology, and biophysics. In turn, new materials and technologies developed in engineering-based biostudies could be utilized for more generic purposes in clinical medicine and industry as well as academic research. Thereby, I propose in this thesis that the dual-directional approaches from engineering to biostudies, and vice versa, are inevitable for developments in the field of biomechanics in the future.

List of Publications and Presentations

A. Publications

Related refereed publications

1. Koichiro Maki, Sung-Woong Han, Taiji Adachi, “β-catenin as a tension transmitter revealed by AFM nanomechanical testing”, *Cellular and Molecular Bioengineering* **8**, pp.14-21 (2015). **(Chapter 2)**

2. Koichiro Maki, Sung-Woong Han, Yoshinori Hirano, Shigenobu Yonemura, Taiji Adachi, “Mechano-adaptive sensory mechanism of α-catenin under tension”, *Scientific Reports* **6**:24878, (2016). **(Chapter 3)**

3. Koichiro Maki, Nobuhiko Nakao, Taiji Adachi, “Nano-mechanical characterization of tension-sensitive helix bundles in talin rod”, *Biochemical and Biophysical Research Communications*, (2017). **(Chapter 3)**

4. Koichiro Maki, Sung-Woong Han, Yoshinori Hirano, Shigenobu Yonemura, Taiji Adachi, “Mechano-guided association mechanism of α-catenin with autoinhibited vinculin revealed by TIRFM-combined AFM”, under revision. **(Chapter 4)**

Review articles in books and journals

1. Milos Spasic, Koichiro Maki, Florian A. Herzog and Christopher R. Jacobs, “Effects of Mechanical Stress on Cells”, Comprehensive Biomaterials, in press.
2. 牧功一郎，安達泰治，“接着結合を介した力の感知－分子引張実験によるアプローチー”，高度物理刺激と生体応答，in press.
3. 牧功一郎，安達泰治，“原子間力顕微鏡による細胞・分子の力学イメージング”，病理と臨床，No. 33-12，pp. 1351-1357，2015 年 12 月
4. 牧功一郎，安達泰治，“メカノセンサーシグナル”，生体の科学，No. 66-5，pp. 450-451，2015 年 9 月
5. 牧功一郎，韓成雄，安達泰治，“AFM でメカノセンサ 1 分子を釣り上げる”，細胞工学，No. 33-9，pp. 917-921，2014 年 9 月

B. Presentations

International conferences

1. Nobuhiko Nakao, Koichiro Maki, Taiji Adachi, “Nano-mechanical measurement of integrin-based focal complex using AFM”, CDB Symposium 2017, Kobe, Japan, Mar. 2017.
2. Stefania Marcotti, Koichiro Maki, Taiji Adachi, Gwendolen C. Reilly, Damien Lacroix, “Nanofishing of Hyaluronic Acid on Murine Osteoblast Precursor Cells”, The Orthopaedic Research Society Annual Meeting, California, USA, Mar. 2017.

B. Presentations

3. Koichiro Maki, Taiji Adachi, “Biomechanical characterization of α-catenin by single-molecule approaches using AFM and TIRFM”, The 15th International Student Seminar (ISS), Kyoto, Japan, Feb. 2017.

4. Koichiro Maki, Taiji Adachi, “Adaptive mechanosensory mechanism of α-catenin revealed by single-molecule AFM and TIRFM”, The 9th Cell, Developmental, and Systems Biology Course Meeting, Kyoto, Japan, Feb. 2017.

5. Nobuhiko Nakao, Koichiro Maki, Taiji Adachi, “Actin remodeling in nascent focal adhesion explored by integrin nanofishing”, IGER International Symposium on "Now in actin study: Motor protein research reaching a new stage", Aichi, Japan, Nov. 2016.

6. Koichiro Maki, Taiji Adachi, “Mechano-adaptive conformational change of α-catenin to sense and transmit intercellular force”, 22nd Congress of the European Society of Biomechanics, Lyon, France, Jul. 2016.

7. Koichiro Maki, Taiji Adachi, “Single-molecule AFM for exploring the force responses of adherens junction proteins”, iCeMS International Symposium -Hierarchical Dynamics in Soft Materials and Biological Matter, Kyoto, Japan, Sept. 2015.

8. Koichiro Maki, Sung-Woong Han, Taiji Adachi, “Mechanical roles of β-catenin for AJ-mediated force transmission”, The 8th Asian-Pacific Conference on Biomechanics, Hokkaido, Japan, Sept. 2015.

9. Koichiro Maki, Sung-Woong Han, Taiji Adachi, “Nanomechanical behaviors of β-catenin revealed by single-molecule AFM”, 21st Congress of the European Society of Biomechanics, Prague, Czech Republic, July 2015.

10. Taiji Adachi, Koichiro Maki, Sung-Woong Han, “Single-molecule analysis of adherens junction-mediated mechanotransduction using AFM”, Frontiers of Single Cell Analysis, Nairobi, Kenya, Sept. 2014.

11. Koichiro Maki, Sung-Woong Han, Taiji Adachi, “Single-molecule mechanical unfolding of α-catenin as an intercellular mechanosensor”, Frontiers of Single Cell Analysis, Nairobi, Kenya, Sept. 2014.

12. Taiji Adachi, Koichiro Maki, Sung-Woong Han, “AFM nanofishing of mechano-sensitive molecules at adherens junction”, The 4th Japan-Switzerland Workshop on Biomechanics, Mie, Japan, Sept. 2014.

13. Koichiro Maki, Sung-Woong Han, Taiji Adachi, “Nanomechanical behaviors of α-catenin as a mechanotransduction switch revealed by AFM nanofishing”, 7th World Congress of Biomechanics, Boston, USA, July 2014.

14. Koichiro Maki, Sung-Woong Han, Taiji Adachi, “α-Catenin switches mechanotransduction ‘on’ under tensile force –based on single-molecule force spectroscopy using AFM”, International symposium on mechanobiology 2014, Okayama, Japan, May 2014.

15. Koichiro Maki, Sung-Woong Han, Taiji Adachi, “Mechanical properties of β-catenin revealed by SMFS”, The 7th Asia Pacific Conference of Biomechanics, Seoul, Korea, Aug. 2013.

16. Koichiro Maki, Sung-Woong Han, Taiji Adachi, “Linear-elastic behaviors of β-catenin revealed by AFM-based SMFS”, Proceeding of the 35th Annual International Conference of the IEEE Engineering in Medicine and Biology Society (EMBC'13), Osaka, Japan, Jul. 2013.

17. Sung-Woong Han, Koichiro Maki, Taiji Adachi, “Evaluation for mechanical behavior for nanospring protein in adherens junction using AFM”, Proceeding of the 12th International Discussion & Conference on Nano Interface Controlled Electronic Devices, Gyeongju, Korea, Oct. 2012.

18. Koichiro Maki, Sung-Woong Han, Taiji Adachi, “Evaluation for mechanical properties of nanospring protein using AFM”, Proceeding of International Symposium on Cellular Mechanobiology, Kyoto, Japan, Mar. 2012.

Domestic conferences

1. 牧功一郎, 安達泰治, “Mechanical, structural and functional dynamics of α-catenin molecule at intercellular adherens junctions”, 日本生物物理学会 第 54 回年会, つくば, 2016 年 11 月

2. 牧功一郎, 安達泰治, “原子間力顕微鏡を用いた張力感知分子のナノフィッシングおよび構造イメージング”, 日本機械学会 第 27 回バイオフロンティア講演会, 北海道, 2016 年 10 月

3. 仲尾信彦, 牧功一郎, 安達泰治, “ECM に刺激されたインテグリン-アクチン構造体の成熟過程におけるナノ力学特性評価”, 日本機械学会 第 27 回バイオフロンティア講演会, 北海道, 2016 年 10 月

4. 牧功一郎, 安達泰治, “細胞間張力を感知する α-カテニンの力学的分子適応メカニズム”, 日本機械学会 第 28 回バイオエンジニアリング講演会, 東京, 2016 年 1 月

5. 広橋佑紀, 牧功一郎, 安達泰治, “α カテニンに対するビンキュリン結合の AFM 分子イメージング”, 日本機械学会 第 28 回バイオエンジニアリング講演会, 東京, 2016 年 1 月

6. 広橋佑紀, 牧功一郎, 安達泰治, “立体構造変化を伴う接着構成分子間の AFM 相互作用測定”, 日本機械学会 2015 年度年次大会, 京都, 2015 年 9 月

7. 牧功一郎, 韓成雄, 安達泰治, “接着結合における張力伝達要素としての β-カテニン”, 日本生物物理学会 第 53 回年会, 石川, 2015 年 9 月

8. 広橋佑紀, 牧功一郎, 安達泰治, “分子間相互作用測定における AFM フォースカーブ解析手法の検討”, 日本機械学会 関西支部第 90 期定時総会講演会, 京都, 2015 年 3 月

9. 牧功一郎, 韓成雄, 安達泰治, “張力感知分子のアンフォールディング経路探索”, 文部科学省　研究開発施設共用等促進費補助金／生命動態システム

科学推進拠点事業「多次元定量イメージングに基づく数理モデルを用いた動的生命システムの革新的研究体系の開発・教育拠点」生命動態の分子メカニズムと数理，京都，2015 年 3 月

10. 安達泰治, 牧功一郎, “メカノセンサー生体分子の AFM ナノフィッシング”, 医工学フォーラム特別講演会 2014，京都，2015 年 2 月

11. 牧功一郎，韓成雄，安達泰治，“構成ドメインの力学的安定性に依存した α-カテニンのアンフォールディング”，日本機械学会 第 27 回バイオエンジニアリング講演会，新潟，2015 年 1 月

12. 牧功一郎，韓成雄，安達泰治，“張力作用下における α-カテニンのナノ力学挙動解析”，日本機械学会 第 26 回バイオエンジニアリング講演会，宮城，2014 年 1 月

13. 牧功一郎，韓成雄，安達泰治，“張力作用下における α-カテニンのナノ力学挙動解析”，京都大学再生医科学研究所　若手発表会，京都，2013 年 12 月

14. 韓成雄, 牧功一郎, 安達泰治, “AFM を用いた接着結合分子の力学挙動解析”, 日本生物物理学会 第 51 回年会，京都，2013 年 10 月

15. 牧功一郎，韓成雄，安達泰治，“原子間力顕微鏡を用いた α-カテニンの単分子力学測定”，日本機械学会 2013 年度年次大会，岡山，2013 年 9 月

16. 牧功一郎, 韓成雄, 安達泰治, “AFM nanofishing of adherens junction component molecules ”，文部科学省科学研究費補助金　新学術領域研究「ミクロからマクロへ階層を超える秩序形成のロジック」第 4 回班会議，北海道，2013 年 6 月

17. 牧功一郎，韓成雄，安達泰治，“AFM ナノフィッシングによる接着結合構成タンパク質の力学的挙動解析”，文部科学省科学研究費補助金　新学術領域研究「細胞機能と分子活性の多次元蛍光生体イメージング」 第 3 回 vivid workshop，石川，2013 年 2 月

18. 牧功一郎，韓成雄，安達泰治，“β-カテニンの AFM 単分子力学測定”，日本機械学会 第 23 回バイオフロンティア講演会，青森，2012 年 10 月

19. 牧功一郎, 韓成雄, 安達泰治, “AFM を用いたβ-カテニンの力学的挙動解析”, 日本生物物理学会 第 50 回年会，名古屋，2012 年 9 月

20. 牧功一郎，韓成雄，安達泰治，“Nanospring behaviors of β-catenin in adherens junctions”，文部科学省科学研究費補助金　新学術領域研究「ミクロからマクロへ階層を超える秩序形成のロジック」第 3 回班会議，北海道，2012 年 6 月

Awards

1. 学生発表賞，日本生物物理学会，2016 年 11 月
2. Student Award Runner-up, The 22nd Congress of the European Society of Biomechanics, July 2016.
3. Travel Award, The 22nd Congress of the European Society of Biomechanics, Lyon, France, July 2016.
4. 優秀発表賞，京都大学再生医科学研究所　若手発表会，京都，2013 年 12 月